Journal of Computational Physics 431 (2021) 109713

Contents lists available at ScienceDirect

Journal of Computational Physics

www.elsevier.com/locate/jcp

The lattice Boltzmann method for nearly incompressible flows

Pierre Lallemand [a], Li-Shi Luo [a,b,*], Manfred Krafczyk [c], Wen-An Yong [d,a]

[a] Computational Science Research Center, Beijing 100193, China
[b] Department of Mathematics and Statistics, Old Dominion University, Norfolk, VA 23529, USA
[c] Institute for Computational Modeling in Civil Engineering (iRMB), Technische Universität Braunschweig, Pockelsstraße 3, 38106 Braunschweig, Germany
[d] Zhou Pei-Yuan Center for Applied Mathematics, Tsinghua University, Beijing 100084, China

ARTICLE INFO

Article history:
Received 10 July 2016
Received in revised form 7 July 2020
Accepted 7 July 2020
Available online 20 November 2020

Keywords:
Lattice Boltzmann equation
Nearly incompressible Navier-Stokes equations
Convergence
Stability
Local analysis and equivalent equations
Boundary conditions

ABSTRACT

This review summarizes the rigorous mathematical theory behind the lattice Boltzmann equation (LBE). Relevant properties of the Boltzmann equation and a derivation of the LBE from the Boltzmann equation are presented. A summary of some important LBE models is provided. Focus is given to results from the numerical analysis of the LBE as a solver for the nearly incompressible Navier-Stokes equations with appropriate boundary conditions. A number of numerical results are provided to demonstrate the efficacy of the lattice Boltzmann method.

1. Introduction

The lattice Boltzmann equation (LBE) has become a popular means of computational fluid dynamics (CFD) in the recent two decades for simulations of near incompressible flows. In particular, the LBE has found popular applications for near incompressible flows with complex and/or moving boundaries, thus, it has been successfully used to simulate a wide variety of flow phenomena, such as micro-scale phenomena of polymer chains or bio-molecules in solvent fluids [1–7] confined in a nano-pore [8,9], flows of biological systems [10], interfacial flows [11–17], flow-structure interactions [18–21], the rheology of red blood cells (RBCs) [22–25] and suspensions in fluids [26–32], flows through realistic porous media [33–44] and in geology [45], to the aerodynamics of insects [46–49], automobiles [50–52], and aircraft [53], or turbulent flows [54–60]. The LBE is particularly popular among those novices who want to write a working CFD code overnight, mostly because of the extremely simple appearance of the basic LBE algorithm. The number of publications on the LBE and its applications has been growing rapidly over the last two decades. There have been numerous reviews [28,61–64] and monographs [65–71] on the LBE method, and they are mostly devoted to the applications of the method. However, there exists no review or

* Corresponding author at: Department of Mathematics and Statistics, Old Dominion University, Norfolk, VA 23529, USA.
E-mail addresses: pierre.lallemand1@free.fr (P. Lallemand), lluo@odu.edu, lluo@csrc.ac.cn (L.-S. Luo), kraft@irmb.tu.bs.de (M. Krafczyk), wayong@mail.tsinghua.edu.cn (W.-A. Yong).
URLs: http://www.lions.odu.edu/~lluo (L.-S. Luo), http://www.tu-braunschweig.de/irmb/institut/mitarbeiter/krafczyk (M. Krafczyk).

https://doi.org/10.1016/j.jcp.2020.109713
0021-9991/

monograph which focuses on the definitive and rigorous analysis of the LBE method to elucidate why and how the method works, from the perspective of numerical analysis. The intent of this review is to fill this void.

Historically, the LBE [72–76] was inspired by the lattice-gas cellular automata [77–80]. However, it was soon understood that a linearized collision term can be used in the LBE to enhance computational efficiency [73,74], and further, the eigenfunctions of the linearized collision operator in the LBE form an orthogonal basis which can be used to expand the distribution functions [75,76]. These developments [74–76] culminated in the generalized LBE [81], which is a system of finite moments evolving in discrete phase space-time, and the collision is modeled by linear relaxations with constant relaxation rates.

On the other hand, it has also been shown that the LBE can be directly derived from the linearized Boltzmann equation [82–85]. Due to its kinetic origin, the LBE differs in principle from *all* traditional CFD methods based on direct discretizations of the Navier-Stokes equations, such as finite difference, finite volume, finite element, and spectral methods. In spite of its kinetic origin, the LBE is a CFD solver for nearly incompressible Navier-Stokes equations, and analysis would reveal that, beneath its surface, the lattice Boltzmann (LB) schemes are equivalent to some existing finite-difference schemes [86–88] with the artificial compressibility method [89–91], but with some features unique to the LBE. In addition, the analysis of the LBE often relies on Chapman-Enskog singular perturbation expansion, which is not conventional for traditional methods in CFD. These factors contribute to the fact that the LBE is not well understood or appreciated in the CFD community at large, in spite of a growing interest in the method. This review intends to emphasize the mathematical validity of the LBE, and to elucidate its pros and cons based on analysis.

To focus on the rigorous analysis of the LBE method, this review will be restricted to the LBE for simple fluid flows and will not discuss the LBE for complex fluids such as immiscible fluids with distinctive interfaces (cf., *e.g.*, [15,16,39,43,92–98]). The remainder of this review is organized as follows. Section 2 provides a brief discussion of the Boltzmann equation, emphasizing the derivation of the hydrodynamic equation and transport coefficients. Section 3 presents the essential features of the LBE, including its connection to the linearized Boltzmann equation, some key mathematical properties of the LBE, and the LBE models for various flow systems. Section 4 focuses on the rigorous numerical analysis of the LBE, which includes derivation of macroscopic equations from the LBE, and convergence and stability proofs for the LBE algorithm. Section 5 discusses the local linear analysis of Fourier and von Neumann, which has been used to optimize the LBE. Section 6 is devoted to the forcing term and various boundaries and initial conditions in the LBE. A particular emphasis is given to the bounce-back type schemes to realize Dirichlet or Neumann boundary conditions. Section 7 discusses very briefly a grid refinement scheme for the LBE. Section 8 provides several examples to demonstrate the capability of the LBE as a method to simulate hydrodynamic flows. Two types of examples are shown. The first are relatively simple test cases which are used to verify the order of convergence, such as the Poiseuille flow and a flow with double shear layers in 2D; and the second are high-Reynolds-number flows which are computationally challenging, such as flows past a sphere or a car body. Finally, Section 9 discusses some outstanding issues in the LBE and concludes this review. For the convenience of the readers, a list of symbols is provided. Although the bibliography includes over four hundred selected references, they are neither comprehensive nor complete, nevertheless, from the authors' perspective they represent the progresses made in the field over the past two decades.

2. The Boltzmann equation and kinetic theory

This section provides a very brief summary of the Boltzmann equation [99–108] — its properties and solution methods in connection with the macroscopic equations, which are relevant to the analysis of the lattice Boltzmann equation to be discussed in the next section. Three solution methods will be mentioned: specifically the Hilbert method, the Chapman-Enskog method, and Grad's moment method.

2.1. The Boltzmann equation and some of its essential properties

Starting from the Liouville theorem for the distribution function in the N-particle phase space of an N-particle Hamiltonian system and via the Bogoliubov–Born–Green–Kirkwood–Yvon (BBGKY) hierarchy of coarse-graining (cf., *e.g.*, [101,102]), *i.e.*, by integrating over $(N-1)$-particle phase space, and the assumption of *stosszahlansatz* that two particles entering a collision have no correlation so their joint distribution function can be factorized into the product of their individual distribution functions, the Boltzmann equation for the time-dependent single particle (mass) distribution function $f(\boldsymbol{r}, \boldsymbol{\xi}, t)$ in single-particle phase space $\mathbb{\Gamma} := (\boldsymbol{r}, \boldsymbol{\xi})$ of the particle position $\boldsymbol{r}$ and velocity $\boldsymbol{\xi}$ is deduced in the so-called Boltzmann-Grad limit [101,102,105,108,109] of large number density n and finite mean free path ℓ (cf., Sec. 2.2 for more discussion on ℓ) as the following:

$$\partial_t f + \boldsymbol{\xi}\cdot\boldsymbol{\partial}_{\boldsymbol{r}} f + \boldsymbol{a}\cdot\boldsymbol{\partial}_{\boldsymbol{\xi}} f = Q[f,\, f_*], \tag{2.1a}$$

$$Q[f, f_*] = \frac{1}{m}\int \mathrm{d}\boldsymbol{\xi}_*\mathrm{d}\Theta\mathrm{d}\epsilon\, B(\Theta, \boldsymbol{\xi}, \boldsymbol{\xi}_*)\left[f' f'_* - f f_*\right], \tag{2.1b}$$

where the notation has been borrowed from the monograph by Harris [101]: $f_* := f(\boldsymbol{r}, \boldsymbol{\xi}_*, t)$ and $f'_* := f(\boldsymbol{r}, \boldsymbol{\xi}'_*, t)$; $(\boldsymbol{\xi}, \boldsymbol{\xi}_*)$ and $(\boldsymbol{\xi}', \boldsymbol{\xi}'_*)$ denote the pre-collision and post-collision particle velocity pairs, respectively; ϵ is the polar angle on the plane

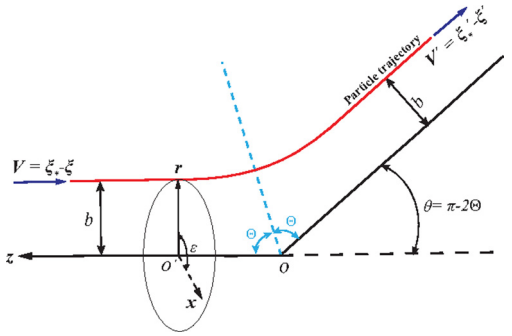

Fig. 1. Illustration of an elastic binary collision. The dashed line is the apse line. The particle trajectory is unbounded, *i.e.*, the interaction potential $U(r_{21})$ is assumed to be purely repulsive thus.

perpendicular to the velocity difference vector $\boldsymbol{V} := \boldsymbol{\xi}_* - \boldsymbol{\xi}$ [101], and Θ is the angle between the apse line and $\boldsymbol{V}$ or $\boldsymbol{V}'$ (cf. Fig. 1), and it is related to the deflection angle θ: $\theta = \pi - 2\Theta$ or $\Theta = (\pi - \theta)/2$ (cf. Fig. 1); $\boldsymbol{a} = \boldsymbol{F}/m$ is the acceleration due to an external force $\boldsymbol{F}$, m is the particle mass which is usually assumed to be 1 unless otherwise specified; Q is the collision operator; and $B(\Theta, \boldsymbol{\xi}, \boldsymbol{\xi}_*) \geq 0$ is the collision kernel depending on the inter-particle potential U [99–103]. Fig. 1 illustrates the variables in the collision integral Eq. (2.1b).

For an *elastic* collision or *reversible* particle dynamics between two *indistinguishable* particles, the collision kernel $B(\Theta, \boldsymbol{\xi}, \boldsymbol{\xi}_*)$ is invariant under the following coordinate transforms (cf., *e.g.*, [110,111]):

$$(\Theta, \boldsymbol{\xi}, \boldsymbol{\xi}_*) \mapsto (\Theta, \boldsymbol{\xi}_*, \boldsymbol{\xi}), \ (\Theta, \boldsymbol{\xi}, \boldsymbol{\xi}_*) \mapsto (\Theta, \boldsymbol{\xi}', \boldsymbol{\xi}'_*), \ (\Theta, \boldsymbol{\xi}, \boldsymbol{\xi}_*) \mapsto (\Theta, \boldsymbol{\xi}'_*, \boldsymbol{\xi}'),$$

therefore,

$$B(\Theta, \boldsymbol{\xi}, \boldsymbol{\xi}_*) = B(\Theta, \boldsymbol{\xi}', \boldsymbol{\xi}'_*) \quad \text{and} \quad B(\Theta, \boldsymbol{\xi}, \boldsymbol{\xi}_*) = B(\Theta, \boldsymbol{\xi}_*, \boldsymbol{\xi}), \tag{2.2}$$

which simply states the reversibility of elastic binary collision and the indistinguishability of particles. In particular, with any spherically symmetric central-force potential $U(\boldsymbol{r}_1, \boldsymbol{r}_2) = U(|\boldsymbol{r}_2 - \boldsymbol{r}_1|) := U(r_{21})$, $r_{12} := |\boldsymbol{r}_1 - \boldsymbol{r}_2|$, between two particles at $\boldsymbol{r}_1$ and $\boldsymbol{r}_2$, one has $|\boldsymbol{\xi}_* - \boldsymbol{\xi}| = |\boldsymbol{\xi}'_* - \boldsymbol{\xi}'| := V$ and

$$B(\Theta, \boldsymbol{\xi}, \boldsymbol{\xi}_*) = B(\Theta, |\boldsymbol{\xi}_* - \boldsymbol{\xi}|) = B(\Theta, V), \tag{2.3}$$

hence satisfying (2.2) automatically.

For an elastic binary collision under the influence of the central-force potential U and with the impact parameter b (cf. Fig. 1):

$$B(\Theta, V) = 2Vb\left|\frac{\mathrm{d}b}{\mathrm{d}\theta}\right|, \quad \Theta(b, V) = \int_0^{\chi_0} \frac{\mathrm{d}\chi}{\sqrt{1 - \chi^2 - \frac{4U(b/\chi)}{mV^2}}}, \quad \chi := \frac{b}{r}, \tag{2.4}$$

where χ_0 is the positive root of $1 - \chi_0^2 - 4U(b/\chi_0)/mV^2 = 0$, corresponding to the particle trajectory $r(\theta)$ at its apse (cf. Fig. 1).

The collision cross section $\sigma(\Theta, V)$ is related to $B(\theta, V)$ by

$$\sigma(\theta, V)\sin\theta\,\mathrm{d}\theta\mathrm{d}\epsilon = \frac{1}{V}B(\Theta, V)\,\mathrm{d}\Theta\mathrm{d}\epsilon. \tag{2.5}$$

It is interesting to note that for the so-called Maxwell molecules [112–114], $\nabla U(r) \propto r^{-5}$, then $B = B(\Theta)$, leading to a considerable simplification of the collision term $Q[f, f_*]$.

Consider the following linear integral operator on a function $\phi(\boldsymbol{\xi})$:

$$\mathcal{I}[\phi(\boldsymbol{\xi})] := \int \phi(\boldsymbol{\xi}) Q[f, f_*]\,\mathrm{d}\boldsymbol{\xi}, \tag{2.6}$$

then the symmetries of $B(\Theta, \boldsymbol{\xi}, \boldsymbol{\xi}_*)$ given by (2.2) directly lead to

$$\mathcal{I}[\phi(\boldsymbol{\xi})] = \frac{1}{4}\left(\mathcal{I}[\phi(\boldsymbol{\xi})] + \mathcal{I}[\phi(\boldsymbol{\xi}_*)] - \mathcal{I}[\phi(\boldsymbol{\xi}')] - \mathcal{I}[\phi(\boldsymbol{\xi}'_*)]\right). \tag{2.7}$$

Note that while it is not indicated in the left-hand side of (2.6), $\mathcal{I}[\phi(\boldsymbol{\xi})]$ indeed depends on f. A function $\phi(\boldsymbol{\xi})$ is a collisional invariant if and only if

$$\phi(\boldsymbol{\xi}) + \phi(\boldsymbol{\xi}_*) = \phi(\boldsymbol{\xi}') + \phi(\boldsymbol{\xi}'_*) \quad \text{or} \quad \phi + \phi_* = \phi' + \phi'_*. \tag{2.8}$$

The symmetries of the *elastic* collision between two *indistinguishable* particles, as stated by (2.2), lead to several significant consequences of the Boltzmann equation (2.1a). The first is that the collision term Q obeys the *microscopic* conservation laws for mass, momentum, and energy:

$$\int \mathrm{d}\boldsymbol{\xi} \begin{pmatrix} 1 \\ \boldsymbol{\xi} \\ \frac{1}{2}\xi^2 \end{pmatrix} Q[f,\, f_*] = \begin{pmatrix} 0 \\ \mathbf{0} \\ 0 \end{pmatrix}, \tag{2.9}$$

where $\xi^2 := \boldsymbol{\xi}\cdot\boldsymbol{\xi}$. Furthermore, the functions $\{1,\, \boldsymbol{\xi},\, \xi^2/2\}$ are the only *collisional invariants*, and they form a basis spanning the *null space* of the collision operator Q. We will use the following notation for the collisional invariants and the corresponding conserved moments:

$$\varphi_0 := 1, \qquad \varphi_{1,2,3} := \xi_{x,y,z}, \qquad \varphi_4 := \xi^2/2, \tag{2.10a}$$

$$\varrho_0 := \rho, \qquad \varrho_{1,2,3} := \rho u_{x,y,z}, \qquad \varrho_4 := \rho(u^2 + d\vartheta)/2, \tag{2.10b}$$

where d is the dimension of the space $\boldsymbol{r} \in \mathbb{R}^d$, $u^2 := \boldsymbol{u}\cdot\boldsymbol{u}$, $\vartheta := k_\mathrm{B}T/m$, k_B is the Boltzmann constant and T is the temperature; so $\rho := \rho(\boldsymbol{r},\, t)$, $\boldsymbol{u} := \boldsymbol{u}(\boldsymbol{r},\, t)$, and $\vartheta := \vartheta(\boldsymbol{r},\, t)$ are the *local* hydrodynamic variables, *i.e.*, mass density, macroscopic velocity, and specific thermal energy, respectively.

The second consequence is that the solution of $Q[f,\, f] = 0$ is $f = f^{(0)}$, the renowned *local* Maxwell-Boltzmann equilibrium distribution function:

$$f^{(0)}(\rho,\, \boldsymbol{u},\, \vartheta) := \frac{\rho}{(2\pi\vartheta)^{d/2}} \exp\left[-\frac{(\boldsymbol{\xi}-\boldsymbol{u})\cdot(\boldsymbol{\xi}-\boldsymbol{u})}{2\vartheta}\right], \tag{2.11}$$

in which $\{\rho,\, \boldsymbol{u},\, \vartheta\}$ are the *local* hydrodynamic variables depending on $(\boldsymbol{r},\, t)$. Thus the equilibrium (2.11) is fully and uniquely defined by the quantities conserved by the collision operator in the system, *i.e.*, $\{\rho,\, \boldsymbol{u},\, \vartheta\}$.

The third, and perhaps the most profound, consequence is the H-theorem. Define

$$\bar{H}(t) := \int H(\boldsymbol{r},\, t)\,\mathrm{d}\boldsymbol{r}, \quad H(\boldsymbol{r},\, t) := \int f \ln f \,\mathrm{d}\boldsymbol{\xi}, \quad \boldsymbol{H}(\boldsymbol{r},\, t) := \int_\Omega \boldsymbol{\xi} f \ln f \,\mathrm{d}\boldsymbol{\xi}, \tag{2.12}$$

where Ω is the region in $\mathbb{R}^d$ containing the gas. For any f satisfying the Boltzmann equation (2.1a), H obeys the following equation:

$$\frac{\mathrm{d}H}{\mathrm{d}t} := \partial_t H + \nabla\cdot\boldsymbol{H} = \int Q[f,\, f]\ln f \,\mathrm{d}\boldsymbol{\xi} \le 0. \tag{2.13}$$

For $H(\boldsymbol{r},\, t)$ to exist, it is understood that f vanishes at $\boldsymbol{\xi} \to \infty$. Integrating (2.13) over Ω leads to [102]:

$$\frac{\mathrm{d}\bar{H}}{\mathrm{d}t} + \int_{\partial\Omega} (\boldsymbol{H} - H\boldsymbol{u}_\mathrm{s})\cdot\hat{\boldsymbol{n}}\mathrm{d}S \le 0, \tag{2.14}$$

where $\boldsymbol{u}_\mathrm{s}$ is the velocity of boundary $\partial\Omega$, and $\hat{\boldsymbol{n}}$ is the out-normal unit vector of the surface ∂V. Thus the H-theorem can be stated as follows (cf., *e.g.*, [102]). For spatially homogeneous systems, $\partial_{\boldsymbol{r}} f = 0$, hence $\partial_t H = 0$ according to (2.13), so H never increases in time, and the equality holds (for suitable regularity of f) if and only if $f = f^{(0)}$ is everywhere a *local* Maxwellian $f^{(0)}$ given by (2.11), in which $\{\rho,\, \boldsymbol{u},\, \vartheta\}$ may vary. Furthermore, for the spatially inhomogeneous systems, H will never increase only if

$$\int_{\partial\Omega} (\boldsymbol{H} - H\boldsymbol{u}_\mathrm{s})\cdot\hat{\boldsymbol{n}}\mathrm{d}S \ge 0. \tag{2.15}$$

The equality in (2.15) holds for the case when the molecules are specularly reflected at the boundary $\partial\Omega$. And again, the equality in (2.14) holds only if $f = f^{(0)}$ is everywhere a *local* Maxwellian $f^{(0)}$.

The H-theorem determines the direction of time, or the irreversibility, of a physical system, due to dissipation. In short, the Boltzmann equation (2.1a) encompasses the conservation laws and the irreversibility of the macroscopic hydrodynamics entirely.

2.2. Dimensionless Boltzmann equation

To analyze the Boltzmann equation (2.1a), relevant spatio-temporal scales in the system should be identified [104,106, 108]. The relevant microscopic spatio-temporal scales are the mean-free path ℓ and the mean-free time τ; and the relevant speed is a reference speed of sound: $c_{s0} := (\gamma\vartheta_0)^{1/2} = O(\ell/\tau)$, where ϑ_0 is a reference thermal energy per unit mass, and

$\gamma = 1 + 2/d$. Suppose L and τ_0 are the macroscopic characteristic spatial and temporal scales, respectively, and V_0 is the characteristic macroscopic flow speed.

The collision term $Q[f, f]$ defined in (2.1b) is of the dimension $n\varsigma^{d-1}V_0$, where ς is the effective particle radius (or effective interaction range) and n is the particle number density. In the thermodynamic limit of $N \to \infty$, $\varsigma \to 0$, and $m \to 0$, the Boltzmann-Grad limit (BGL) assumes that $N\varsigma^{d-1} \sim O(1)$ and $Nm \sim O(1)$, thus $\ell \sim 1/(n\varsigma^{d-1}) \sim O(1)$.

Using the following scalings:

$$\boldsymbol{r} \to \boldsymbol{r}/L, \quad t \to t/\tau_0, \quad \boldsymbol{\xi} \to \boldsymbol{\xi}/c_{s0}, \quad \boldsymbol{a} \to \boldsymbol{a}/G, \tag{2.16}$$

where G is a constant acceleration, and multiplying L/c_{s0} to both sides of (2.1a), we obtain the following dimensionless form of the Boltzmann equation:

$$\mathrm{St}\,\partial_t f + \boldsymbol{\xi}\cdot\boldsymbol{\partial}_{\boldsymbol{x}} f + \frac{\mathrm{Ma}^2}{\mathrm{Fr}^2}\boldsymbol{a}\cdot\boldsymbol{\partial}_{\boldsymbol{\xi}} f = \frac{1}{\mathrm{Kn}}Q[f, f], \tag{2.17}$$

where it has been assumed that $\ell \sim c_{s0}\tau$; $\mathrm{St} := L/\tau_0 c_{s0}$ is the kinetic Strouhal number, $\mathrm{Ma} := V_0/c_{s0}$ is the Mach number, $\mathrm{Fr} := V_0/\sqrt{LG}$ is the Froude number, and $\mathrm{Kn} := \ell/L$ is the Knudsen number. If indeed $V_0 \sim O(L/\tau_0)$, then $\mathrm{St} = \mathrm{Ma}$, and the dimensionless Boltzmann equation (2.17) reduces to the following:

$$\partial_t f + \frac{1}{\mathrm{Ma}}\boldsymbol{\xi}\cdot\boldsymbol{\partial}_{\boldsymbol{x}} f + \frac{\mathrm{Ma}}{\mathrm{Fr}^2}\boldsymbol{a}\cdot\boldsymbol{\partial}_{\boldsymbol{\xi}} f = \frac{1}{\mathrm{MaKn}}Q[f, f]. \tag{2.18}$$

One important task in kinetic theory is to derive hydrodynamic equations from the Boltzmann equation in some proper limits.

In hydrodynamic regimes, Kn is small by definition, *i.e.*, $\mathrm{Kn} \sim O(\varepsilon) \ll 1$, there are several hydrodynamic limits (cf., *e.g.*, [102,106,108]). First, with $\mathrm{Kn} = O(\varepsilon)$, the compressible Euler equations are obtained in the zeroth-order approximation of $f \approx f^{(0)}$; and with $\mathrm{Ma} = O(\varepsilon)$ and $\mathrm{Kn} = O(\varepsilon^2)$, the *incompressible* Euler equations are obtained. If $\mathrm{Ma} \sim \mathrm{Kn} = O(\varepsilon)$, considering $f \approx f^{(0)} + \varepsilon f^{(1)}$, the *incompressible* Navier-Stokes equations can be derived, and this is the so-called *diffusive* scaling. Finally, the *compressible* Navier-Stokes equations are obtained with $\mathrm{Ma} \sim O(1)$ and by considering the viscous correction of $f \approx f^{(0)} + \varepsilon f^{(1)}$, in the so-called *acoustic* scaling.

2.3. Hydrodynamic equations

The distribution function f can be characterized by its velocity moments:

$$\mathbf{M}^{(n)}(\boldsymbol{r}, t) := \int \mathrm{d}\boldsymbol{\xi}\, \boldsymbol{\Psi}^{(n)} f(\boldsymbol{r}, \boldsymbol{\xi}, t) := \left\langle \boldsymbol{\Psi}^{(n)} f \right\rangle, \tag{2.19}$$

where $\boldsymbol{\Psi}^{(n)} := \boldsymbol{\Psi}^{(n)}(\boldsymbol{\xi})$ is an n-th order tensorial polynomial of $\boldsymbol{\xi}$. The first few velocity moments of the distribution function, corresponding to the collisional invariants (cf. Sec. 2.1 and Eq. (2.9) in particular), are the familiar *macroscopic* variables in hydrodynamics:

$$\int \mathrm{d}\boldsymbol{\xi} \begin{pmatrix} 1 \\ \boldsymbol{\xi} \\ \frac{1}{2}\xi^2 \end{pmatrix} f(\boldsymbol{r}, \boldsymbol{\xi}, t) = \rho \begin{pmatrix} 1 \\ \boldsymbol{u} \\ \frac{1}{2}\left(u^2 + d\vartheta\right) \end{pmatrix}, \tag{2.20}$$

where $u^2 := \boldsymbol{u}\cdot\boldsymbol{u}$. The Boltzmann equation (2.1a) can be cast into an *infinite* hierarchy of moment equations:

$$\partial_t \mathbf{M}^{(n)} + \nabla\cdot\mathbf{M}^{(n+1)} = \left\langle Q\boldsymbol{\Psi}^{(n)} \right\rangle, \tag{2.21}$$

and the first few moment equations are the *macroscopic* conservation laws of mass, momentum, and energy:

$$\partial_t \rho + \rho\boldsymbol{u}\cdot\nabla\rho = -\rho\nabla\cdot\boldsymbol{u}, \tag{2.22a}$$

$$\rho\partial_t \boldsymbol{u} + \rho\boldsymbol{u}\cdot\nabla\boldsymbol{u} = -\nabla\cdot\boldsymbol{\Pi}, \qquad \boldsymbol{\Pi} := \langle f\boldsymbol{c}\boldsymbol{c}\rangle, \tag{2.22b}$$

$$\rho\partial_t e + \rho\boldsymbol{u}\cdot\nabla e = -\boldsymbol{\Pi} : \nabla\boldsymbol{u} - \nabla\cdot\boldsymbol{q}, \qquad \boldsymbol{q} := \frac{1}{2}\left\langle f\boldsymbol{c}c^2 \right\rangle, \tag{2.22c}$$

where $\boldsymbol{c} := \boldsymbol{\xi} - \boldsymbol{u}$ is the peculiar velocity, $e := d\vartheta/2$ is the specific total thermal energy, and the pressure tensor $\boldsymbol{\Pi}$ and the heat flux vector $\boldsymbol{q}$ in general cannot be expressed in terms of hydrodynamic variables $(\rho, \boldsymbol{u}, \vartheta)$ and thus are unknown unless f is given. Kinetic theory provides various *approximations* of f to obtain the pressure tensor $\boldsymbol{\Pi}$ and the heat flux $\boldsymbol{q}$, which are to be discussed next.

2.4. Solution methods of the Boltzmann equation

This section will provide brief outlines of three solution methods for the Boltzmann equation: the Hilbert expansion, the Chapman-Enskog expansion, and the moment methods due to Maxwell [112–114] and Grad later [109]. These methods are chosen to be mentioned because of their relevance to the lattice Boltzmann equation. In this section, the forcing term $\boldsymbol{a}\cdot\boldsymbol{\partial}_{\boldsymbol{\xi}} f$ shall be neglected unless otherwise stated.

2.4.1. The Hilbert expansion

There are several approaches to solve the Boltzmann equation. The first one is to seek the so-called *normal* solutions of the Boltzmann equation, of which the initial value problem is fully determined by certain non-singular initial values of the *hydrodynamic* variables $\{\rho, \boldsymbol{u}, \vartheta\}$. In the Hilbert expansion, f is expanded about the equilibrium $f^{(0)}$ as a power series in the Knudsen number $\mathrm{Kn} := \varepsilon$:

$$f = \sum_{n=0}^{\infty} \varepsilon^n f^{(n)}, \quad f^{(n)} := f^{(0)}\phi^{(n)}, \quad \phi^{(0)} = 1, \tag{2.23}$$

and the hydrodynamic variables are expanded as a power series of ε as well:

$$\varrho_i = \sum_{n=0}^{\infty} \varepsilon^n \varrho_i^{(n)}, \quad \varrho_i^{(n)} := \left\langle \varphi_i f^{(n)} \right\rangle, \ 0 \le i \le (d+1), \tag{2.24}$$

where $\{\varphi_i | 0 \le i \le d+1\}$ are collisional invariants defined in (2.10a). With the acoustic scaling, the Boltzmann equation (2.17) (with $\mathrm{St} = 1$ and without the forcing term) is expanded as a hierarchy of Fredholm integral equations for $f^{(n)}$:

$$Q[f^{(0)}, f^{(0)}] = 0, \qquad n = 0, \tag{2.25a}$$

$$2Q[f^{(n)}, f^{(0)}] = \mathrm{d}_t f^{(n-1)} - \sum_{k=1}^{n-1} Q[f^{(k)}, f^{(n-k)}], \qquad n \ge 1, \tag{2.25b}$$

where $\mathrm{d}_t := \partial_t + \boldsymbol{\xi}\cdot\nabla$, $f^{(n)} = 0$ if $n < 0$, and the sum $\sum_{k=1}^{n-1}$ is zero if $n < 1$, the collision term is re-written in the following bilinear form due to the symmetries of $B(\Theta, \boldsymbol{\xi}, \boldsymbol{\xi}_*)$ given in (2.2):

$$Q[f^{(n)}, f^{(k)}] := \frac{1}{2m} \int \mathrm{d}\boldsymbol{\xi}_* \mathrm{d}\Theta \mathrm{d}\epsilon \, B \left[f'^{(n)} f_*'^{(k)} + f'^{(k)} f_*'^{(n)} - f^{(n)} f_*^{(k)} - f^{(k)} f_*^{(n)} \right], \tag{2.26}$$

and in particular, $Q[f^{(n)}, f^{(0)}]$ is the linear operator $\mathcal{L}$ defined as the following:

$$f^{(0)}\mathcal{L}[\phi^{(n)}] := 2Q[f^{(0)}, f^{(n)}] = \frac{f^{(0)}}{m} \int \mathrm{d}\boldsymbol{\xi}_* \mathrm{d}\Theta \mathrm{d}\epsilon \, B \, f_*^{(0)} \left[\phi'^{(n)} + \phi_*'^{(n)} - \phi^{(n)} - \phi_*^{(n)} \right]. \tag{2.27}$$

Equations (2.25a) and (2.25b) are the homogeneous and inhomogeneous Fredholm equations of second kind (cf., *e.g.*, [115,116]), respectively, and they can be concisely written in one equation:

$$f^{(0)}\mathcal{L}[\phi^{(n)}] = \mathrm{d}_t f^{(n-1)} - \mathcal{S}^{(n-1)}, \quad \mathcal{S}^{(n-1)} := \sum_{k=1}^{n-1} Q[f^{(k)}, f^{(n-k)}]. \tag{2.28}$$

For $n = 0$, the solution of the homogeneous equation $Q[f^{(0)}, f^{(0)}] = 0$ is the Maxwellian $f^{(0)}(\rho^{(0)}, \boldsymbol{u}^{(0)}, \vartheta^{(0)})$. For $n \ge 1$, the only unknown in Eq. (2.28) is $\phi^{(n)}$ on the left-hand side, and the source terms $\mathrm{d}_t f^{(n-1)}$ and $\mathcal{S}^{(n-1)}$ on the right-hand side involve only $f^{(k)}$ for $k \le n-1$, which have been obtained in previous orders. Thus, Eq. (2.28) is solved successively.

The solution of the inhomogeneous equation (2.28) consists of two parts: the general solution of the homogeneous equation $f^{(0)}\mathcal{L}[\phi^{(n)}] = 0$, which is $\phi_0^{(n)} = \sum_{i=0}^{d+1} \gamma_i^{(n)}(\boldsymbol{r}, t)\varphi_i(\boldsymbol{\xi})$, and the particular solution $\phi_p^{(n)}$ of the inhomogeneous equation, which must be orthogonal to the general solution (the Fredholm solubility condition). Because $\{\varphi_i\}$ are the collisional invariants, $\langle \varphi_i Q[f^{(k)}, f^{(n-k)}] \rangle = 0$ is always satisfied, so the Fredholm solubility condition for (2.25b) reduces to $\langle \varphi_i \mathrm{d}_t f^{(n-1)} \rangle = 0$ for $0 \le i \le (d-1)$, which leads to the following equations:

$$\partial_t \varrho_i^{(n-1)} + \nabla\cdot\boldsymbol{j}_i^{(n-1)} = 0, \quad \varrho_i^{(n)} := \langle \varphi_i f^{(n)} \rangle, \ \boldsymbol{j}_i^{(n)} := \langle \boldsymbol{\xi}\varphi_i f^{(n)} \rangle. \tag{2.29}$$

The above equations are the evolution equations for the coefficients $\{\gamma_i^{(n)}(\boldsymbol{r}, t)\}$, with the initial values of $\{\varrho_i\}$ given. The infinite sum of the above equations is the compressible Euler equations for $\{\rho, \boldsymbol{u}, \vartheta\}$ with $\boldsymbol{\Pi} = p\mathbf{I}$, where $p := \rho\vartheta$ is the ideal-gas equation of state and $\mathbf{I}$ is the $d \times d$ identity matrix, and $\boldsymbol{q} = \mathbf{0}$.

The convergence of the Hilbert expansion establishes Hilbert's theorem that the evolution of $f(\boldsymbol{r}, \boldsymbol{\xi}, t)$ is uniquely determined by the initial values of only five hydrodynamic moments $\{\varrho_i(\boldsymbol{r}, t)\}$. However, the Hilbert expansion cannot be used to derive the Navier-Stokes equation, because Eq. (2.28) gives the linearized Euler equation, usually inhomogeneous, and the second-order spatial derivative for the viscous stress in the Navier-Stokes equation will never appear, as can be seen in Eq. (2.29)

2.4.2. The Chapman-Enskog expansion

The Chapman-Enskog (C-E) method is the device to derive the Navier-Stokes equations [99,103,106,109,117]. The key idea behind the C-E method is to expand the fluxes $\langle \boldsymbol{\xi}\varphi_i f\rangle$ which are non-conserved quantities, while leaving the hydrodynamic or conserved quantities unexpanded, *i.e.*,

$$\varrho_i = \langle \varphi_i f\rangle = \left\langle \varphi_i f^{(0)}\right\rangle. \tag{2.30}$$

The C-E *ansatz* assumes that the spatio-temporal dependence of f is only through a *functional* dependence on the hydrodynamic variables and their spatial derivatives:

$$f(\boldsymbol{r},\,\boldsymbol{\xi},\,t) = f(\boldsymbol{\xi};\,\rho,\,\boldsymbol{u},\,\vartheta) \implies \frac{\partial f}{\partial t} = \sum_{k=0}^{\infty}\sum_{i=0}^{d+1}\frac{\partial f}{\partial(\nabla^k\varrho_i)}\cdot\frac{\partial(\nabla^k\varrho_i)}{\partial t}, \tag{2.31}$$

this implies that the time t has to be expanded implicitly through the expansion of the operator ∂_t. This is accomplished by expanding the equations for the hydrodynamic variables to introduce the operator $\partial^{(n)}/\partial t$ on $\{\rho,\,\boldsymbol{u},\,\vartheta\}$ as the following:

$$\frac{\partial^{(0)}\rho}{\partial t} = -\nabla\cdot(\boldsymbol{u}\rho), \qquad \frac{\partial^{(n)}\rho}{\partial t} = 0, \qquad n\geq 1, \tag{2.32a}$$

$$\frac{\partial^{(0)}\boldsymbol{u}}{\partial t} = -\boldsymbol{u}\cdot\nabla\boldsymbol{u} - \frac{1}{\rho}\nabla\cdot\boldsymbol{\Pi}^{(0)}, \qquad \frac{\partial^{(n)}\boldsymbol{u}}{\partial t} = -\frac{1}{\rho}\nabla\cdot\boldsymbol{\Pi}^{(n)}, \qquad n\geq 1, \tag{2.32b}$$

$$\frac{\partial^{(0)}\vartheta}{\partial t} = -\boldsymbol{u}\cdot\nabla\vartheta - \frac{2}{3\rho}\left(\boldsymbol{\Pi}^{(0)}:\nabla\boldsymbol{u} + \nabla\cdot\boldsymbol{q}^{(0)}\right), \qquad \frac{\partial^{(n)}\vartheta}{\partial t} = -\frac{2}{3\rho}\left(\boldsymbol{\Pi}^{(n)}:\nabla\boldsymbol{u} + \nabla\cdot\boldsymbol{q}^{(n)}\right), \qquad n\geq 1, \tag{2.32c}$$

where both the pressure tensor $\boldsymbol{\Pi}$ and the heat flux $\boldsymbol{q}$ are expanded as series of ε:

$$\boldsymbol{\Pi} = \textstyle\sum_{n=0}^{\infty}\varepsilon^n\boldsymbol{\Pi}^{(n)}, \qquad \boldsymbol{\Pi}^{(n)} := \left\langle f^{(n)}\boldsymbol{c}\boldsymbol{c}\right\rangle, \tag{2.33a}$$

$$\boldsymbol{q} = \textstyle\sum_{n=0}^{\infty}\varepsilon^n\boldsymbol{q}^{(n)}, \qquad \boldsymbol{q}^{(n)} := \frac{1}{2}\left\langle f^{(n)}\boldsymbol{c}c^2\right\rangle. \tag{2.33b}$$

With the expansion of f defined by (2.23), $\partial^{(n)}/\partial t$ by (2.32), and $\boldsymbol{\Pi}^{(n)}$ and $\boldsymbol{q}^{(n)}$ by (2.33), $\partial f/\partial t$ can be recast in the following expansion of multiple time scales:

$$\frac{\partial f}{\partial t} = \sum_{n=0}^{\infty}\varepsilon^n\sum_{m=0}^{n}\frac{\partial^{(m)}}{\partial t}\left(\rho\frac{\partial}{\partial\rho} + \boldsymbol{u}\cdot\frac{\partial}{\partial\boldsymbol{u}} + \vartheta\frac{\partial}{\partial\vartheta}\right)f^{(n-m)} := \sum_{n=0}^{\infty}\varepsilon^n\frac{\partial^{(n)}f}{\partial t}. \tag{2.34}$$

Consequently, one obtains a hierarchy of Fredholm integral equations identical to Eqs. (2.25) in form, except that the term $\mathrm{d}_t f^{(n)}$ in (2.25b) is replaced by:

$$\mathrm{d}_t^{(n)}f := \partial_t^{(n)}f + \boldsymbol{\xi}\cdot\nabla f^{(n)} = \sum_{m=0}^{n}\frac{\partial^{(m)}}{\partial t}\left(\rho\frac{\partial}{\partial\rho} + \boldsymbol{u}\cdot\frac{\partial}{\partial\boldsymbol{u}} + \vartheta\frac{\partial}{\partial\vartheta}\right)f^{(n-m)} + \boldsymbol{\xi}\cdot\nabla f^{(n)}. \tag{2.35}$$

The uniqueness of the solutions of the inhomogeneous integral equation requires the following solubility condition:

$$\left\langle\varphi_i f^{(n)}\right\rangle = 0,\ n\geq 1,\ 0\leq i\leq(d+1), \tag{2.36}$$

which is equivalent to, and implies, (2.30), then the Fredholm orthogonal condition $\left\langle\varphi_i\mathrm{d}_t^{(n)}f\right\rangle = 0$ is

$$\sum_{m=0}^{n}\frac{\partial^{(m)}}{\partial t}\left(\rho\frac{\partial}{\partial\rho} + \boldsymbol{u}\cdot\frac{\partial}{\partial\boldsymbol{u}} + \vartheta\frac{\partial}{\partial\vartheta}\right)\left\langle\varphi_i f^{(n-m)}\right\rangle + \nabla\cdot\left\langle\boldsymbol{\xi}\varphi_i f^{(n)}\right\rangle = 0. \tag{2.37}$$

The only non-zero term in the sum of (2.37) is for $m=n$, thus the orthogonal condition is nothing more than the definition of $\partial_t^{(n)}\varrho_i$ given in Eqs. (2.32). Therefore, not only the deviation from the equilibrium as a whole, but also the non-equilibrium distribution function $f^{(n)}$ at each given order $n\geq 1$ has no contribution to the hydrodynamic variables $\{\rho,\,\rho\boldsymbol{u},\,\vartheta\}$, as required by the Fredholm solubility condition, but they do contribute to the fluxes.

For $n=0$ the homogeneous integral equation (2.25a) leads to the equilibrium of *local* Maxwellian $f^{(0)}(\rho,\,\boldsymbol{u},\,\vartheta)$, in which the hydrodynamic variables $\{\rho,\,\boldsymbol{u},\,\vartheta\}$ are *exact* in the sense that they are unexpanded; and the solubility condition $\langle\varphi_i(\mathrm{d}^{(0)}f^{(0)}/\mathrm{d}t)\rangle = 0$ yields the *compressible Euler equations* for an ideal gas with $\boldsymbol{\Pi}^{(0)} = p\mathbf{I}$, $p=\rho\vartheta$, and $\boldsymbol{q}^{(0)} = \mathbf{0}$.

For $n=1$, the solution $\phi^{(1)} := f^{(1)}/f^{(0)}$ obtained with the Chapman-Enskog analysis is

$$\phi^{(1)}(\boldsymbol{\xi}) = \frac{1}{\rho}\left[\sqrt{2\vartheta}\boldsymbol{A}\cdot\nabla\ln\vartheta + \mathbf{B}:\nabla\boldsymbol{u}\right], \tag{2.38a}$$

$$\mathcal{L}(\boldsymbol{A}) = \rho\left(\bar{\boldsymbol{c}}\cdot\bar{\boldsymbol{c}} - \frac{d+2}{2}\right)\bar{\boldsymbol{c}}, \quad \boldsymbol{A} = A(\vartheta,\bar{\boldsymbol{c}})\bar{\boldsymbol{c}}, \tag{2.38b}$$

$$\mathcal{L}(\mathbf{B}) = 2\rho\widehat{\mathbf{C}}, \qquad \mathbf{B} = B(\vartheta,\bar{\boldsymbol{c}})\widehat{\mathbf{C}}, \quad \widehat{\mathbf{C}} := \bar{\boldsymbol{c}}\bar{\boldsymbol{c}} - \frac{1}{d}\bar{c}^2\mathbf{I}, \tag{2.38c}$$

where $\bar{\boldsymbol{c}} := \boldsymbol{c}/\sqrt{\vartheta}$. Note that $B(\vartheta,\bar{\boldsymbol{c}})$ here in (2.38c) is not the collision kernel. The result of $\phi^{(1)}$ given by (2.38a) leads to

$$\boldsymbol{\Pi}^{(1)} = -2\mu\widehat{\boldsymbol{\Sigma}} := -\widehat{\boldsymbol{\sigma}}, \qquad \widehat{\boldsymbol{\Sigma}} := \boldsymbol{\Sigma} - \frac{1}{d}(\nabla\cdot\boldsymbol{u})\mathbf{I}, \qquad \boldsymbol{\Sigma} := \frac{1}{2}\left[(\nabla\boldsymbol{u}) + (\nabla\boldsymbol{u})^{\dagger}\right], \tag{2.39a}$$

$$\boldsymbol{q}^{(1)} = -\kappa\nabla\vartheta, \tag{2.39b}$$

where $\dagger$ denotes the transpose, $\widehat{\boldsymbol{\sigma}}$ is the traceless part of the shear stress tensor $\boldsymbol{\sigma}$, $\boldsymbol{\Sigma}$ is the rate of strain tensor, $\widehat{\boldsymbol{\Sigma}}$ is the traceless part of $\boldsymbol{\Sigma}$, and the dynamic viscosity μ and the heat diffusivity κ are given by $B(\vartheta,\bar{\boldsymbol{c}})$ and $A(\vartheta,\bar{\boldsymbol{c}})$ given by (2.38c) and (2.38b), respectively:

$$\mu = -\frac{\vartheta}{5\rho^2}\int \mathrm{d}\boldsymbol{\xi}\, f^{(0)}\,\mathbf{B}:\mathcal{L}(\mathbf{B}) = -\frac{2\vartheta}{5\rho}\int \mathrm{d}\bar{\boldsymbol{c}}\, f^{(0)}\, B(\vartheta,\bar{\boldsymbol{c}})\widehat{\mathbf{C}}:\widehat{\mathbf{C}}, \tag{2.40a}$$

$$\kappa = -\frac{2\vartheta}{3\rho^2}\int \mathrm{d}\boldsymbol{\xi}\, f^{(0)}\,\boldsymbol{A}\cdot\mathcal{L}(\boldsymbol{A}) = -\frac{2\vartheta}{3\rho}\int \mathrm{d}\bar{\boldsymbol{c}}\, f^{(0)}\, A(\vartheta,\bar{\boldsymbol{c}})\left[\bar{\boldsymbol{c}}\cdot\bar{\boldsymbol{c}} - \frac{d+2}{2}\right]\bar{\boldsymbol{c}}\cdot\bar{\boldsymbol{c}}, \tag{2.40b}$$

where $A(\vartheta,\bar{\boldsymbol{c}})$ and $B(\vartheta,\bar{\boldsymbol{c}})$ are defined by (2.38b) and (2.38c), respectively. Beyond the compressible Navier-Stokes-Fourier (NSF) system, the Chapman-Enskog analysis can also lead to the Burnett and super-Burnett equations (cf., *e.g.*, [102,109]), however, these higher-order systems are ill-posed and they are beyond the scope of this review.

It is useful to introduce the Reynolds number $\mathrm{Re} := V_0 L/\nu$ and its relation to Kn and Ma. Since the kinematic (shear) viscosity is $\nu := \mu/\rho \sim \ell c_s$ and $c_s = \sqrt{\gamma\vartheta}$, then

$$\mathrm{Kn} := \frac{\ell}{L} \sim \frac{\nu}{L c_s} \sim \frac{\nu}{L V_0}\frac{V_0}{c_s} \sim \frac{\mathrm{Ma}}{\mathrm{Re}}. \tag{2.41}$$

The above relationship is also known as the von Kármán relationship, which can also be independently derived from the dimensional analysis of the viscous term of the Navier-Stokes equation. If $\mathrm{Kn} \sim \mathrm{Ma} \sim O(\varepsilon)$ and $\mathrm{Re} \sim O(1)$, the incompressible Navier-Stokes equations are invariant under the following *diffusive* scaling:

$$(\boldsymbol{r},\, t,\, \boldsymbol{u},\, p) \longrightarrow (\varepsilon\boldsymbol{r},\, \varepsilon^2 t,\, \varepsilon^{-1}\boldsymbol{u},\, \varepsilon^{-2}p), \tag{2.42}$$

where p is the pressure. Consequently, $\mathrm{Fr} \sim O(\mathrm{Ma}^2) = O(\varepsilon^2)$ with this scaling, which will be used later in Sec. 3.

2.4.3. Moment methods

With the Chapman-Enskog approach, it is difficult, if possible at all, to derive equations beyond the order of the super-Burnett equations, *i.e.*, $f^{(3)}$, unless the collision term is simplified. An alternative approach, the method of moments, is considered to obtain the *non-normal* solutions. It was Maxwell who first realized that the r^{-5} force law eliminates the dependence of the collision cross section $\sigma(\chi, V)$ or the collision kernel $B(\Theta, \boldsymbol{\xi}, \boldsymbol{\xi}_*)$ on the relative speed $V := |\boldsymbol{\xi} - \boldsymbol{\xi}_*|$ [101,112–114]. Consequently the hierarchical equations of moments (2.21) are drastically simplified, because the moment of the collision term, $\left\langle \boldsymbol{\Psi}^{(n)} Q \right\rangle$, does *not* generate moments of order higher than n, so the equations are not closed only due to the advection term $\nabla\cdot\mathbf{M}^{(n+1)}$. Maxwell devised an iterative procedure to solve the moment equations for $\boldsymbol{\Psi}^{(n)} = \boldsymbol{c}^n$, starting with vanishing collision term for moments of the order 2 or higher, *i.e.*, $\langle \boldsymbol{c}^n Q\rangle = \mathbf{0}\ \forall n \geq 2$, which leads to the local equilibrium $f^{(0)}$, and then proceeding with

$$\left\langle \boldsymbol{c}^n\left[\partial_t f + \nabla\cdot(\boldsymbol{c}+\boldsymbol{u})f\right]\right\rangle^{[k+1]} = \left\langle \boldsymbol{c}^n Q\right\rangle^{[k]}, \tag{2.43}$$

where the superscript $[k]$ indicates the iteration of order k. For the Maxwell molecules of the r^{-5} force law, both $\boldsymbol{\Pi}^{(1)}$ and $\boldsymbol{q}^{(1)}$ are identical to that obtained by the Chapman-Enskog expansion, but the higher-order results differ.

Grad proposed to expand the distribution function in terms of the tensorial Hermite orthogonal polynomials $\mathbf{H}^{(n)}(\bar{\boldsymbol{c}})$ [109,118–120] defined as the following:

$$\mathbf{H}^{(n)}(\bar{\boldsymbol{c}}) = (-1)^n\frac{\nabla_{\bar{\boldsymbol{c}}}^n\omega(\bar{\boldsymbol{c}})}{\omega(\bar{\boldsymbol{c}})}, \quad \omega(\bar{\boldsymbol{c}}) := \frac{\exp(-\bar{\boldsymbol{c}}\cdot\bar{\boldsymbol{c}}/2)}{(2\pi)^{3/2}}, \tag{2.44}$$

or the recurrence relation

$$\mathbf{H}^{(n)}(\bar{\boldsymbol{c}}) = (\bar{\boldsymbol{c}} - \nabla_{\bar{\boldsymbol{c}}})\,\mathbf{H}^{(n-1)}(\bar{\boldsymbol{c}}), \tag{2.45}$$

and the first few tensorial Hermite polynomials are:

$$\mathbf{H}^{(0)} = 1,\ \mathbf{H}^{(1)} = \bar{\boldsymbol{c}},\ \mathbf{H}^{(2)} = \bar{\boldsymbol{c}}\bar{\boldsymbol{c}} - \mathbf{I},\ H^{(3)}_{ijk} = \bar{c}_i\bar{c}_j\bar{c}_k - (\bar{c}_i\delta_{jk} + \bar{c}_j\delta_{ki} + \bar{c}_k\delta_{ij}). \tag{2.46}$$

The distribution function f is expanded in terms of $\mathbf{H}^{(n)}(\bar{\boldsymbol{c}})$ as the following:

$$f = f^{(0)}\sum_{n=0}^{\infty}\frac{1}{n!}\mathbf{a}^{(n)}(\boldsymbol{r},\,t) : \mathbf{H}^{(n)}(\bar{\boldsymbol{c}}), \tag{2.47a}$$

$$\mathbf{a}^{(0)} = 1, \quad \mathbf{a}^{(1)} = \mathbf{0}, \quad \mathbf{a}^{(2)} = \frac{1}{p}\boldsymbol{\Pi} - \mathbf{I} := \frac{1}{p}\mathbf{p}, \quad \mathbf{a}^{(3)} = \frac{\langle f\boldsymbol{c}^3\rangle}{p\sqrt{\vartheta}},\ \ldots, \tag{2.47b}$$

where $p = \rho\vartheta$, thus the Boltzmann equation becomes a hierarchy of equations for the expansion coefficients $\{\mathbf{a}^{(n)}|n \geq 0\}$, which are the moments of f with respect to the Hermite polynomials $\{\mathbf{H}^{(n)}\}$. A closure of order n for $\{\mathbf{a}^{(k)}|0 \leq k \leq n\}$ is attained by truncating the expansion (2.47a) to n-th order and omitting $\nabla\cdot\mathbf{a}^{(n+1)}$ in the equation of $\mathbf{a}^{(n)}$. With $n = 3$ and retaining only the heat flux vector $\boldsymbol{q} = \mathbf{a}^{(3)}_{\alpha\beta\beta}/2$, where $\alpha,\,\beta \in \{x,\,y,\,z\}$ and the repeated indices imply summation, instead of the full $\mathbf{a}^{(3)}$ tensor, the distribution function is approximated by

$$f = f^{(0)}\left[1 + \frac{\bar{\mathbf{p}} : \bar{\boldsymbol{c}}\bar{\boldsymbol{c}}}{2} + \frac{\bar{\boldsymbol{q}}\cdot\bar{\boldsymbol{c}}}{2}\left(1 - \frac{\bar{\boldsymbol{c}}\cdot\bar{\boldsymbol{c}}}{(d+2)}\right)\right], \quad \bar{\mathbf{p}} := \frac{\mathbf{p}}{p}, \quad \bar{\boldsymbol{q}} := \frac{\boldsymbol{q}}{p\sqrt{\vartheta}}. \tag{2.48}$$

This is the renowned thirteen-moment system of Grad [119], which includes the evolution equations for $\boldsymbol{\Pi}$ and $\boldsymbol{q}$ and is beyond the Navier-Stokes-Fourier system. It should be pointed out that Grad's 13-moment system is not hyperbolic globally [121,122], thus becomes ill-posed as an initial value problem when it loses hyperbolicity, and this problem has only been solved recently [122–125].

2.5. Linearized model equations

The collision term in the Boltzmann equation (2.1a) is a nonlinear integral Q in $d+2$ dimensional space (cf. the definition of $Q[f,\,f_*]$ in (2.1a)). To make the solution of the Boltzmann equation more manageable, the collision term is often linearized based on the practical consideration that most flows may not be too far from the equilibrium. Perhaps the most general model equation based on the linearized collision term is that of Gross and Jackson [126].

Consider the linear operator $\mathcal{L}$ (cf. Eqs. (2.26) and (2.27)), the linearized Boltzmann equation is:

$$\partial_t f + \boldsymbol{\xi}\cdot\boldsymbol{\partial}_{\boldsymbol{x}} f = f^{(0)}\mathcal{L}[\phi] - \boldsymbol{a}\cdot\boldsymbol{\partial}_{\boldsymbol{\xi}} f, \quad f := f^{(0)}(1+\phi). \tag{2.49}$$

Denote $\mathcal{L}_{\mathrm{M}}$ the linearized collision operator for Maxwell molecules with eigenfunctions $\{\varphi_i\}$ and the corresponding eigenvalues $\{\lambda_i\}$, thus ϕ can be expanded in terms of $\{\varphi_i\}$:

$$\phi = \sum_{i=1}^{\infty}\alpha_i\varphi_i, \quad \mathcal{L}_{\mathrm{M}}[\phi] = \sum_{i=1}^{\infty}\alpha_i\lambda_i\varphi_i, \tag{2.50}$$

where $\{\varphi_i\}$ are orthogonal with respect to the Maxwellian equilibrium $f^{(0)}$. The linearized collision operator $\mathcal{L}_{\mathrm{M}}$ can be approximated by the Gross-Jackson model [126] which replaces the eigenvalues λ_i for $i \geq N$ by a constant λ_N, leaving only a finite number, N, of distinctive eigenvalues, *i.e.*,

$$\begin{aligned}\mathcal{L}_N[\phi] &:= \sum_{i=0}^{N-1}\alpha_i\lambda_i\varphi_i - \lambda_N\sum_{i=N}^{\infty}\alpha_i\varphi_i = \sum_{i=0}^{N-1}\alpha_i(\lambda_i+\lambda_N)\varphi_i - \lambda_N\phi \\ &= \left[\sum_{i=0}^{N-1}\alpha_i(\lambda_i+\lambda_N)\varphi_i + \lambda_N\right] - \lambda_N(1+\phi) := \mathcal{J}_N - \lambda_N(1+\phi),\end{aligned} \tag{2.51}$$

where $\mathcal{L}_N$ is also called the mutilated linearized operator. The first $d+2$ eigenfunctions are the collisional invariants, *i.e.*, $\lambda_i = 0$ for $0 \leq i \leq d+1$. Hence, by choosing $N = d+2$ leaves only one free parameter in $\mathcal{L}_N$, which is the renowned single-relaxation time model due to Bhatnagar, Gross, and Krook (BGK) [127]; and with $N = (d+2)+1$, there are two distinctive eigenvalues (or relaxation rates) λ_i, the Gross-Jackson model reduces to that of Shakhov [128], in which both shear viscosity and the heat diffusivity can be independently adjusted. The Gross-Jackson model has been generalized for arbitrary inter-particle potentials [129].

2.6. Kinetic boundary conditions

The Boltzmann equation must be supplemented with appropriate boundary conditions, which describe the particle-wall interaction in the presence of a solid wall. The particle-wall interaction is described by the kernel $B_{\rm w}(\boldsymbol{\xi}', \boldsymbol{\xi}, \boldsymbol{r})$ which is the probability that a particle with incident velocity $\boldsymbol{\xi}'$ which strikes the wall at $\boldsymbol{r}$ will emerge with velocity $\boldsymbol{\xi}$ at $\boldsymbol{r}$. The simplest models for the boundary conditions are the bounce-back and specular reflections. The former implies velocity at the wall vanishes with respect to the wall velocity $\boldsymbol{u}_{\rm w}$, and the latter imposes the reflection symmetry about the normal of the boundary plane, which ensures that the velocity component normal to the wall vanishes at the wall at rest.

Perhaps the most widely used boundary conditions in kinetic theory are the Maxwell diffusive reflection model, which assumes that the particles striking a boundary are completely thermalized by the wall with the velocity $\boldsymbol{u}_{\rm w}$ and temperature $T_{\rm w}$ (accommodation effect). Slightly more general boundary conditions are to consider that a fraction α of the particles is diffusively deflected, while the remaining fraction $(1-\alpha)$ is specularly reflected, such that

$$B_{\rm w}(\boldsymbol{\xi}', \boldsymbol{\xi}, \boldsymbol{r}) = (1-\alpha)\delta(\boldsymbol{\xi}' - \boldsymbol{\xi} + 2\hat{\boldsymbol{n}}(\hat{\boldsymbol{n}}\cdot\boldsymbol{\xi})) + \alpha(\hat{\boldsymbol{n}}\cdot\boldsymbol{\xi}) f^{(0)}(\rho_{\rm w}, \boldsymbol{u}_{\rm w}, T_{\rm w}), \tag{2.52}$$

where $\delta(\cdot)$ is the Dirac delta function, and $\hat{\boldsymbol{n}}$ is the out-normal unit vector at the collision point of the wall such that $\boldsymbol{\xi}'\cdot\hat{\boldsymbol{n}} < 0$ and $\boldsymbol{\xi}\cdot\hat{\boldsymbol{n}} > 0$, and $f^{(0)}(\rho_{\rm w}, \boldsymbol{u}_{\rm w}, T_{\rm w})$ is the Maxwellian equilibrium defined in (2.11), *i.e.*, the *wall equilibrium*. Also,

$$(\hat{\boldsymbol{n}}\cdot\boldsymbol{\xi}) f(\boldsymbol{\xi}) = -\int\limits_{\hat{\boldsymbol{n}}\cdot\boldsymbol{\xi}'\le 0} (\hat{\boldsymbol{n}}\cdot\boldsymbol{\xi}') f(\boldsymbol{\xi}') B_w(\boldsymbol{\xi}', \boldsymbol{\xi}, \boldsymbol{r}) d\boldsymbol{\xi}'. \tag{2.53}$$

The normalization condition of $B_{\rm w}(\boldsymbol{\xi}', \boldsymbol{\xi}, \boldsymbol{r})$,

$$\int\limits_{\boldsymbol{\xi}\cdot\hat{\boldsymbol{n}}>0} B_{\rm w}(\boldsymbol{\xi}', \boldsymbol{\xi}, \boldsymbol{r})\, {\rm d}\boldsymbol{\xi} = 1, \tag{2.54}$$

leads to $\rho_{\rm w} = \sqrt{2\pi/RT_{\rm w}}$, where R is the gas constant. The parameter α in (2.52) is the so-called (momentum) accommodation coefficient. The cases of $\alpha = 1$ and $\alpha = 0$ correspond to total diffusive deflection and total specular reflection, respectively. One deficiency of the Maxwell boundary conditions (2.52) is that they do not distinguish the accommodation effects of momentum and energy, nor that between the tangential and normal momentum, which may be different [102,130,131].

In closing this very brief discourse on the Boltzmann equation and kinetic theory, we would like to remark that, while in principle the Boltzmann equation was constructed for rarefied gases in which the correlations are neglected (*stosszahlansatz*), nonetheless, it can be extended to more complicated fluid systems. For dense gases, the Enskog equation is a natural extension [99–101], and for particles with internal structures, the generalizations include the Boltzmann-Curtiss model and its quantum counterpart, the Wang Chang-Uhlenbeck model (cf. [102, §II.4] for a brief discussion and [132]). There exists also kinetic theory for complex fluids such as polymers [133,134]. However, it should be noted that the kinetic theory of polymers [133,134] differs from the kinetic theory of gases. In the case of polymers, the Stokes hydrodynamic equations are given, and a distribution of bead and spring objects suspended in such a fluid is considered. In addition, kinetic theory can be used to derive the equations of state and transport coefficients for dense gases or more complex fluids, which are to be used in continuum theory. Most importantly, kinetic theory serves as the bridge between macroscopic continuum theory and underlying microscopic physics, and forms the basis of coarse-grained models.

3. The lattice Boltzmann equation

This section summarizes key mathematical properties and features of the lattice Boltzmann equation: The first is about the explicit connection between the LBE and the continuous Boltzmann equation with a linearized collision model, including the low-Mach number expansion of the distribution function discussed in Sec. 3.1, the coherent discretization of phase-space and time which is unique to the LBE in Sec. 3.2, Sec. 3.3, and Sec. 3.4, and the construction of the collision models based on moments of the distribution function in Sec. 3.5. The second part concerns the numerical efficiency related to the over-relaxation feature of the LBE in Sec. 3.6. The LBE model for one conserved scalar, *i.e.*, the LBE model for the advection-diffusion equation, and the LBE models for thermal flows are discussed in Sec. 3.7 and Sec. 3.8, respectively. And finally, the third part deals with the LBE model based on the cumulants, as opposed to moments, of the distribution function and some recent developments in Sec. 3.9 and Sec. 3.10, respectively.

We should start with a mathematical description of the LBE first. The lattice Boltzmann equation comprises three ingredients:

(a) A symmetric discrete velocity set $\mathbb{X}_q := \{\boldsymbol{\xi}_i \in \mathbb{Z}^d | 0 \le i \le (q-1)\} = -\mathbb{X}_q$, and the corresponding set of distribution functions on a d dimensional lattice $\delta_x\mathbb{Z}_d$ of a lattice spacing δ_x and with a discrete time $t_n := n\delta_t$ of a time step size δ_t, $n \in \mathbb{N}_0$, *i.e.*, $\{f_i(\boldsymbol{x}_j, t_n) | f_i : \delta_x\mathbb{Z}_d \times \delta_t\mathbb{N}_0 \mapsto \mathbb{R}\}$;

(b) A *local* collision process $Q_i[\{f_k(\boldsymbol{x}_j, t_n)|\forall k\}]$ which respects necessary conservation laws;
(c) And finally an evolution equation:

$$f_i(\boldsymbol{x}_j + \boldsymbol{\xi}_i\delta_t, t_n + \delta_t) = f_i(\boldsymbol{x}_j, t_n) + Q_i[\{f_k(\boldsymbol{x}_j, t_n)|\forall k\}] + G_i, \tag{3.1}$$

where G_i comes from an external forcing.

What is special about the LBE is that the lattice space $\delta_x\mathbb{Z}_d$, the discrete velocity set $\mathbb{X}_q$, and the discrete time step size δ_t are tied together such that

$$\boldsymbol{x}_j + \boldsymbol{\xi}_i\delta_t \in \delta_x\mathbb{Z}_d, \quad \forall\, \boldsymbol{x}_j \in \delta_x\mathbb{Z}_d \text{ and } \forall\, \boldsymbol{\xi}_i \in \mathbb{X}_q. \tag{3.2}$$

In the remainder of this section, the lattice Boltzmann equation (3.1) will be directly derived from the linearized Boltzmann equation.

As will be shown later, the discrete velocity set $\mathbb{X}_q = \{\boldsymbol{\xi}_i|0 \le i \le (q-1)\}$ in the LBE is symmetric by construction, *i.e.*, $\mathbb{X}_q = -\mathbb{X}_q$, therefore,

$$\textstyle\sum_i \boldsymbol{\xi}_i^{2k+1} = \sum_i (\boldsymbol{\xi}_i\boldsymbol{\xi}_i)^k\boldsymbol{\xi}_i = \mathbf{0}.$$

This property of $\mathbb{X}_q$ is related to an expansion of the distribution function around $\boldsymbol{u} = \mathbf{0}$, as employed below. It will also be shown that for each discrete velocity $\boldsymbol{\xi}_i$, there is a corresponding quadrature weight coefficient w_i satisfying the following normalization condition:

$$\textstyle\sum_i w_i = 1. \tag{3.3}$$

3.1. Truncated expansions of distributions and linearized collision term

Two essential steps are required to derive the LBE from the Boltzmann equation with a linearized collision term (2.49). The first is the truncation of the distribution functions $f^{(0)}$ (cf. (2.11)) and f expanded in terms of the Hermite polynomials (cf. Sec. 2.4.3), which is equivalent to the low-Mach-number expansion, and the second is a *coherent* discretization of the phase space $\mathbb{\Gamma} := (\boldsymbol{r}, \boldsymbol{\xi})$ and the time t.

The first step is straightforward. The expansions of $f^{(0)}$ and f in terms of the tensor Hermite polynomials $\{\mathbf{H}^{(n)}\}$ are:

$$f^{(0)} = \rho\frac{e^{-\bar{\boldsymbol{\xi}}\cdot\bar{\boldsymbol{\xi}}/2}}{(2\pi\vartheta)^{d/2}}\sum_{n=0}^{\infty}\frac{1}{n!}\bar{\boldsymbol{u}}^n : \mathbf{H}^{(n)}(\bar{\boldsymbol{\xi}}), \quad \bar{\boldsymbol{u}}^n := \underbrace{\bar{\boldsymbol{u}}\bar{\boldsymbol{u}}\cdots\bar{\boldsymbol{u}}}_{n}, \tag{3.4a}$$

$$f = \rho\frac{e^{-\bar{\boldsymbol{\xi}}\cdot\bar{\boldsymbol{\xi}}/2}}{(2\pi\vartheta)^{d/2}}\sum_{n=0}^{\infty}\frac{1}{n!}\mathbf{b}^{(n)} : \mathbf{H}^{(n)}(\bar{\boldsymbol{\xi}}), \quad \mathbf{b}^{(n)} := \frac{(2\pi\vartheta)^{d/2}}{\rho}\langle\mathbf{H}^{(n)}(\bar{\boldsymbol{\xi}})f\rangle, \tag{3.4b}$$

where $\bar{\boldsymbol{u}} := \boldsymbol{u}/\sqrt{\vartheta}$, $\bar{\boldsymbol{\xi}} := \boldsymbol{\xi}/\sqrt{\vartheta}$, and $\bar{\boldsymbol{u}}^n$ denotes the n-th order tensor produced by the tensor product of n $\bar{\boldsymbol{u}}$'s; $\mathbf{b}^{(0)} = 1$ and $\mathbf{b}^{(1)} = \bar{\boldsymbol{u}}$. The coefficient $\mathbf{b}^{(n)}$ is the same as $\mathbf{a}^{(n)}$ defined in (2.47a), except that for $\mathbf{b}^{(n)}$ here the variable is the normalized particle velocity $\bar{\boldsymbol{\xi}}$, as opposed to the normalized peculiar velocity $\bar{\boldsymbol{c}}$ in (2.47a). With f given in (3.4b), we have

$$\boldsymbol{a}\cdot\partial_{\boldsymbol{\xi}}f = -\rho\frac{e^{-\bar{\boldsymbol{\xi}}\cdot\bar{\boldsymbol{\xi}}/2}}{(2\pi\vartheta)^{d/2}}\sum_{n=0}^{\infty}\frac{1}{n!}(\boldsymbol{a}\mathbf{b}^{(n)}) : \mathbf{H}^{(n+1)}(\bar{\boldsymbol{\xi}}). \tag{3.5}$$

It is clear that the number of the linearly independent moments is equal to the number of discrete velocities, q, for the moments are linear combinations of the distribution functions, therefore the number of independent eigenfunctions $\mathbf{H}^{(n)}$ in a truncated expansion of $f^{(0)}$ or f is also fixed to be q. For a system with d_c conservative moments, there are only $q - d_c$ dissipative moments; consequently, there are at most an equal number of independently adjustable eigenvalues $\{\lambda_i\}$ in the collision term if the symmetry of the moments is not considered. The LBE is in fact a discrete version of the Gross-Jackson model.

A few remarks are in order here. First, the expansion of f in terms of $\{\mathbf{H}^{(n)}\}$ is identical to Grad's moment method [101,119], except that the variable of $\mathbf{H}^{(n)}$ is the dimensionless peculiar velocity $\bar{\boldsymbol{c}} := (\boldsymbol{\xi} - \boldsymbol{u})/\sqrt{\vartheta}$ in Grad's expansion, as opposed to the dimensionless particle velocity $\bar{\boldsymbol{\xi}}$ in the LBE [135]. The Prandtl number, Pr, can be easily adjusted by tuning the relaxation rates for the contracted third-order moments and the off-diagonal second-order moments related to the components of the stress tensor. However, the expansion of the equilibrium $f^{(0)}$ is unique to the LBE, it can be seen as the Taylor expansion in powers of $\bar{\boldsymbol{u}} := \boldsymbol{u}/\sqrt{\vartheta}$ [83,84], which is essentially the local Mach number. Thus the expansion is effectively a low-Mach-number expansion. Also, the coefficients $\{\mathbf{b}^{(n)}\}$ are implicitly computed in the LBE — they are not required as inputs in the LBE calculations.

Second, when the velocity space $\boldsymbol{\xi}$ is discretized to $\{\boldsymbol{\xi}_i|0 \le i \le (q-1)\}$, the tensor Hermite polynomials $\{\mathbf{H}^{(n)}\}$ will be replaced by their counterparts on the discrete velocity set $\mathbb{X}_q := \{\boldsymbol{\xi}_i\}$, as discussed later in Sec. 3.2.

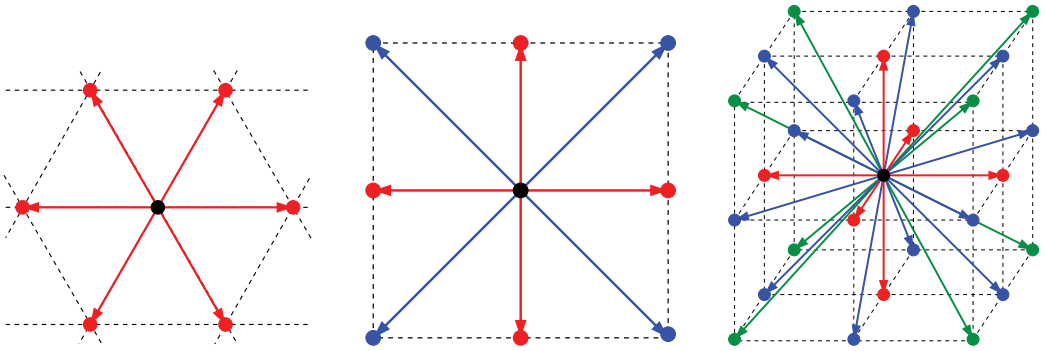

Fig. 2. Some discrete velocity sets in 2D and 3D. From left to right: D2Q7, D2Q9, and D3Q27 velocities. In D3Q27 velocity set, red, blue, and green indicate velocities in groups $\mathbb{F}_6$ of speed $1c$, $\mathbb{E}_{12}$ of speed $\sqrt{2}c$, and $\mathbb{V}_8$ of speed $\sqrt{3}c$, respectively. Note that D2Q9 and D3Q27 sets are the tensor product of D1Q3 set in 2D and 3D, respectively. (For interpretation of the colors in the figure(s), the reader is referred to the web version of this article.)

Third, to recover the *athermal* Stokes or Navier-Stokes equations [81,83,84,135], it is necessary and sufficient to retain the terms up to or including $\boldsymbol{u}^2$ in $f^{(0)}$, respectively, provided that the discrete velocity set $\mathbb{X}_q$ is sufficiently large to retain the required tenor structures (cf., *e.g.*, [136]), that is, not only the hydrodynamic variables, but also their fluxes, must be accurately simulated. By *athermal* we mean that the energy is not a conserved variable in the model.

And fourth, if the expansion of $f^{(0)}$ (thus implicitly the expansion of f) retains terms only up to $\boldsymbol{u}^2$, then the error is of the order $O(u^3)$ (cf., *e.g.*, [137]). However, the equilibria of second-order expansion in $\boldsymbol{u}$ are not the only source of this error, more importantly, it is due to the defect that the discrete velocity set cannot accommodate the corresponding third-order tensor moment $\mathbf{M}^{(3)}$ (cf., *e.g.*, [136]). Therefore, complete removal of $O(u^3)$ error requires the equilibria including all the terms up to third order and a sufficiently large number of discrete velocities to accommodate all the tensor moments up to the order three. More discussion on this issue is deferred to Sec. 3.8.

3.2. Discretization of velocity space $\boldsymbol{\xi}$ based on quadrature

The next step is to discretize the velocity space $\boldsymbol{\xi}$. For *athermal* flows, the discretized velocity space $\{\boldsymbol{\xi}_i\}$ must satisfy the following *quadrature* rules to conserve the mass and momentum [83,84]:

$$\sum_i f_i = \sum_i f_i^{(0)} = \int f \mathrm{d}\boldsymbol{\xi} = \int f^{(0)} \mathrm{d}\boldsymbol{\xi} = \rho, \tag{3.6a}$$

$$\sum_i f_i \boldsymbol{\xi}_i = \sum_i f_i^{(0)} \boldsymbol{\xi}_i = \int f \boldsymbol{\xi} \mathrm{d}\boldsymbol{\xi} = \int f^{(0)} \boldsymbol{\xi} \mathrm{d}\boldsymbol{\xi} = \rho \boldsymbol{u}, \tag{3.6b}$$

where $f_i := f_i(\boldsymbol{r}, t)$ and $f_i^{(0)} := f_i^{(0)}(\boldsymbol{r}, t)$ are the distributions and equilibria corresponding to the discrete velocity $\boldsymbol{\xi}_i$, respectively. We will restrict ourselves to the athermal LBE model for now, so ϑ is a fixed constant, and reserve the discussion of thermal LBE model to Sec. 3.8.

We will use the notation DdQq for a model in d dimensional space with q discrete velocities. With the polar coordinates in 2D, one can derive the D2Q7 model (cf. Fig. 2), of which discrete velocities include a zero velocity and six velocities evenly distributed on a circle, *i.e.*, $\boldsymbol{\xi}_0 = (0, 0)$, and

$$\boldsymbol{\xi}_i = (\cos[(i-1)\pi/3], \sin[(i-1)\pi/3])c, \quad i = 1, 2, \ldots 6, \tag{3.7}$$

where $c := \delta_x/\delta_t = \sqrt{2\vartheta}$ is the unit of velocity. The D2Q7 model evolves on the triangular lattice in 2D.

With Cartesian coordinates in 2D, one can derive the D2Q9 model with the following discrete velocities:

$$\boldsymbol{\xi}_i = \begin{cases} (0, 0), & i = 0, \\ (1, 0)c,\ (0, 1)c,\ (-1, 0)c,\ (0, -1)c, & i = 1, 2, 3, 4, \\ (1, 1)c,\ (-1, 1)c,\ (-1, -1)c,\ (1, -1)c, & i = 5, 6, 7, 8, \end{cases} \tag{3.8}$$

where $c := \delta_x/\delta_t = \sqrt{3\vartheta}$, which differs from the value of c for D2Q7 model on the triangular lattice. It should be noted that the discrete velocity set of the D2Q9 model is the tensor product of two velocity sets of the D1Q3 model [83,84], and the D2Q9 model evolves on a square lattice.

Similarly, with Cartesian coordinates in 3D, a number of models evolving on cubic lattices can be derived [84,138,139]. The discrete velocities are generated from the rotation of a cube, which has one center ($\mathbb{O}_1$), six faces ($\mathbb{F}_6$), eight vertices ($\mathbb{V}_8$), and twelve edges ($\mathbb{E}_{12}$). The combinations of these symmetry groups form the D3Q13 ($\mathbb{O}_1 \cup \mathbb{E}_{12}$) [138], D3Q15 ($\mathbb{O}_1 \cup \mathbb{F}_6 \cup \mathbb{V}_8$), D3Q19 ($\mathbb{O}_1 \cup \mathbb{F}_6 \cup \mathbb{E}_{12}$), and D3Q27 ($\mathbb{O}_1 \cup \mathbb{F}_6 \cup \mathbb{V}_8 \cup \mathbb{E}_{12}$) models. The D3Q27 model is in fact the tensor product of three velocity sets of the D1Q3 model in three coordinates $\{x, y, z\}$. For these 3D LB models, $c := \sqrt{3\vartheta}$. In

summary, if the equilibrium is obtained by the Taylor expansion of the Maxwellian [83,84], then for the LB models on square lattice in 2D and cubic lattice in 3D, $c = \sqrt{3\vartheta}$.

3.3. Discretization of time t

The Boltzmann equation with a *fixed* set of discrete velocities $\mathbb{X}_q = \{\boldsymbol{\xi}_i\}$ can be written as a differential equation along the characteristic $(\boldsymbol{r}', t') := (\boldsymbol{r} + \boldsymbol{\xi} s, t + s)$ parameterized by s [83,84]:

$$\frac{\mathrm{d}}{\mathrm{d}s} f_i(\boldsymbol{r} + \boldsymbol{\xi}_i s, t + s) = Q_i(\boldsymbol{r} + \boldsymbol{\xi}_i s, t + s) + G_i(\boldsymbol{r} + \boldsymbol{\xi}_i s, t + s), \quad \frac{\mathrm{d}}{\mathrm{d}s} := \partial_s + \boldsymbol{\xi}_i \cdot \boldsymbol{\nabla}, \tag{3.9}$$

where Q_i is a collision term to be discussed in detail later (in Sec. 3.5) and G_i is the forcing term coming from $\boldsymbol{a} \cdot \boldsymbol{\partial}_{\boldsymbol{\xi}} f$. Integrating both sides of Eq. (3.9) along the characteristic in the interval $s \in [0, \delta_t]$ and approximating the integrand on the right-hand side by the trapezoidal rule give [140–142]:

$$\begin{aligned} f_i(\boldsymbol{r} + \boldsymbol{\xi}_i \delta_t, t + \delta_t) - f_i(\boldsymbol{r}, t) = & \frac{1}{2}\delta_t \left[Q_i(\boldsymbol{r}, t) + Q_i(\boldsymbol{r} + \boldsymbol{\xi}_i \delta_t, t + \delta_t) \right] \\ & + \frac{1}{2}\delta_t \left[G_i(\boldsymbol{r}, t) + G_i(\boldsymbol{r} + \boldsymbol{\xi}_i \delta_t, t + \delta_t) \right] + O(\delta_t^3). \end{aligned} \tag{3.10}$$

The above equation is implicit because of the dependence of $Q_i(\boldsymbol{r} + \boldsymbol{\xi}_i \delta_t, t + \delta_t)$ and $G_i(\boldsymbol{r} + \boldsymbol{\xi}_i \delta_t, t + \delta_t)$ on $f_i(\boldsymbol{r} + \boldsymbol{\xi}_i \delta_t, t + \delta_t)$. However, it can be made explicit by the following change of variable [140,141]:

$$\bar{f}_i(\boldsymbol{r}, t) := f_i(\boldsymbol{r}, t) - \frac{1}{2}\delta_t \left[Q_i(\boldsymbol{r}, t) + G_i(\boldsymbol{r}, t) \right], \tag{3.11}$$

so that Eq. (3.10) becomes:

$$\bar{f}_i(\boldsymbol{r} + \boldsymbol{\xi}_i \delta_t, t + \delta_t) - \bar{f}_i(\boldsymbol{r}, t) = \delta_t \left[Q_i(\boldsymbol{r}, t) + G_i(\boldsymbol{r}, t) \right] + O(\delta_t^3). \tag{3.12}$$

Note that the change of variable from f_i to $\bar{f}_i$ due to the collision term Q_i does *not* affect the conserved moments ρ and $\rho\boldsymbol{u}$ because they are collisional invariants; but it does affect non-conserved moments.

The forcing term G_i does affect the momentum and higher order moments, which are to be discussed next. Assuming that $\boldsymbol{a}$ due to an external force field is independent of the velocity $\boldsymbol{\xi}$ for the sake of simplicity, then the first few velocity moments of the forcing term, $G := -\boldsymbol{a} \cdot \boldsymbol{\partial}_{\boldsymbol{\xi}} f$ (cf. Eq. (3.5)), are the following [141,143,144]:

$$\langle G \rangle = 0, \quad \langle \boldsymbol{\xi} G \rangle = \rho \boldsymbol{a}, \quad \langle \boldsymbol{\xi}\boldsymbol{\xi} G \rangle = \rho \left(\boldsymbol{a}\boldsymbol{u} + \boldsymbol{u}\boldsymbol{a} \right), \tag{3.13}$$

therefore, the forcing term G can be consistently approximated by the following expansion in terms of the tensor Hermite polynomials $\{\mathbf{H}^{(n)}\}$ up to second order [141,143,144]:

$$G_i = w_i \rho \left[\bar{\boldsymbol{\xi}}_i \cdot \bar{\boldsymbol{a}} + \frac{1}{2}(\bar{\boldsymbol{\xi}}_i \bar{\boldsymbol{\xi}}_i - \mathbf{I}) : (\bar{\boldsymbol{a}}\bar{\boldsymbol{u}} + \bar{\boldsymbol{u}}\bar{\boldsymbol{a}}) \right] = w_i \rho \left[\mathbf{H}^{(1)}(\bar{\boldsymbol{\xi}}_i) \cdot \bar{\boldsymbol{a}} + \frac{1}{2}\mathbf{H}^{(2)}(\bar{\boldsymbol{\xi}}_i) : (\bar{\boldsymbol{a}}\bar{\boldsymbol{u}} + \bar{\boldsymbol{u}}\bar{\boldsymbol{a}}) \right], \tag{3.14}$$

where $\bar{\boldsymbol{a}} := \boldsymbol{a}/\sqrt{\vartheta}$.

The mass density ρ is not affected by the discrete forcing term G_i, but the momentum $\rho\boldsymbol{u}$ is. The equilibrium value of the velocity in $\bar{f}_i^{(0)}(\rho, \boldsymbol{u}^*)$ can be modified to account for this effect [143,144]:

$$\rho \boldsymbol{u}^* := \textstyle\sum_i \boldsymbol{\xi}_i \bar{f}_i = \sum_i \boldsymbol{\xi}_i f_i - \frac{1}{2}\delta_t \rho \boldsymbol{a} = \rho \left(\boldsymbol{u} - \frac{1}{2}\delta_t \boldsymbol{a} \right). \tag{3.15}$$

The implementations of the forcing term will be discussed more later in Sec. 6.1.

3.4. Coherent discretization of phase space $(\boldsymbol{r}, \boldsymbol{\xi})$ and time t

In the LBE, the discretization of space $\boldsymbol{r}$ is done coherently with that of velocity $\boldsymbol{\xi}$ and time t as follows. The discretized space $\{\boldsymbol{x}_j\}$ is required to form a lattice with the lattice spacing δ_x, *i.e.*, $\boldsymbol{x}_j \in \delta_x \mathbb{Z}_d$. Furthermore, it is also required that the unit of the discrete velocities $\{\boldsymbol{\xi}_i\}$ is $c := \delta_x/\delta_t = \sqrt{3\vartheta}$ and

$$\boldsymbol{x}_j + \boldsymbol{\xi}_i \delta_t \in \delta_x \mathbb{Z}_d, \qquad \forall \boldsymbol{x}_j \in \delta_x \mathbb{Z}_d, \quad \forall \boldsymbol{\xi}_i \in \mathbb{X}, \tag{3.16}$$

that is, the particle with the velocity $\boldsymbol{\xi}_i$ hops from one lattice point $\boldsymbol{x}_j$ to another $\boldsymbol{x}_{j'} = \boldsymbol{x}_j + \boldsymbol{\xi}_i \delta_t$ in one discrete time step δ_t. In this manner, the discretization of phase space $\mathbb{\Gamma} := (\boldsymbol{r}, \boldsymbol{\xi})$ and time t are closely tied together, *i.e.*, they are discretized *coherently*.

The lattice Boltzmann equation in fully discretized phase space and time can be expressed in the following concise vector form:

$$\bar{\mathbf{f}}(\boldsymbol{x}_j + \boldsymbol{\xi}\delta_t,\, t_n + \delta_t) - \bar{\mathbf{f}}(\boldsymbol{x}_j,\, t_n) = \delta_t \left[\mathbf{Q}(\boldsymbol{x}_j,\, t_n) + \mathbf{G}(\boldsymbol{x}_j,\, t_n)\right], \tag{3.17}$$

where the symbols in the upright bold-font are q-dimensional vectors in $\mathbb{R}^q$, specifically, with $\boldsymbol{\xi}_0 := \mathbf{0}$,

$$\begin{aligned}
&\bar{\mathbf{f}}(\boldsymbol{x}_j + \boldsymbol{\xi}\delta_t,\, t_n + \delta_t) := (\bar{f}_0(\boldsymbol{x}_j,\, t_n + \delta_t),\, \bar{f}_1(\boldsymbol{x}_j + \boldsymbol{\xi}_1\delta_t,\, t_n + \delta_t),\, \ldots,\, \bar{f}_b(\boldsymbol{x}_j + \boldsymbol{\xi}_b\delta_t,\, t_n + \delta_t))^\dagger,\\
&\bar{\mathbf{f}}(\boldsymbol{x}_j,\, t_n) := (\bar{f}_0(\boldsymbol{x}_j,\, t_n),\, \bar{f}_1(\boldsymbol{x}_j,\, t_n),\, \ldots,\, \bar{f}_b(\boldsymbol{x}_j,\, t_n))^\dagger,\\
&\mathbf{Q}(\boldsymbol{x}_j,\, t_n) := (Q_0(\boldsymbol{x}_j,\, t_n),\, Q_1(\boldsymbol{x}_j,\, t_n),\, \ldots,\, Q_b(\boldsymbol{x}_j,\, t_n))^\dagger,\\
&\mathbf{G}(\boldsymbol{x}_j,\, t_n) := (G_0(\boldsymbol{x}_j,\, t_n),\, G_1(\boldsymbol{x}_j,\, t_n),\, \ldots,\, G_b(\boldsymbol{x}_j,\, t_n))^\dagger,
\end{aligned}$$

where $\dagger$ denotes the transpose, $b := (q-1)$ is the number of non-zero discrete velocities $\boldsymbol{\xi}_i \neq \mathbf{0}$, and G_i is given by (3.14) or otherwise provided.

3.5. Collision models

We now specify the collision operator $\mathbf{Q}$ in the LBE (3.17). Given q number of discrete velocities $\{\boldsymbol{\xi}_i\}$, the corresponding distributions $\{f_i\}$ can be linearly mapped to an equal number of velocity moments $\{m_i\}$ without losing or gaining any information. The moments, especially the low-order ones, have clear physical significance and thus are convenient to be used in collision process — the effect of the $\mathcal{L}_M$ in (2.50) or $\mathcal{L}_N$ in (2.51) in fact consists of the relaxation of its eigenmodes. Since the velocity space $\boldsymbol{\xi}$ is discretized into a finite set $\{\boldsymbol{\xi}_i\}$, the set of the eigenfunctions of $\mathcal{L}$ is also finite.

The construction of the orthogonal polynomials on a finite, discrete velocity set $\{\boldsymbol{\xi}_i\}$ is not unique. We will follow the methodology proposed by d'Humières [81] — the orthogonal polynomials are obtained by applying the Gram-Schmidt procedure to orthogonalize combinations of monomials ξ_i^k of the same order. We will restrict our discussion to 2D space and focus on the D2Q9 model in what follows. Denote $\{\psi_i(\boldsymbol{\xi})\}$ the orthogonal polynomials on $\{\boldsymbol{\xi}_i\}$ with a unit weight, then

$$\langle \psi_i(\boldsymbol{\xi}),\, \psi_j(\boldsymbol{\xi})\rangle := \textstyle\sum_{k=0}^{q-1} \psi_i(\boldsymbol{\xi}_k)\psi_j(\boldsymbol{\xi}_k) = \boldsymbol{\Psi}_i \cdot \boldsymbol{\Psi}_j = |\boldsymbol{\Psi}_i|^2 \delta_{ij}, \tag{3.18}$$

where $\boldsymbol{\Psi}_i \in \mathbb{R}^q$ is an eigenvector of $\mathbf{Q}$, whose elements are $\psi_i(\boldsymbol{\xi}_k)$, $0 \le k \le (q-1)$. The first three orthogonal polynomials corresponding to the conserved moments are

$$\psi_0(\boldsymbol{\xi}) = |\boldsymbol{\xi}|^0 = 1, \quad \psi_1(\boldsymbol{\xi}) = \xi_x, \quad \psi_2(\boldsymbol{\xi}) = \xi_y, \tag{3.19}$$

where ξ_x and ξ_y and the x and y component of $\boldsymbol{\xi}$. The remaining six orthogonal polynomials for non-conserved moments are:

$$\begin{aligned}
&\psi_3(\boldsymbol{\xi}) = \xi_x^2 - \xi_y^2, \quad \psi_4(\boldsymbol{\xi}) = \xi_x\xi_y, \quad \psi_5(\boldsymbol{\xi}) = -4|\boldsymbol{\xi}|^0 + 3|\boldsymbol{\xi}|^2,\\
&\psi_{6,7}(\boldsymbol{\xi}) = (-5|\boldsymbol{\xi}|^0 + 3|\boldsymbol{\xi}|^2)\xi_{x,y}, \quad \psi_8 = 4|\boldsymbol{\xi}|^0 - \frac{21}{2}|\boldsymbol{\xi}|^2 + \frac{9}{2}|\boldsymbol{\xi}|^4.
\end{aligned} \tag{3.20}$$

For the D2Q9 model, the discrete velocities are given in (3.8), so the definitions (3.19) become

$$\boldsymbol{\Psi}_0 = (1,\, 1,\, 1,\, 1,\, 1,\, 1,\, 1,\, 1,\, 1)^\dagger, \tag{3.21a}$$
$$\boldsymbol{\Psi}_1 = (0,\, 1,\, 0,\, -1,\, 0,\, 1,\, -1,\, -1,\, 1)^\dagger, \tag{3.21b}$$
$$\boldsymbol{\Psi}_2 = (0,\, 0,\, 1,\, 0,\, -1,\, 1,\, 1,\, -1,\, -1)^\dagger. \tag{3.21c}$$

Note that $\boldsymbol{\Psi}_0$, $\boldsymbol{\Psi}_1$, and $\boldsymbol{\Psi}_2$ are mutually orthogonal, but they are not normalized, and they span the null space of the collision operator. The components of $\boldsymbol{\Psi}_1$ and $\boldsymbol{\Psi}_2$ specify the order of the labeling of the discrete velocities $\{\boldsymbol{\xi}_i | 0 \le i \le (q-1)\}$. Another six orthogonal vectors can be generated by the above three, and they can be *chosen* to be:

$$\boldsymbol{\Psi}_3 = (0,\, 1,\, -1,\, 1,\, -1,\, 0,\, 0,\, 0,\, 0)^\dagger, \tag{3.22a}$$
$$\boldsymbol{\Psi}_4 = (0,\, 0,\, 0,\, 0,\, 0,\, 1,\, -1,\, 1,\, -1)^\dagger, \tag{3.22b}$$
$$\boldsymbol{\Psi}_5 = (-4,\, -1,\, -1,\, -1,\, -1,\, 2,\, 2,\, 2,\, 2)^\dagger, \tag{3.22c}$$
$$\boldsymbol{\Psi}_6 = (0,\, -2,\, 0,\, 2,\, 0,\, 1,\, -1,\, -1,\, 1)^\dagger, \tag{3.22d}$$
$$\boldsymbol{\Psi}_7 = (0,\, 0,\, -2,\, 0,\, 2,\, 1,\, 1,\, -1,\, -1)^\dagger, \tag{3.22e}$$
$$\boldsymbol{\Psi}_8 = (4,\, -2,\, -2,\, -2,\, -2,\, 1,\, 1,\, 1,\, 1)^\dagger. \tag{3.22f}$$

Note that due to the discreteness of the velocity set $\{\boldsymbol{\xi}_i\}$, some polynomials are missing, so the polynomials $\{\psi_i\}$ on $\{\boldsymbol{\xi}_i\}$ cannot be arranged into complete n-th order tensors in an orderly fashion for a given order $n \geq 3$ [136]. For example, there are only two third-order polynomials and one fourth-order one in the D2Q9 model, and it is impossible to construct a complete third-order tensor with the D2Q9 velocity set [136]. This is the cause of the cubic error in the viscous stress. The complete third-order tensor requires the D2Q13 model [136,145,146]. The incomplete tensors associated with discrete velocity sets generate anisotropy, and are the origin of some defects observed in the LBE simulations [147,148]. This issue was first mentioned in Sec. 3.1 and will be further discussed in Sec. 3.8.

The transform matrix $\mathbf{M}$ which maps the distributions to the moments can be given as the following:

$$\mathbf{M} = \begin{pmatrix} 1 & 1 & 1 & 1 & 1 & 1 & 1 & 1 & 1 \\ 0 & 1 & 0 & -1 & 0 & 1 & -1 & -1 & 1 \\ 0 & 0 & 1 & 0 & -1 & 1 & 1 & -1 & -1 \\ 0 & 1 & -1 & 1 & -1 & 0 & 0 & 0 & 0 \\ 0 & 0 & 0 & 0 & 0 & 1 & -1 & 1 & -1 \\ -4 & -1 & -1 & -1 & -1 & 2 & 2 & 2 & 2 \\ 0 & -2 & 0 & 2 & 0 & 1 & -1 & -1 & 1 \\ 0 & 0 & -2 & 0 & 2 & 1 & 1 & -1 & -1 \\ 4 & -2 & -2 & -2 & -2 & 1 & 1 & 1 & 1 \end{pmatrix}. \tag{3.23}$$

The rows of $\mathbf{M}$ are $\boldsymbol{\Psi}_i^\dagger$, $0 \leq i \leq 8$, are mutually orthogonal, therefore

$$\mathbf{M}\mathbf{M}^\dagger = \mathrm{diag}\left(|\boldsymbol{\Psi}_0|^2, |\boldsymbol{\Psi}_1|^2, \ldots, |\boldsymbol{\Psi}_8|^2\right)$$

is diagonal, hence $\mathbf{M}^{-1}$ can be easily obtained. If $\{\boldsymbol{\Psi}_i\}$ are normalized, $\mathbf{M}$ becomes an orthogonal matrix.

With $\mathbf{M}$ given, the moments can be easily obtained:

$$\mathbf{m} = \mathbf{M}\mathbf{f}, \quad \mathbf{f} = \mathbf{M}^{-1}\mathbf{m}, \tag{3.24}$$

where $\mathbf{m} := (m_0, m_1, \ldots, m_8)^\dagger$, $m_0 = \rho$ is the (mass) density, $m_1 = \rho u_x$ and $m_2 = \rho u_y$ are the x and y component of the flow momentum, respectively, m_3 and m_4 are the second-order moments related to the components of the traceless stress tensor, m_5 is the second-order moment related to the diagonal components of the stress tensor, m_6 and m_7 are third-order moments, which behave as the x- and y-components of a vector, and m_8 is a fourth-order moment. The collision operator with multiple relaxation times (MRT) is naturally written in terms of relaxations of non-conserved moments:

$$\mathbf{Q} = -\mathbf{M}^{-1}\mathbf{S}\left(\mathbf{m} - \mathbf{m}^{(0)}\right), \quad \mathbf{S} := \mathrm{diag}(\underbrace{1, \ldots, 1}_{d+1}, \underbrace{s_{d+1}, \ldots, s_b}_{q-(d+1)}), \tag{3.25}$$

where $\mathbf{S}$ is the diagonal matrix of the relaxation rates $\{s_i\}$ in the unit of $\delta_t = 1$, of which $s_i = 1$ for the conserved moments with $0 \leq i \leq d$, $s_i \in (0, 2)$ for non-conserved moments; and $\mathbf{m}^{(0)}$ is the vector of equilibrium moments:

$$\begin{aligned} &m_0^{(0)} = \rho, \quad m_{1,2}^{(0)} = \rho u_{x,y}, \\ &m_3^{(0)} = \rho(u_x^2 - u_y^2), \quad m_4^{(0)} = \rho u_x u_y, \quad m_5^{(0)} = -\rho(2 - 3u^2), \\ &m_{6,7}^{(0)} = -\rho u_{x,y}, \quad m_8^{(0)} = \rho(1 - 3u^2). \end{aligned} \tag{3.26}$$

Note that for the conserved moments, their equilibria are equal to themselves, *i.e.*, $m_i^{(0)} = m_i$, for ρ and $\rho\boldsymbol{u} := \rho(u_x, u_y)$ in this case. The equilibrium moments $\{m_i^{(0)}\}$ can be constructed by linear analysis (or Fourier-von Neumann analysis, cf. Sec. 5 and [149–151]) and the above result is identical to the truncation of the Maxwell-Boltzmann equilibrium expanded in Hermite polynomials up to second-order (cf. (3.4b)), *i.e.*, $\mathbf{m}^{(0)} = \mathbf{M}^{-1}\mathbf{f}^{(0)}$, and

$$f_i^{(0)} = w_i\rho\left\{1 + \bar{\boldsymbol{\xi}}_i \cdot \bar{\boldsymbol{u}} + \frac{1}{2}\left(\bar{\boldsymbol{\xi}}_i\bar{\boldsymbol{\xi}}_i - \mathbf{I}\right) : \bar{\boldsymbol{u}}\bar{\boldsymbol{u}}\right\} = w_i\rho\left\{\mathbf{H}^{(0)} + \bar{\boldsymbol{u}} \cdot \mathbf{H}^{(1)}(\bar{\boldsymbol{\xi}}_i) + \frac{1}{2}\bar{\boldsymbol{u}}\bar{\boldsymbol{u}} : \mathbf{H}^{(2)}(\bar{\boldsymbol{\xi}}_i)\right\}, \tag{3.27}$$

where $\mathbf{H}^{(n)}$ is the n-th order Hermite tensor in d dimensions (cf. (2.44) and (2.46)); $\bar{\boldsymbol{u}} := \boldsymbol{u}/c_s$, $\bar{\boldsymbol{\xi}}_i := \boldsymbol{\xi}_i/c_s$; $w_0 = 4/9$ for $|\boldsymbol{\xi}_0| = 0$, $w_{1,2,3,4} = 1/9$ for $|\boldsymbol{\xi}_{1,2,3,4}| = 1$, and $w_{5,6,7,8} = 1/36$ for $|\boldsymbol{\xi}_{5,6,7,8}| = \sqrt{2}$ [83,84], the flow mass density ρ and momentum $\rho\boldsymbol{u}$ are given by:

$$\sum_i f_i(\boldsymbol{x}, t) = \sum_i f_i^{(0)}(\boldsymbol{x}, t) = \rho(\boldsymbol{x}, t), \tag{3.28a}$$

$$\sum_i \boldsymbol{\xi}_i f_i(\boldsymbol{x}, t) = \sum_i \boldsymbol{\xi}_i f_i^{(0)}(\boldsymbol{x}, t) = \rho(\boldsymbol{x}, t)\boldsymbol{u}(\boldsymbol{x}, t). \tag{3.28b}$$

The speed of sound c_s in the LBE is determined by the trace of the symmetric second-order moment, *i.e.*, the thermal energy:

$$\frac{1}{2}\int (\boldsymbol{\xi}-\boldsymbol{u})\cdot(\boldsymbol{\xi}-\boldsymbol{u}) f \mathrm{d}\boldsymbol{\xi} = \frac{d}{2}\rho\vartheta = \frac{d}{2}\rho c_s^2,$$

and with the discrete velocities $\{\boldsymbol{\xi}_i\}$ about $\boldsymbol{u}=\mathbf{0}$, it leads to

$$c_s^2 = \frac{1}{d}\sum_i w_i \boldsymbol{\xi}_i\cdot\boldsymbol{\xi}_i. \tag{3.29}$$

Thus, $c_s=(1/\sqrt{3})c$ for the D2Q9 model. In general, for athermal LBE models, c_s depends solely on the discrete velocity set $\mathbb{X}_q$ and the corresponding weights $\{w_i\}$, however, it can also be a tunable parameter to be determined by linear analysis [149,151].

The collision with multiple-relaxation times (MRT) can be rewritten as the following:

$$\mathbf{Q}=\mathbf{M}^{-1}\mathbf{S}\delta\mathbf{m}=\mathbf{M}^{\dagger}\boldsymbol{\Psi}^{-1}\mathbf{S}\delta\mathbf{m}=\mathbf{M}^{\dagger}\mathbf{S}'\delta\mathbf{m}, \tag{3.30}$$

where $\delta\mathbf{m}:=\mathbf{m}-\mathbf{m}^{(0)}$, $\mathbf{S}':=\boldsymbol{\Psi}^{-1}\mathbf{S}$, and specifically for the D2Q9 model,

$$\begin{aligned}\boldsymbol{\Psi}^{-1} :=& \mathrm{diag}\left(|\boldsymbol{\Psi}_0|^2,\ |\boldsymbol{\Psi}_1|^2,\ \ldots,\ |\boldsymbol{\Psi}_8|^2\right)^{-1}\\ =& \mathrm{diag}\left(\tfrac{1}{9},\tfrac{1}{6},\tfrac{1}{6},\tfrac{1}{4},\tfrac{1}{4},\tfrac{1}{36},\tfrac{1}{12},\tfrac{1}{12},\tfrac{1}{36}\right)=\tfrac{1}{36}\mathrm{diag}(4,6,6,9,9,1,3,3,1).\end{aligned} \tag{3.31}$$

The relaxation rates s_i are rescaled by $|\boldsymbol{\Psi}_i|^2$ in the pre-processing, then $\mathbf{M}^{\dagger}$ can be used to transfer $\mathbf{m}$ to $\mathbf{f}$.

We emphasize that $\mathbf{M}$ given in the form of (3.23) is constructed to optimize algorithmic simplicity and computational efficiency. The matrix $\mathbf{M}$ has several symmetry properties allowing for efficient coding. One can simplify the collision process further by pre-processing $\tilde{\mathbf{S}}:=\mathbf{M}^{-1}\cdot\mathbf{SM}$, and write out the collision $\mathbf{Q}=-\tilde{\mathbf{S}}\delta\mathbf{m}$ explicitly in codes.

As aforementioned, the construction of the orthogonal polynomial set $\{\psi_i\}$ is not unique. The orthogonality of the polynomials $\{\psi_i\}$ on $\{\boldsymbol{\xi}_i\}$ given in (3.20) is with respect to a unity weight. The polynomials can also be constructed with respect to the weight $\{w_i\}$ corresponding to the velocity set $\{\boldsymbol{\xi}_i\}$ (cf. (3.3)) [85,87,152–155]. In this case, the orthogonality (3.18) becomes:

$$\langle\psi_i'(\boldsymbol{\xi}),\ \psi_j'(\boldsymbol{\xi})\rangle_w := \sum_{k=0}^{q-1} w_i\psi_i'(\boldsymbol{\xi}_k)\psi_j'(\boldsymbol{\xi}_k)=\boldsymbol{\Psi}_i'\cdot\boldsymbol{\Psi}_j'=|\boldsymbol{\Psi}_i'|^2\delta_{ij}, \tag{3.32}$$

and the new orthogonal polynomials $\{\psi_i'\}$ for the D2Q9 model are [85,87,154,155]:

$$\begin{aligned}&\psi_3'(\boldsymbol{\xi})=\xi_x^2-\xi_y^2,\quad \psi_4'(\boldsymbol{\xi})=\xi_x\xi_y,\quad \psi_5'(\boldsymbol{\xi})=-2|\boldsymbol{\xi}|^0+3|\boldsymbol{\xi}|^2,\\ &\psi_{6,7}'(\boldsymbol{\xi})=(-4|\boldsymbol{\xi}|^0+3|\boldsymbol{\xi}|^2)\xi_{x,y},\quad \psi_8'=2|\boldsymbol{\xi}|^0-15|\boldsymbol{\xi}|^2+9|\boldsymbol{\xi}|^4,\end{aligned} \tag{3.33}$$

and the corresponding equilibria of the non-conserved moments are:

$$m_3'^{(0)}=\rho(u_x^2-u_y^2),\quad m_4'^{(0)}=\rho u_x u_y,\quad m_5'^{(0)}=3\rho u^2,\quad m_{6,7,8}'^{(0)}=0. \tag{3.34}$$

With the above equilibrium moments, the consequences of the weighted orthogonal polynomials become apparent — all the equilibria of the non-conserved moments are decoupled from the conserved moments ρ and $\rho\boldsymbol{u}$. This is essential for the fluctuating LBE in which thermal fluctuations cannot affect the conserved quantities [152–155]. In particular, by comparing (3.34) and (3.26), it can be seen that the equilibrium of m_5', which is related to the diagonal components of the stress tensor, no longer has a projection on the density ρ, and the equilibria of two third-order moments, m_6 and m_7, no longer have the projections on ρu_x and ρu_y, respectively. Hence, by using the weighted polynomials $\{\psi_i'\}$, the boundary conditions in the LBE may be altered, because the decoupling between the third-order moments $m_{6,7}$ and the momentum $\rho\boldsymbol{u}$ affects the relationship between the relaxation rates of even and odd order moments (cf. (3.44) and Sec. 6.3).

3.6. The over-relaxation feature of the LBE

The change of variable from $\mathbf{f}$ to $\bar{\mathbf{f}}$ (cf. (3.11)) has important consequences [141]. First of all, it makes an implicit algorithm (3.10) explicit (3.12). Secondly, despite the appearance of having a first-order Euler method, the LBE is in fact a second-order accurate scheme [141,156]. Thirdly, the LBE can work in the over-relaxed regime making it rather efficient computationally. To elucidate the latter two points, as an example let's first examine the lattice BGK model with the collision model of single relaxation time (SRT) τ_v in the continuous BGK counterpart:

$$Q_{\mathrm{BGK}} := -\frac{1}{\tau_v}[f-f^{(0)}]. \tag{3.35}$$

In what follows, τ_v is used solely to denote the relaxation time in the above continuous BGK model, and it is the relaxation time in the lattice BGK equation for the distribution function f_i without the correction of $\delta_t/2$ as discussed in Sec. 3.3 (cf. (3.10) – (3.12)). If the first-order forward Euler method is applied to discretize (3.9) with the BGK collision model (3.35), then the equation for f_i is [83,84]:

$$\mathbf{f}(\boldsymbol{x}_j+\boldsymbol{\xi}\delta_t,\, t_n+\delta_t) = \mathbf{f}(\boldsymbol{x}_j,\, t_n) - \frac{\delta_t}{\tau_\nu}\left[\mathbf{f}(\boldsymbol{x}_j,\, t_n) - \mathbf{f}^{(0)}(\rho,\, \boldsymbol{u};\, \boldsymbol{x}_j,\, t_n)\right] + \delta_t\mathbf{G}$$
$$= \left(1-\frac{\delta_t}{\tau_\nu}\right)\mathbf{f}(\boldsymbol{x}_j,\, t_n) + \frac{\delta_t}{\tau_\nu}\mathbf{f}^{(0)}(\rho,\, \boldsymbol{u};\, \boldsymbol{x}_j,\, t_n) + \delta_t\mathbf{G}. \tag{3.36}$$

Therefore $\mathbf{f}(\boldsymbol{x}_j+\boldsymbol{\xi}\delta_t,\, t_n+\delta_t)$ is in fact a convex combination of $\mathbf{f}(\boldsymbol{x}_j,\, t_n)$ and $\mathbf{f}^{(0)}(\rho,\, \boldsymbol{u};\, \boldsymbol{x}_j,\, t_n)$ in (3.36), if the forcing term $\mathbf{G}$ is ignored and $\delta_t/\tau_\nu \le 1$ [141,156]. This of course imposes a severe restriction on $\tau_\nu \ge \delta_t$, and thus the viscosity, ν, for $\nu = (2\tau_\nu - \delta_t)c^2/6 \ge \delta_x c/6$ (with $\vartheta = c^2/3$), which in turn would severely limit the Reynolds number $\mathrm{Re} := UL/\nu$. In contrast, (3.12) in terms of $\bar{\mathbf{f}}$ and with the BGK model (3.35) becomes:

$$\bar{\mathbf{f}}(\boldsymbol{x}_j+\boldsymbol{\xi}\delta_t,\, t_n+\delta_t) = (1-\beta)\bar{\mathbf{f}}(\boldsymbol{x}_j,\, t_n) + \beta\bar{\mathbf{f}}^{(0)}(\rho,\, \boldsymbol{u};\, \boldsymbol{x}_j,\, t_n) + \delta_t\mathbf{G}, \tag{3.37}$$

$$\bar{\mathbf{f}}^{(0)}(\rho,\, \boldsymbol{u};\, \boldsymbol{x}_j,\, t_n) := \mathbf{f}^{(0)}(\rho,\, \boldsymbol{u}^*;\, \boldsymbol{x}_j,\, t_n) = \mathbf{f}^{(0)}(\rho,\, \boldsymbol{u};\, \boldsymbol{x}_j,\, t_n) - \frac{\delta_t}{2}\mathbf{G}, \tag{3.38}$$

$$\beta := \frac{\delta_t}{\tau_\nu + \delta_t/2},$$

where $\boldsymbol{u}^* := \boldsymbol{u} - \boldsymbol{a}\delta_t/2$ (cf. (3.15) and pertinent discussion, and Sec. 6.1).

Eq. (3.37) is in fact the Crank-Nicolson discretization of (3.9) with the BGK collision model (3.35), and it is second-order accurate in δ_t [141]. The contrast between (3.37) and (3.36) indicates that the restriction on τ_ν becomes $\tau_\nu > 0$ for the system of $\bar{\mathbf{f}}$ (as opposed to $\tau_\nu/\delta_t > 1/2$ for the system of $\mathbf{f}$), and the viscosity becomes $\nu = \tau_\nu/3$, which can be significantly reduced so long as the scheme is numerically stable, so the numerical efficiency is greatly enhanced. It must be noted that the above analysis can be immediately applied to the LBE with the MRT collision model [141].

Hence, with $1 > \tau_\nu/\delta_t > 0$, the LBE (when formulated in terms of $\bar{\mathbf{f}}$) is operating in the over-relaxation regime of (3.9) [141,156,157], which permits small viscosity so to achieve high Reynolds number in simulations. therefore is very useful, hence most LBE flow simulations are carried out in this regime (cf., *e.g.*, [52,158,159]). It should be stressed that the over-relaxation does not ease the intrinsic restriction on δ_t, or the Mach number, which is equivalent to the Courant-Friedrichs-Lewy (CFL) number in the LBE. In addition, it should be cautioned that, while the LBE method operating in the over-relaxation region is numerically efficient to simulation flows with small viscosity (equivalently high Reynolds number Re) when stable, it is by no means to imply that the LBE simulation adequately resolves the physics corresponding to the given Re.

3.7. The LB model for advection-diffusion equation

When the collision model in an LB model respects both mass and momentum conservation as discussed in the previous section, the LB model solves the incompressible Navier-Stokes equations for athermal fluid systems. If the collision respects the conservation for one scalar quantity, *e.g.*, the mass conservation, the LB system models the advection-diffusion equation for the scalar field [160–170]. The LB system for the advection-diffusion equation of a scalar requires a fewer number of discrete velocities than that for the Navier-Stokes equations. In 2D, for example, the system of one conserved scalar can be simulated by the D2Q5 model, of which the discrete velocities are a subset of $\mathbb{X}_9$ defined in (3.8), *i.e.*, $\{\boldsymbol{\xi}_i | 0 \le i \le 4\}$ in $\mathbb{X}_9$.

In the D2Q5 model, there are five moments $\{m_i | 0 \le i \le 4\}$: one zeroth-order, two first-order, and two second-order ones, and the corresponding transformation matrix, similar to $\mathbf{M}$ of (3.23) for the D2Q9 model:

$$\begin{pmatrix} 1 & 1 & 1 & 1 & 1 \\ 0 & 1 & 0 & -1 & 0 \\ 0 & 0 & 1 & 0 & -1 \\ -4 & 1 & 1 & 1 & 1 \\ 0 & 1 & -1 & 1 & -1 \end{pmatrix}. \tag{3.39}$$

The orthogonal polynomials corresponding to four non-conserved moments are:

$$\phi_1(\boldsymbol{\xi}) = \xi_x, \quad \phi_2(\boldsymbol{\xi}) = \xi_y, \quad \phi_5(\boldsymbol{\xi}) = -4 + 5|\boldsymbol{\xi}|^2, \quad \phi_4(\boldsymbol{\xi}) = \xi_x^2 - \xi_y^2. \tag{3.40}$$

Assuming the conserved quantity is the scalar $m_0 = \rho$, then the equilibria in the D2Q5 model are chosen as the following:

$$m_1^{(0)} = \rho u, \quad m_2^{(0)} = \rho v, \quad m_3^{(0)} = a\rho, \quad m_4^{(0)} = 0, \tag{3.41}$$

where a is a parameter to be determined, and $(u,\, v) = \boldsymbol{u}$ is the external advection velocity. The D2D5 model leads to the advection-diffusion equation satisfied by the conserved scalar ρ:

$$\partial_t\rho + \boldsymbol{u}\cdot\nabla\rho = \kappa\nabla^2\rho. \tag{3.42}$$

There are three relaxation rates for the D2Q5 model, s_κ for m_1 and m_2, and s_e and s_ν for m_3 and m_4 defined in (3.41), respectively. In the absence of an advective velocity $\boldsymbol{u}$, the diffusion coefficient κ in (3.42) is determined by the parameter a and the relaxation rate s_κ for the first-order moments:

$$\kappa = \frac{(4+a)}{10}\sigma_\kappa, \quad \sigma_\kappa := \left(\frac{1}{s_\kappa} - \frac{1}{2}\right), \tag{3.43}$$

where the notation $\sigma_i := (1/s_i - 1/2)$ is used [171]. To attain the isotropy for the fourth-order (error) term in the advection-diffusion equation derived from the D2Q5 model, σ_e and σ_ν must satisfy the following relationship (cf. [172] and refs. therein):

$$\sigma_\kappa \sigma_\nu = \left(\frac{1}{s_\kappa} - \frac{1}{2}\right)\left(\frac{1}{s_\nu} - \frac{1}{2}\right) = \frac{1}{6}. \tag{3.44}$$

It is also possible to cancel the remaining fourth-order error terms. One way is to set $\sigma_e = \sigma_\nu$ and

$$\sigma_\kappa = \frac{\sqrt{3}}{6}, \tag{3.45}$$

such that (3.44) leads to

$$\sigma_e = \sigma_\nu = \frac{\sqrt{3}}{3}, \tag{3.46}$$

thus the diffusivity κ is solely determined by the value of a:

$$\kappa = \frac{\sqrt{3}\,(4+a)}{60}. \tag{3.47}$$

The stability of the scheme requires $-4 < a < 1$, where the condition $a < 1$ is to avoid the instability due to "checkerboard" modes (cf. [167–169,172] and refs. therein).

In the presence of non-zero advection velocity $\boldsymbol{u}$, the conserved variable ρ is correctly advected at velocity $\boldsymbol{u}$ provided it varies slowly in space. It can be shown that the effective diffusivity κ becomes velocity dependent in the D2Q5 model [173]. These defects of the model have been analyzed in detail [161,174], they can be removed by using a larger number of discrete velocities. It should also be noted that *anisotropic* diffusivity can be achieved by using different relaxation rates for the moments m_1 and m_2 and modified equilibria of m_3 and m_4 [160–163,168,175].

3.8. The thermal LBE

The LBE considered in the preceding discussion only respects the conservation of mass and momentum, as stipulated in conservation constraints (3.6) and the corresponding equilibria (3.20), so the energy is *not* a conserved quantity, hence the LBE so constructed is in *principle athermal* (as opposed to isothermal). For thermal flows, the conservation laws of mass, momentum, and energy must be respected simultaneously. For the Boltzmann equation, the total energy is given by the diagonal second-order moment of the velocity distribution function $f(\boldsymbol{r}, \boldsymbol{\xi}, t)$:

$$\rho E := \tfrac{1}{2}\int \boldsymbol{\xi}\cdot\boldsymbol{\xi} f \mathrm{d}\boldsymbol{\xi} = \tfrac{1}{2}\int \boldsymbol{\xi}\cdot\boldsymbol{\xi} f^{(0)} \mathrm{d}\boldsymbol{\xi} = \tfrac{1}{2}\textstyle\sum_i \boldsymbol{\xi}_i\cdot\boldsymbol{\xi}_i f_i = \tfrac{1}{2}\sum_i \boldsymbol{\xi}_i\cdot\boldsymbol{\xi}_i f_i^{(0)}, \tag{3.48}$$

which includes both the flow kinetic energy $\rho\boldsymbol{u}\cdot\boldsymbol{u}/2$ and the thermal energy $d\rho\vartheta/2$, *i.e.*, for a Maxwellian equilibrium $f_i^{(0)}$ in d dimensional space,

$$\rho E = \frac{1}{2}\int \boldsymbol{\xi}_i\cdot\boldsymbol{\xi}_i f_i^{(0)} \mathrm{d}\boldsymbol{\xi} = \frac{1}{2}\rho u^2 + \frac{d}{2}\rho\vartheta. \tag{3.49}$$

It follows from the ideal gas equations of state for the pressure $p = \rho\vartheta$ and the internal energy $\rho e = p/(\gamma - 1)$, where $\gamma := C_\mathrm{P}/C_\mathrm{V}$ is the ratio of the specific heats or the adiabatic exponent (cf., *e.g.*, [176]), that

$$\rho E = \rho e + \frac{1}{2}\rho u^2 = \frac{p}{\gamma - 1} + \frac{1}{2}\rho u^2, \tag{3.50}$$

thus in the Boltzmann equation for structureless particles, $\gamma = 1 + 2/d$ in d dimensional space, which is a fixed constant, even though in reality γ depends on the degrees of freedom of constituent particles and temperature.

There are several approaches to model the energy conservation in the LBE. With the appropriate moment constraints including energy and heat fluxes, the Navier-Stokes-Fourier (NSF) system can be derived from the LBE [177–179]. Thus the most direct and obvious approach seems to be simply imposing the energy conservation condition (3.48) on the collision, *i.e.*, the energy-conserving LBE which leads to the correct PDEs for the NSF system [177–182]. It should be mentioned that to

correctly model the NSF system, the energy-conserving LBE requires a larger number of discrete velocities than its athermal counterpart. It requires at least five velocities in 1D [183] with a fixed $\gamma = 3$, or seven velocities in 1D [179], thirteen in 2D [177], and twenty-seven in 3D [178]. However, it has also been found that the energy-conserving LBE with polynomial equilibria are endowed with some inherent defects. First, there exists an unphysical coupling between the longitudinal (acoustic) and shear modes [151], which leads to numerical instability for short wavelengths [182]. It must be emphasized that this coupling is a direct consequence of the space-time discretization described in preceding Sections 3.2–3.4. In addition, for the energy-conserving LBE with a *linear* collision model (cf. Eq. (3.25) and related discussion), achieving stability leads to a restriction on γ in a very narrow range of variation about 1.0 — the stable value of γ is neither 7/5 nor 5/3 (corresponding to diatomic and monatomic gases, respectively), and it does not depend on the temperature correctly as with real gases [151]. The point is that the energy-conserving LBE does not accommodate the degree of freedom for a tunable parameter γ. It should be stressed that the aforementioned defects are *inherent* to the energy-conserving LBE with no internal degrees of freedom derived in the preceding sections and cannot be removed by, *e.g.*, increasing the number of discrete velocities alone. However, it should be stressed that this is perhaps not a pressing issue concerning LBE's capability to simulate fully compressible viscous flow.

There are several avenues to circumvent the aforementioned defects. First, it has been observed that some shortcomings of the energy-conserving LBE can be easily removed by simply separating the energy conservation from the mass and momentum conservation in the spirit of Boussinesq approximation [151,184]. In 2D, for instance, the mass and momentum conservation is solved by the D2Q9 model, while the energy conservation can be separately solved by either a finite-difference scheme [151,184,185] or the D2Q5 LB model [140,172,185–188]. In the approach with dual distribution functions, one set for mass-momentum conservation and the other for the energy conservation, the viscosity and heat diffusivity can be easily adjusted by the relaxation rates for the moments related to the viscous stresses and the energy fluxes, thus the Prandtl number Pr can be easily adjusted in a wide range. Also, the boundary conditions for the velocity and temperature fields can be consistently realized via the bounce-back boundary conditions [151,185], which are also easy to implement. The thermal LBE with dual distributions can adequately and effectively simulate near-incompressible thermal flows [172, 185,188,189] and enjoys some attractive properties, such as superior numerical stability while retaining the simplicity of the LBE algorithm [151]. Thus this approach appears to be the most widely used thermal LBE model [140,172,185,186,188,189].

Since the fully compressible Euler or NSF system can be derived from the LBE [81,177–182], there have been continuous efforts to extend the LBE for fully compressible thermal inviscid [190–199] or viscous flows [179,196,199–209] with shocks and contact discontinuities. There are essentially three approaches to extend the LBE for fully compressible flows. The first is to modify the equilibrium distribution function to extend the validity of the low-Mach number expansion. The equilibria of second-order polynomials in the LBE are basically the truncated Maclaurin series expansions of the Maxwellian (cf. Eq. (3.26) and (3.27)), which may become invalid when local Mach number grows sufficiently large, and thus are a major suspect responsible for the numerical instability observed in the thermal LBE. There are several alternative forms of the equilibria tailored to address this issue, *i.e.*, the Maxwellian (*i.e.*, the exponential) [196,204], the Dirac delta function [205–207], or polynomials of higher than second order [200,202,203,208]. However, it turns out that the Maxwellian type of equilibria [204] leads to a system of partial differential equations inconsistent with the Euler system at the leading order [195]. It is worth noting, in particular, that even though this system is shown to satisfy the entropic condition *i.e.*, the H theorem [204], it is nonetheless an ineffective approach for compressible flow simulation.

The second approach is to introduce the internal energy as an additional degree of freedom in the distribution functions [179,192–194,208–210] so to allow the adiabatic exponent γ to be an independent and tunable parameter.

The third approach is to abandon the approximation of the transport term $\partial_t f + \boldsymbol{\xi}\cdot\nabla f$ in the Boltzmann equation (2.1a) by exact "hopping" on lattice (cf. Eq. (3.17)):

$$\tilde{\mathbf{f}}(\boldsymbol{r}_j + \boldsymbol{\xi}\delta_t,\, t_n + \delta_t) = \tilde{\mathbf{f}}^*(\boldsymbol{r}_j,\, t_n), \quad \boldsymbol{r}_j,\, \boldsymbol{r}_j + \boldsymbol{\xi}_i \in \mathbb{Z}_d,$$

where $\tilde{\mathbf{f}}^*$ denotes the post-collision value of $\tilde{\mathbf{f}}$. Instead, the particle velocity $\boldsymbol{\xi}_i$ is decomposed into the local flow velocity $\boldsymbol{u}$ and the peculiar velocity $\boldsymbol{c}_i := \boldsymbol{\xi}_i - \boldsymbol{u}$ is fixed as a constant discrete velocity set, thus the "hopping" by $\boldsymbol{\xi}_i$ is adapted to the local flow velocity $\boldsymbol{u}$ and no longer from one lattice node to another, and interpolations or other means have to be used to obtain values of $\tilde{\mathbf{f}}$ on the underlying lattice [205–207]. Alternatively, the transport term can also be approximated with finite-difference schemes (or otherwise), such as backward Euler with respect to $\boldsymbol{\xi}_i$ [193], second-order total variation diminishing (TVD) scheme [194], Crank-Nicholson [208], or Beam-Warming method [179]. These "off-lattice" approaches immediately avoid the numerical instability intrinsic to the simple hopping-collision algorithm of the LBE [151]. It should also be noted that the above approaches are usually used in combination to effectively overcome the numerical instabilities in the thermal LBE. In addition, one can use asymmetric velocity sets, *i.e.*, $\mathbb{V}_q \neq -\mathbb{V}_q$, such that $\sum_i \boldsymbol{c}_i = \boldsymbol{U} \neq \boldsymbol{0}$. In essence, the use of the asymmetric velocity means that the expansions of the distribution functions are about the non-zero velocity $\boldsymbol{U}$, instead of at the rest frame of reference with $\boldsymbol{U} = \boldsymbol{0}$. Because $\boldsymbol{U}$ may vary in space, so does the asymmetric velocity set. Consequently, one of the important properties of the LBE, *i.e.*, $\nabla\cdot\boldsymbol{\xi}_i f_i = \boldsymbol{\xi}_i\cdot\nabla f_i$ no longer holds. In any event, the model of this type has yet to subject to rigorous analyses and tests.

Many of the aforementioned thermal LBE schemes have successfully simulated 1D shocks, *i.e.*, the Sod tests [190–192,194, 196,197,201], viscous flows [179,196,200,202,203,205,208] or more complex compressible flows with strong shocks, such as compressible flows over a forward-facing step [207]. It should be pointed out that the off-lattice approach must utilize

interpolations of some sort to approximate advection, which inevitably increase the higher-order numerical viscosities and therefore also improve the numerical stability. A specific effect of interpolations is that they annihilate the checker-board or staggered modes, which are the eigen-modes of the collision operator with the eigenvalue -1 [149,211].

The error of $O(u^3)$ due to the approximation of the equilibria using the second-order polynomial of $\mathbf{H}^{(n)}$ is the leading order error in terms of Ma which can be significant for high-speed compressible flows, and there have been a considerable effort to remove the u^3 error [145,146,200,202,203,208,212–216]. To illustrate the origin of the cubic error, D2Q9 model with the BGK collision model can serve as an example for the sake of simplicity. The second-order moment is

$$\mathbf{m}^{(2)} = \sum_i \boldsymbol{\xi}_i \boldsymbol{\xi}_i f_i = \tau_\nu \vartheta \rho [(\nabla \boldsymbol{u}) + (\nabla \boldsymbol{u})^\dagger] + \tau_\nu \nabla \cdot \rho \boldsymbol{uuu}, \tag{3.51}$$

where τ_ν is the relaxation time in the BGK model. The error term of $\nabla \cdot \rho \boldsymbol{uuu}$ is due to the second-order truncation of the equilibrium $f_i^{(0)}$ (cf. Eq. (3.27)). This term cannot be eliminated by including $O(\boldsymbol{u}^3)$ terms in $f_i^{(0)}$, because for the discrete velocities $\{\boldsymbol{\xi}_i\}$ with the components of $\{-1, 0, +1\}$, $\xi_{i\alpha}^3 = \xi_{i\alpha}$, $\alpha \in \{x, y\}$, consequently $\sum_i \boldsymbol{\xi}_i^3 f_i = \sum_i \boldsymbol{\xi}_i f_i$. That is, the third-order moment is incomplete and its non-zero components linearly depend on the first-order ones. Thus, a complete removal of the cubic error term $\nabla \cdot \rho \boldsymbol{uuu}$ requires not only the equilibria with the terms of $\boldsymbol{u}^3$, but also the discrete velocity set which can accommodate independent third-order moments [145,146,200,213]. A recently proposed model that replaces the velocities of $(\pm 1, \pm 1, \pm 1)$ in D3Q27 model with that of $(\pm 1/2, \pm 1/2, \pm 1/2)$ can effectively eliminate the cubic error term [217].

It has been shown that it requires 39 velocities in 3D to fully eliminate the cubic error by brute force [213], which significantly enhances the computational cost and communication band width requirement. Since degeneracies of moments are at the root of this problem, off-lattice velocity sets determined by the higher-order Gauss-Hermite quadratures have been proposed [218,219], however, this approach requires interpolation of distribution functions between lattice points which increases computational cost and may also introduce numerical instability [85] as well as dissipation at grid scales [151]. However, with the number of velocities less than the required order of symmetry, partial elimination of some terms related to cubic error is possible. For example, the D2Q17 model [146] with correct equilibria [212,220] can eliminate some terms of $\nabla \cdot \rho \boldsymbol{uuu}$. Even with the D2Q9 model, some cubic terms can be included in the equilibria [220]. Using u-dependent relaxation times for the mode corresponding to the diagonal components of the stress tensor can mitigate the remaining problems, reducing the error from $O(\mathrm{Ma}^3)$ to $O(\mathrm{Ma}^5)$ [159,214]. A cancellation of the cubic term can also be realized by explicitly including the necessary terms obtained by finite difference [215]. For multi-phase or multi-component flows, explicit inclusion of the density gradient $\nabla \rho$ in the forcing term can eliminate the term $\boldsymbol{uuu} \cdot \nabla \rho$, which is significant in the interface region [216,221].

It is a fair observation that the thermal LBE for fully compressible flows is not as mature as its athermal counterpart. Much of the efforts along this direction are from the physics perspective based on the kinetic theory, as indicated in the preceding discussions, and not so much on the numerics pertaining to the compressible flows. Thus, it should be noted that correct and effective numerical techniques are essential for compressible flow simulations. For instance, the lattice Boltzmann schemes with a symmetric discrete velocity set are in fact connected to the central difference schemes [86,87,222], while the techniques based on upwind method are prevailing and preferred treatments for compressible flows (cf., *e.g.*, [223]), and yet they have not been effectively incorporated into the LB method [220,224–230]. Nevertheless, the efforts to reformulate the LBE using some mature techniques which have been widely used in CFD have begun [198,199,231–236], but the benefits, if any, of these approaches remain to be seen. The issue one must keep in mind is how to make the LB method effective for the compressible flow simulation while maintaining its simplicity and numerical efficiency. Clearly, much more analysis along this direction is still waiting to be done.

Finally, we would like to mention that the LBE has been successfully applied to simulate aeroacoustics [237–251]. The reason attributing to the success of the LBE simulation of aeroacoustics seems to be the fact that the LBE has a relatively low numerical dissipation [149,151] thus high fidelity.

3.9. Cumulant lattice Boltzmann equation (CLBE)

Before we proceed to discuss the details of the cumulant LBE, a brief introduction of some pertaining concepts seems to be in order. For a probability density distribution function $f(x)$, its moments $\{\mu_n\}$

$$\mu_n := \langle x^n \rangle := \int x^n f(x)\, \mathrm{d}x, \quad n \geq 0, \tag{3.52}$$

can be generated by the moment generating function of $f(x)$ (cf., *e.g.*, [252])

$$m(t) := \langle e^{tx} \rangle := \int f(x) e^{tx}\, \mathrm{d}x = \sum_n \frac{t^n}{n!} \mu_n. \tag{3.53}$$

It is sometime convenient to use the moments about the mean, *i.e.*,

$$\chi_n := \langle (x - \mu_1)^n \rangle := \int (x - \mu_1)^n f(x)\, \mathrm{d}x, \tag{3.54}$$

of which the generating function is

$$M(t) := \langle e^{t(x-\mu_1)} \rangle := \int f(x) e^{t(x-\mu_1)} \, \mathrm{d}x = \sum_n \frac{t^n}{n!} \chi_n. \tag{3.55}$$

Obviously,

$$\mu_n = \left. \frac{\mathrm{d}^n m(t)}{\mathrm{d}t^n} \right|_{t=0} \quad \text{and} \quad \chi_n = \left. \frac{\mathrm{d}^n M(t)}{\mathrm{d}t^n} \right|_{t=0}.$$

Suppose

$$\kappa(t) := \ln m(t) := \kappa_0 + \kappa_1 t + \frac{\kappa_2}{2!} t^2 + \cdots + \frac{\kappa_n}{n!} t^n + \cdots, \tag{3.56}$$

then the function $\kappa(t)$ is the cumulant generating function for cumulants $\{\kappa_i\}$, *i.e.*, $\kappa_n = \mathrm{d}^n \kappa(t)/\mathrm{d}t^n$ at $t = 0$. It can be seen that the first few cumulants are:

$$\kappa_i = \mu_i, \quad \kappa_{2,3} = \chi_{2,3}, \quad \kappa_4 = \chi_4 - 3\chi_2^2.$$

The usefulness of the cumulant representation can be seen through the example of the normal distribution

$$f(x) = \frac{1}{\sigma\sqrt{2\pi}} e^{-(x-x_0)^2/2\sigma^2},$$

which has an infinite number of nonzero moments, but only two non-zero cumulants:

$$\kappa_1 = x_0, \quad \kappa_2 = \frac{1}{\sigma^2}, \quad \kappa_n = 0 \; \forall n \geq 3.$$

The MRT LBE derived in the preceding sections is based on the moments of the microscopic velocity $\boldsymbol{\xi}$. The cumulant LBE is based on the moments of the peculiar velocity $\boldsymbol{c} := (\boldsymbol{\xi} - \boldsymbol{u})$ [253–257]. Let $F(\boldsymbol{x}, \boldsymbol{K}, t)$ be the generating function of the distribution function $f(\boldsymbol{x}, \boldsymbol{c}, t)$, *i.e.*, $F(\boldsymbol{x}, \boldsymbol{K}, t) := \langle e^{\boldsymbol{K}\cdot\boldsymbol{c}} f \rangle$, then the corresponding cumulants are [159]:

$$C_{lmn}(\boldsymbol{x}, t) := c^{-(l+m+n)} \left. \frac{\partial^l \partial^m \partial^n \ln F}{\partial K_x^l \partial K_y^m \partial K_z^n} \right|_{\boldsymbol{K}=\boldsymbol{0}}, \quad \boldsymbol{K} := (K_x, K_y, K_z). \tag{3.57}$$

For the Maxwell-Boltzmann equilibrium $f^{(0)}$,

$$\ln F^{(0)} = \ln(\rho/\rho_0) - \boldsymbol{K}\cdot\boldsymbol{u} + \frac{c^2\vartheta}{2} \boldsymbol{K}\cdot\boldsymbol{K}, \tag{3.58}$$

thus the equilibrium has $(d+2)$ non-zero cumulants in d dimensions in terms of ρ, $\boldsymbol{u}$ and ϑ.

The collision in terms of the cumulants $\{C_{lmn}\}$ can be taken to be:

$$C^*_{lmn} = C_{lmn} - s_{lmn}\left[C_{lmn} - C^{(0)}_{lmn}\right], \tag{3.59}$$

where C_{lmn} and C^*_{lmn} denote the pre- and post-collision value of a cumulant, $C^{(0)}_{lmn}$ denotes the equilibrium of C_{lmn}, and $s_{lmn} \in (0, 2)$ is the relaxation rate for the cumulant C_{lmn}. When $\ln F$ is given in terms of a finite number of cumulants $\{C_{lmn}\}$, the distribution function, $f(\boldsymbol{x}, \boldsymbol{\xi}, t)$ can be obtained by inverse Fourier transform of F. In the case of the LBE, the finite number of linearly independent cumulants $\{C_{lmn}\}$ is equal to that of the discrete velocities $\{\boldsymbol{\xi}_i\}$. However, the higher-order cumulants depend on the lower-order ones in a complicated nonlinear manner [253–257]. For this reason, the cumulant LBE with an SRT collision model differs significantly from its LBGK counterpart based on the moments, because the relaxation of a lower-order moment affects that for the next order moment, which is not the case for the LBE based on moments, which are orthogonal to each other.

Perhaps the most noteworthy feature of the cumulant presentation is the elimination of redundancy of the moment representation. As demonstrated in Eq. (3.58), the equilibrium has only nonzero cumulants up to second order, all higher order cumulants are zero. In contrast, there is an infinite number of nonzero moments of the equilibrium, which are products of ρ, $\boldsymbol{u}$ and ϑ. Thus, the non-zero higher-order cumulants represent the nonequilibrium information which is not present in lower-order cumulants. It is also observed that the cumulant LBE has superior stability [258] which cannot be explained by linear analysis.

3.10. Other models and further developments

The lattice Boltzmann equation has also been developed for viscoelastic fluids [150,259–261] and magnetohydrodynamics [262–265]. The gist of these LBE models is the construction of certain second-order tensors and relaxation processes (collision operator) appropriate to the physics. In addition, the fluctuating LBE [152,153,155,266–268] has been formulated to simulate fluctuating hydrodynamics [269]. The fluctuating LBE relies on the correct implementation of the viscous stress tensor with fluctuations so that the fluctuation-dissipation theorem is obeyed. To do so, the orthogonal basis must be constructed with respect to the weights $\{w_i\}$ (cf. (3.33) and related discussions) [85,270].

It has been revealed that the LBE has direct connections to finite difference scheme [86,87,222,271] and the artificial compressibility method [90,91]. These revelations help us understand the LBE in terms of our knowledge about existing methods.

Another notable development is to extending the capability of the LBE beyond the hydrodynamics of NSF system. Since the number of discrete velocity is equal to that of moments in the LBE, the LBE capable of solving the kinetic equation would certainly require a larger number of discrete velocities than the LBE which is only adequate to solve the macroscopic hydrodynamic equations [272,273]. However, enlarging the discrete velocity set can be problematic if the exact streaming step is to be maintained, which requires the velocity set to conform with integer lattice (cf. Sec. 3.2), and this approach may be problematic because it is difficult to remove degeneracy among the moments [136] and to construct boundary conditions, among other issues.

One solution to the above problems is to abandon the exact streaming paradigm and instead employ interpolation methods to compute the advection and time stepping with finite-difference techniques. The finite-difference lattice Boltzmann (FDLB) method uses the so-called off-lattice velocity sets, which do not conform with the lattice structure in the LBE and which are often chosen to be some quadrature points. Also, instead of using the Hermite polynomials on the entire space (cf. (2.44) – (2.46) and related discussion), one can use the Hermite polynomials on the half space (half-range Hermite polynomials) [274–276]. These new approaches have shown some promising results for benchmark cases such as the Couette and Poiseuille flows in kinetic regime [277–281].

4. LBE: macroscopic equations, stability, and convergence

In what follows, we will show that the solution of the LBE for suitably constructed initial data has an asymptotic expansion in the lattice spacing δ_x, and the first two moments of the LBE solution converge to a solution of the incompressible Navier-Stokes equations for the corresponding initial data.

We first pose an expansion of the solution of the lattice Boltzmann equation as a formal power series in the lattice spacing $\delta_x := \varepsilon$, and use it to motivate expressions for the expansion coefficients $\{f^{(k)}(\boldsymbol{x}, t)\}$ in terms of their moments $\{\rho^{(k)}\}$ and $\{\boldsymbol{u}^{(k)}\}$ that satisfy a hierarchy of quasi-linear and linear PDEs. By considering the linear stability of perturbations to the global equilibrium with $\rho = 1$ and $\boldsymbol{u} = \boldsymbol{0}$, we show that the series so defined is in fact an asymptotic expansion of the solution of the LBE for initial conditions obtained from the $f^{(k)}(\boldsymbol{x}, t)$ at $t = 0$. We also show that the $\rho^{(2)}$ and $\boldsymbol{u}^{(1)}$ obtained from moments of this expansion converge to a solution of the incompressible Navier-Stokes equations. This approach is based on the Hilbert expansion in the sense that both the distribution function and conserved quantities are expanded (cf. §2.4.1).

The results given below have been presented as theorems for the LBE with the periodic boundary conditions [270,282–286] as well as the bounce-back boundary conditions [287], which will be discussed in §6. In what follows, all analyses are applied to the distribution functions f_i, as opposed to $\bar{f}_i$ (cf. the discussions in Sec. 3.3 and 3.6), *i.e.*, pertaining to the discretization with the first-order forward Euler method, as shown by (3.36) in the case of the BGK collision model, so the relaxation times and the relaxation rates are those without the correction of $\delta_t/2$.

4.1. Formal expansion to the solution of the LBE and macroscopic equations

To derive the *incompressible* Navier-Stokes equations from the LBE, we adopt the following dimensionless diffusive scaling:

$$\delta_x = \varepsilon, \quad \delta_t = \varepsilon^2. \tag{4.1}$$

The forcing term in the LBE corresponding to an external force density $\boldsymbol{F}$ in the Navier-Stokes equations can be approximated by:

$$G_i = 3 w_i \varepsilon^3 \boldsymbol{\xi}_i \cdot \boldsymbol{F}, \tag{4.2}$$

which is the first-order approximation in terms of the Hermite polynomials (or equivalently in terms of $\boldsymbol{u}$, cf. Eq. (3.14)). The solution $\mathbf{f}$ of the LBE (3.17) depends on ε as a parameter, *i.e.*, $\mathbf{f} := \mathbf{f}(\boldsymbol{x}_j, t_n; \varepsilon)$, so we seek the following formal expansion (*i.e.*, an ansatz or Strang expansion [288]):

$$\mathbf{f}(\boldsymbol{x}_j, t_n; \varepsilon) \sim \textstyle\sum_{k \geq 0} \varepsilon^k \mathbf{f}^{(k)}(\boldsymbol{x}_j, t_n). \tag{4.3}$$

Correspondingly, both ρ and $\boldsymbol{u}$ are given by:

$$\rho_\varepsilon \sim \textstyle\sum_{k\geq 0} \varepsilon^k \rho^{(k)}, \qquad \rho^{(k)} := \textstyle\sum_i f_i^{(k)}, \tag{4.4a}$$

$$\boldsymbol{u}_\varepsilon \sim \textstyle\sum_{k\geq 0} \varepsilon^k \boldsymbol{u}^{(k)}, \qquad \boldsymbol{u}^{(k)} := \textstyle\sum_i \boldsymbol{\xi}_i f_i^{(k)}. \tag{4.4b}$$

For now the right-hand sides of (4.3) and (4.4) are *formal* sums which we show later in §4.3 are in fact *asymptotic* expansions. The *ansatz* (4.3) is similar to the Hilbert expansion (cf. (2.24) in §2).

In the following analysis, define

$$\mathbf{f}^{(0)} := \mathbf{f}^{(0)}(\rho = 1, \boldsymbol{u} = \mathbf{0}) = \mathbf{w} := (w_0,\ w_1,\ \ldots,\ w_{q-1})^\dagger.$$

It follows from the definition of $\{w_i\}$, Eq. (4.4), and the symmetry of $\{\boldsymbol{\xi}_i\}$ that

$$\rho^{(0)} = 1, \quad \boldsymbol{u}^{(0)} = \mathbf{0}. \tag{4.5}$$

Define $\mathbf{R} := \mathbf{f}(\boldsymbol{x}_j + \boldsymbol{\xi}\varepsilon,\ t_n + \varepsilon^2) - \mathbf{f}(\boldsymbol{x}_j,\ t_n) - \mathbf{Q}(\boldsymbol{x}_j,\ t_n)$, and substitute the ansatz (4.3) into $\mathbf{R}$:

$$\begin{aligned}\mathbf{R} :=& \textstyle\sum_{k\geq 0} \varepsilon^k \mathbf{f}^{(k)}(\boldsymbol{x}_j + \boldsymbol{\xi}\varepsilon,\ t_n + \varepsilon^2) - \sum_{k\geq 0} \varepsilon^k \mathbf{f}^{(k)}(\boldsymbol{x}_j,\ t_n) \\ &+ \tilde{\mathbf{S}} \left[\textstyle\sum_k \varepsilon^k \mathbf{f}^{(k)} - \mathbf{f}^{(0)}(\sum_k \varepsilon^k \rho^{(k)},\ \sum_k \varepsilon^k \boldsymbol{u}^{(k)})\right](\boldsymbol{x}_j,\ t_n) - \varepsilon^3 \mathbf{G},\end{aligned} \tag{4.6}$$

where $\mathbf{G} := 3(0,\ w_1 \boldsymbol{\xi}_1 \cdot \boldsymbol{F},\ w_2 \boldsymbol{\xi}_2 \cdot \boldsymbol{F},\ \ldots,\ w_b \boldsymbol{\xi}_b \cdot \boldsymbol{F})^\dagger$, and $\tilde{\mathbf{S}} := \mathbf{M}^{-1}\mathbf{S}\mathbf{M}$. Using the Taylor expansion for $\mathbf{f}(\boldsymbol{x}_j + \boldsymbol{\xi}\delta_t,\ t_n + \delta_t)$, we have

$$\begin{aligned}\mathbf{R} =& \sum_{n>0,\, k\geq 0} \frac{\varepsilon^k}{n!} \mathbf{D}^n \mathbf{f}^{(k)} + \tilde{\mathbf{S}} \sum_{k\geq 0} \varepsilon^k \left[\mathbf{f}^{(k)} - \mathbf{f}_{\mathrm{L}}^{(0)}(\mathbf{f}^{(k)})\right] - \tilde{\mathbf{S}} \sum_{k\geq 0,\, q+p=k} \varepsilon^k \mathbf{f}_{\mathrm{Q}}^{(0)}(\boldsymbol{u}^{(p)},\ \boldsymbol{u}^{(q)}) - \varepsilon^3 \mathbf{G} \\ =& \sum_{l,\, k>0,\, m} \varepsilon^{k+m+l} \mathbf{D}^{[l+m]} \mathbf{f}^{(k)} + \tilde{\mathbf{S}} \sum_{k\geq 0} \varepsilon^k \left[\mathbf{f}^{(k)} - \mathbf{f}_{\mathrm{L}}^{(0)}(\mathbf{f}^{(k)})\right] - \tilde{\mathbf{S}} \sum_{k\geq 0,\, q+p=k} \varepsilon^k \mathbf{f}_{\mathrm{Q}}^{(0)}(\boldsymbol{u}^{(p)},\ \boldsymbol{u}^{(q)}) - \varepsilon^3 \mathbf{G}\end{aligned} \tag{4.7}$$

where $\mathbf{f}_{\mathrm{L}}^{(0)}$ and $\mathbf{f}_{\mathrm{Q}}^{(0)}$ are the parts of the local equilibrium that are linear and quadratic in $\boldsymbol{u}$, respectively,

$$\begin{aligned}\mathbf{D} :=& \operatorname{diag}\left(\varepsilon^2\partial_t,\ \varepsilon^2\partial_t + \varepsilon\boldsymbol{\xi}_1 \cdot \nabla,\ \ldots,\ \varepsilon^2\partial_t + \varepsilon\boldsymbol{\xi}_b \cdot \nabla\right) \\ =& \varepsilon \operatorname{diag}\left(\varepsilon\partial_t,\ \varepsilon\partial_t + \boldsymbol{\xi}_1 \cdot \nabla,\ \ldots,\ \varepsilon\partial_t + \boldsymbol{\xi}_b \cdot \nabla\right),\end{aligned} \tag{4.8}$$

$\mathbf{D}^{[k]}$ is the diagonal matrix operator with the diagonal elements

$$\mathbf{D}_i^{[k]} := \sum_{2m+n=k} \frac{\partial_t^m (\boldsymbol{\xi}_i \cdot \nabla)^n}{m!n!}.$$

Define $\bar{\imath}$ such that $\boldsymbol{\xi}_{\bar{\imath}} := -\boldsymbol{\xi}_i$, so $(\boldsymbol{\xi}_{\bar{\imath}} \cdot \nabla)^n = (-1)^n (\boldsymbol{\xi}_i \cdot \nabla)^n$, and it can be shown that

$$\mathrm{D}_{\bar{\imath}}^{[k]} = (-1)^k \mathrm{D}_i^{[k]}. \tag{4.9}$$

Equating the coefficients of ε^n for $n \geq 0$ in the right-hand side of (4.7) to zero gives the following hierarchy of equations similar to (2.25):

$$\mathbf{f}_{\mathrm{L}}^{(0)}(\mathbf{f}^{(1)}) - \mathbf{f}^{(1)} = \mathbf{0}, \tag{4.10a}$$

$$\mathbf{f}_{\mathrm{L}}^{(0)}(\mathbf{f}^{(2)}) - \mathbf{f}^{(2)} = \tilde{\mathbf{S}}^{-1} \mathbf{D}^{[1]} \mathbf{f}^{(1)} - \mathbf{f}_{\mathrm{Q}}^{(0)}(\boldsymbol{u}^{(1)},\ \boldsymbol{u}^{(1)}), \tag{4.10b}$$

$$\mathbf{f}_{\mathrm{L}}^{(0)}(\mathbf{f}^{(3)}) - \mathbf{f}^{(3)} = \tilde{\mathbf{S}}^{-1} \left(\mathbf{D}^{[1]} \mathbf{f}^{(2)} + \mathbf{D}^{[2]} \mathbf{f}^{(1)} - \mathbf{G}\right) - 2\mathbf{f}_{\mathrm{Q}}^{(0)}(\boldsymbol{u}^{(1)},\ \boldsymbol{u}^{(2)}), \tag{4.10c}$$

$$\mathbf{f}_{\mathrm{L}}^{(0)}(\mathbf{f}^{(k)}) - \mathbf{f}^{(k)} = \sum_{n=1}^{k-1} \left(\tilde{\mathbf{S}} \mathbf{D}^{[n]} \mathbf{f}^{(k-n)} - \mathbf{f}_{\mathrm{Q}}^{(0)}(\boldsymbol{u}^{(n)},\ \boldsymbol{u}^{(k-n)})\right),\ k \geq 4, \tag{4.10d}$$

where $\mathbf{f}_{\mathrm{L}}^{(0)}$ and $\mathbf{f}_{\mathrm{Q}}^{(0)}$ are defined under (4.7).

The $\rho^{(n)}$ and $\boldsymbol{u}^{(n)}$, for $n = 1, 2, \ldots, k$, are uniquely determined as solutions of the hierarchy of PDEs implied by (4.10) [282,283]. In particular, $\rho^{(1)} \equiv 0$; and $(\rho^{(2)},\ \boldsymbol{u}^{(1)})$ satisfies the incompressible Navier-Stokes equations:

$$\nabla \cdot \boldsymbol{u}^{(1)} = 0, \quad \partial_t \boldsymbol{u}^{(1)} + \nabla \cdot (\boldsymbol{u}^{(1)} \boldsymbol{u}^{(1)}) = -\nabla p + \nu \nabla^2 \boldsymbol{u}^{(1)} + \boldsymbol{F}, \tag{4.11}$$

where $p := \rho^{(2)}/3$, and $\nu := (1/s_3 - 1/2)/3$ [171], provided that $s_3 = s_4$ (cf. (3.25) for the definition of relaxation rates $\{s_i\}$). The $\rho^{(n)}$ for $n \geq 3$ and $\boldsymbol{u}^{(n)}$ for $n \geq 2$ are solutions of linear PDEs of Oseen type. We will show that (4.11) are indeed the macroscopic equations solved by the LBE in the diffusive scaling.

Define the truncated expansion $\widehat{\mathbf{f}}$ for $\mathbf{f}$ as the following:

$$\widehat{\mathbf{f}} := \sum_{k=0}^{2m+1} \varepsilon^k \mathbf{f}^{(k)}, \quad m \geq 2, \tag{4.12}$$

and correspondingly

$$\widehat{\rho} = 1 + \sum_{k=1}^{m} \varepsilon^{2k} \rho^{(2k)}, \quad \widehat{\boldsymbol{u}} = \varepsilon \boldsymbol{u}^{(1)} + \sum_{k=1}^{m} \varepsilon^{2k+1} \boldsymbol{u}^{(2k+1)}, \tag{4.13}$$

so $\widehat{\mathbf{f}}$ satisfies the equation

$$\widehat{\mathbf{f}}(\boldsymbol{x}_j + \varepsilon\boldsymbol{\xi},\, t_n + \varepsilon^2) = \widehat{\mathbf{f}}(\boldsymbol{x}_j\, t_n) + \mathbf{Q}(\widehat{\mathbf{f}}) + \varepsilon^3 \mathbf{G} + O(\varepsilon^{2(m+1)}). \tag{4.14}$$

In spite of this, we cannot claim *a priori* that the LB solution is close to $\widehat{\mathbf{f}}$.

The difference $\delta\mathbf{f} := \mathbf{f} - \widehat{\mathbf{f}}$ between $\widehat{\mathbf{f}}$ and $\mathbf{f}$ satisfies

$$\delta\mathbf{f}(\boldsymbol{x}_j + \varepsilon\boldsymbol{\xi},\, t_n + \varepsilon^2) = \delta\mathbf{f}(\boldsymbol{x}_j,\, t_n) + \mathbf{Q}(\mathbf{f}) - \mathbf{Q}(\widehat{\mathbf{f}}) + O(\varepsilon^{2(m+1)}). \tag{4.15}$$

Our convergence proof will be based on this equation.

4.2. Linear stability of the absolute equilibrium

Consider the linearized lattice Boltzmann equation:

$$\mathbf{f}(\boldsymbol{x}_j + \boldsymbol{\xi}\delta_t,\, t_n + \delta_t) = \mathbf{f}(\boldsymbol{x}_j,\, t_n) + \mathbf{J}\mathbf{f}(\boldsymbol{x}_j,\, t_n) = (\mathbf{I} + \mathbf{J})\mathbf{f}(\boldsymbol{x}_j,\, t_n), \tag{4.16}$$

where $\mathbf{J}$ is the Jacobian matrix at the absolute equilibrium corresponding to the quiescent state of $\rho = 1$ and $\boldsymbol{u} = \mathbf{0}$:

$$\mathbf{J} := \left.\frac{\partial \mathbf{Q}}{\partial \mathbf{f}}\right|_{\substack{\rho=1 \\ \boldsymbol{u}=\mathbf{0}}} = -\tilde{\mathbf{S}}\,(\mathbf{I} - \mathbf{W}\mathbf{E}), \qquad \mathbf{W} := \operatorname{diag}\left(w_0,\, w_1,\, \ldots,\, w_{q-1}\right), \tag{4.17a}$$

$$\mathbf{E} := \frac{\partial \mathbf{W}^{-1}\mathbf{f}^{(0)}}{\partial \mathbf{f}}, \qquad \mathrm{E}_{ij} := \frac{1}{w_i}\frac{\partial f_i^{(0)}}{\partial f_j} = \left(1 + \frac{\boldsymbol{\xi}_i \cdot \boldsymbol{\xi}_j}{c_s^2}\right). \tag{4.17b}$$

The Jacobian $\mathbf{J}$ can be diagonalized as

$$\mathbf{P}\mathbf{J}\mathbf{P}^{-1} = -\boldsymbol{\Lambda}, \quad \boldsymbol{\Lambda} := \operatorname{diag}\left(0,\, 0,\, 0,\, s_3,\, \ldots,\, s_{q-1}\right), \quad s_i \geq 0, \tag{4.18}$$

where $\mathbf{P} \in \mathbb{R}^{q\times q}$ in general for a model with q velocities, $\mathbf{P}^\dagger\mathbf{P} = \mathbf{W}^{-1}$, and $\boldsymbol{\Lambda}$ is in fact the diagonal matrix $\mathbf{S}$ of relaxation rates given in (3.25), except that the relaxation rates for the conserved modes are set to be zero in $\boldsymbol{\Lambda}$, as opposed to 1 in $\mathbf{S}$. The matrix $\mathbf{P}$ can be easily constructed explicitly [85,270]. Just as $\mathbf{M}$ maps the $\{f_i\}$ to the moments $\{m_i\}$, $\mathbf{P}^\dagger$ maps the $\{f_i\}$ to some other set of moments [85,270]. The structure of $\mathbf{J}$ can also be related to an Onsager-like relation for the LBE [286]. The reason why the Jacobian $\mathbf{J}$ can be diagonalized is the following. The matrices $\mathbf{E}$, $\mathbf{W}$, and $\mathbf{S}$ are all real and symmetric. And $\mathbf{M}$ can be made orthogonal by normalizing its row vectors (cf. §3.5). Thus, $\mathbf{J}$ can be made symmetric, hence is diagonalizable.

The property of $\mathbf{J}$ immediately leads to the stability of the linearized LBE (4.16) on a periodic domain with a weighted L^2 norm [270]:

$$|\mathbf{P}\mathbf{f}(\cdot,\, t_n)|_2 = |\mathbf{P}\,(\mathbf{I} + \mathbf{J})\,\mathbf{P}^{-1}\mathbf{P}\mathbf{f}(\cdot,\, t_{n-1})|_2 = |\left(\mathbf{I} - \boldsymbol{\Lambda}\right)\mathbf{P}\mathbf{f}(\cdot,\, t_{n-1})|_2 \leq |\mathbf{P}\mathbf{f}(\cdot,\, t_{n-1})|_2 \leq |\mathbf{P}\mathbf{f}(\cdot,\, 0)|_2, \tag{4.19}$$

if $s_i \in [0,\, 2]$ for non-conserved moments, and the equality holds when $s_i = 2$, where $|\cdot|_2$ is defined as

$$|\mathbf{f}(\cdot)|_2^2 := \sum_j |\mathbf{f}(\boldsymbol{x}_j)|^2,$$

which is a finite sum on a periodic or bounded domain.

4.3. Convergence

Based on the error equation (4.15) and the property (4.18) of $\mathbf{J}$ with $s_i \in (0,\, 2)$ for the non-conserved moments, we use an energy argument to obtain

$$|\mathbf{P}\delta\mathbf{f}(\cdot,\, t_{n+1})|^2 \leq (1 + c\varepsilon)|\mathbf{P}\delta\mathbf{f}(\cdot,\, t_n)|^2 + c|\mathbf{P}\delta\mathbf{f}(\cdot,\, t_n)|^4 + O(\varepsilon^{4m+2}). \tag{4.20}$$

It must be emphasized that the above inequality needed for the convergence requires $s_i \in (0, 2)$ for non-conserved moments, as opposed $s_i \in [0, 2]$ needed for linear stability (cf. (4.20) in the previous section). To control the $|\mathbf{P}\delta\mathbf{f}(\cdot, t_n)|^4$ term relative to the $|\mathbf{P}\delta\mathbf{f}(\cdot, t_n)|^2$ term in the above inequality with a sufficiently small h and the following initial conditions:

$$\mathbf{f}(\boldsymbol{x}_j, 0) = \sum_{k=0}^{2m-1} \varepsilon^k \mathbf{f}^{(k)}(\boldsymbol{x}_j, 0), \tag{4.21}$$

an inductive argument establishes that

$$|\mathbf{P}\delta\mathbf{f}(\cdot, t_n)|^2 = o(\varepsilon). \tag{4.22}$$

Consequently, (4.20) reduces to

$$|\mathbf{P}\delta\mathbf{f}(\cdot, t_{n+1})|^2 \le (1 + C\varepsilon)|\mathbf{P}\delta\mathbf{f}(\cdot, t_n)|^2 + O(\varepsilon^{4m+2}), \tag{4.23}$$

where C is a constant independent of both n and h, and for a given fixed T:

$$|\mathbf{P}\delta\mathbf{f}(t_n)|_2^2 \le \left(1 + C\varepsilon^2\right)^n |\mathbf{P}\delta\mathbf{f}(0)|_2^2 + CT\varepsilon^{4m}, \tag{4.24}$$

for $0 \le t_n = n\varepsilon^2 \le T$. Therefore, the solution of the LBE (3.17) with the initial conditions (4.21) can be given by the following *asymptotic* expansion:

$$\mathbf{f}(\boldsymbol{x}_j, t_n) = \widehat{\mathbf{f}}(\boldsymbol{x}_j, t_n) + O(\varepsilon^{2m}) = \sum_{k=0}^{2m-1} \varepsilon^k \mathbf{f}^{(k)}(\boldsymbol{x}_j, t_n) + O(\varepsilon^{2m}), \tag{4.25}$$

in the interval of time $0 \le t_n = n\varepsilon^2 \le T$.

Now assume the initial conditions are such that $\rho^{(2k+1)}|_{t=0} = 0$ and $\boldsymbol{u}^{(2k)}|_{t=0} = \mathbf{0}$ for $k \ge 0$, and $s_3 = s_4$, then, with the periodic boundary conditions, the expansion coefficients possess the following property due to the symmetry of the velocity set $\{\boldsymbol{\xi}_i\}$:

$$f_i^{(k)} = (-1)^k f_{\bar{i}}^{(k)}, \quad \boldsymbol{\xi}_{\bar{i}} := -\boldsymbol{\xi}_i.$$

Consequently, the density and velocity moments of the LB solution $f_i = f_i(x, t; \varepsilon)$ can be expanded as

$$\rho_\varepsilon := \sum_i f_i \sim \sum_{k\ge 0} \varepsilon^k \rho^{(k)} = 1 + \varepsilon^2\rho^{(2)} + \varepsilon^4\rho^{(4)} + \varepsilon^6\rho^{(6)} + \cdots,$$
$$\boldsymbol{u}_\varepsilon := \sum_i \boldsymbol{\xi}_i f_i \sim \sum_{k\ge 0} \varepsilon^k \boldsymbol{u}^{(k)} = \varepsilon\boldsymbol{u}^{(1)} + \varepsilon^3\boldsymbol{u}^{(3)} + \varepsilon^5\boldsymbol{u}^{(5)} + \cdots,$$

so from (4.25) with $m \ge 2$, we have

$$\frac{\rho_\varepsilon - 1}{\varepsilon^2} - \rho^{(2)} = \varepsilon^2\left(\rho^{(4)} + \varepsilon^2\rho^{(6)} + \cdots + \varepsilon^{2(m-3)}\rho^{(2m-2)}\right) + O(\varepsilon^{2(m-1)}) = O(\varepsilon^2), \tag{4.26a}$$

$$\frac{\boldsymbol{u}_\varepsilon}{\varepsilon} - \boldsymbol{u}^{(1)} = \varepsilon^2\left(\boldsymbol{u}^{(3)} + \varepsilon^2\boldsymbol{u}^{(5)} + \cdots + \varepsilon^{2(m-2)}\boldsymbol{u}^{(2m-1)}\right) + O(\varepsilon^{2m-1}) = O(\varepsilon^2). \tag{4.26b}$$

Therefore the rescaled moments $(\rho_\varepsilon - 1)/\varepsilon^2$ and $\boldsymbol{u}_\varepsilon/\varepsilon$ obtained by the LBE (3.17) are indeed the approximations of the pressure $p := \rho^{(2)}/3$ and the velocity $\boldsymbol{u}^{(1)}$, respectively, with second-order accuracy in space and first-order accuracy in time.

One can also use (4.26) to compute the solutions of a higher-order accuracy based on the Richardson extrapolation [289]. By computing, for example, a solution $\rho_{\varepsilon/2}$ with grid spacing $\varepsilon/2$, then combine

$$\frac{\rho_{\varepsilon/2} - 1}{\varepsilon^2/4} - \rho^{(2)} = \varepsilon^2\left(\frac{1}{4}\rho^{(4)} + \frac{\varepsilon^2}{16}\rho^{(6)} + \ldots\right) = O(\varepsilon^2), \tag{4.27}$$

with ρ_ε in (4.26) and $m \ge 3$, we have

$$\frac{16\rho_{\varepsilon/2} - \rho_\varepsilon - 15}{3\varepsilon^2} - \rho^{(2)} = -\frac{\varepsilon^4}{4}\rho^{(6)} + \ldots = O(\varepsilon^4), \tag{4.28}$$

and similarly for the velocity field, we have

$$\frac{8\boldsymbol{u}_{\varepsilon/2} - \boldsymbol{u}_\varepsilon}{3\varepsilon^2} - \boldsymbol{u}^{(1)} = -\frac{\varepsilon^4}{4}\boldsymbol{u}^{(5)} + \ldots = O(\varepsilon^4). \tag{4.29}$$

Therefore, both ρ and $\boldsymbol{u}$ can achieve fourth-order convergence via above extrapolations.

4.4. Further results and discussions

In preceding sections, we proved that the LBE (3.17) with the collision model (3.25) indeed approximates the incompressible Navier-Stokes equations in the diffusive limit with first-order accuracy in time and second-order accuracy in space, thus the rigorous analysis of the LBE is established. The accuracy of the LBE with a forcing term can also be shown through Strang splitting [141].

The proofs can be extended to generalized Newtonian fluids with a non-constant viscosity depending on local fields [290], *e.g.*, such as the shear-stress dependent viscosity $\nu = \nu(\|\boldsymbol{\Sigma}\|)$ used in the Smagorinsky model for large-eddy simulation of turbulent flows [291–298] or the power-law fluids [148,296,299–308].

While the *linear* stability of the LBE can be proven, it must be stressed that the LBE does not have an H theorem [309,310]. Also, these theoretical analysis do not address one important issue related to the computational efficiency of the LBE, *i.e.*, the maximum and optimal time-step size possible under certain flow conditions.

With the diffusive scaling, the limit of $\delta_x^2 \sim \delta_t \to 0$ is equivalent to the limit of $\mathrm{Ma} \to 0$ (cf., §2.2 and *e.g.*, [106,108]). One may work with departures from uniform equilibrium at density ρ_0. Thus, the difference between the equilibrium (3.27) and the absolute equilibrium $f_i^{(0)}(\rho = 1, \boldsymbol{u} = 0)$ can be approximated by [311]:

$$f_i^{(0)} = w_i \left\{ \delta\rho + 3\boldsymbol{\xi}_i \cdot \boldsymbol{u} + \frac{1}{2}\left[9(\boldsymbol{\xi}_i \cdot \boldsymbol{u})^2 - 3\boldsymbol{u} \cdot \boldsymbol{u} \right] \right\}, \tag{4.30}$$

where $\delta\rho := \rho - \rho^{(0)}$ with $\rho^{(0)} = 1$. And in the equilibrium moments of (3.26), ρ is replaced by $\delta\rho$ in $m_0^{(0)}$ and by 1 in all other equilibrium moments $\{m_i^{(0)} | i \geq 1\}$. This practice can improve the computational efficiency slightly [312], however, it introduces some unwanted terms in the viscous stress [214] and an error of $O(\mathrm{Ma}^2)$ in the acoustic waves (cf. related discussion in §5.2).

It should be mentioned that the compressible Navier-Stokes equations can be derived from the LBE with acoustic scaling $\delta_x \sim \delta_t$ through either the Chapman-Enskog analysis [80,81] or Maxwell iteration [313]. However, this does not mean that the LBE based on truncated expansion of the Maxwell equilibrium can simulate fully compressible flows with $\mathrm{Ma} > 1$, because it is still inherently limited by the low-Mach-number approximation of $f^{(0)}$ discussed in §3.1.

With the acoustic scaling $\delta_x = O(\delta_t)$, the stress can be obtained through the Chapman-Enskog analysis of the second-order moments m_4 and m_5, or equivalently the nonequilibrium momentum flux [314], or the Maxwell iteration [313]:

$$\begin{aligned} \boldsymbol{\Sigma} &= -\textstyle\sum_i \boldsymbol{\xi}_i \boldsymbol{\xi}_i \dfrac{(f_i - f_i^{(0)}) + (f_i^* - f_i^{(0)})}{2} \\ &= \rho\nu \left[(\nabla \boldsymbol{u}) + (\nabla \boldsymbol{u})^\dagger - \frac{2}{d}(\nabla \cdot \boldsymbol{u})\mathbf{I} \right] + \rho\zeta\, (\nabla \cdot \boldsymbol{u})\mathbf{I} + O(\delta_t^2) + \delta_t O(\mathrm{Ma}^3), \end{aligned} \tag{4.31}$$

where f_i and f_i^* the pre- and post-collision state, respectively, and the kinematic shear viscosity ν and bulk viscosity ζ [171] of the D2Q9 model are:

$$\nu = \frac{1}{3}\left(\frac{1}{s_\nu} - \frac{1}{2} \right), \quad \zeta = \frac{1}{3}\left(\frac{1}{s_e} - \frac{1}{2} \right). \tag{4.32}$$

If the discretization error of $O(\delta_t^2)$ is of the same order of the truncation error of $\delta_t O(\mathrm{Ma}^3)$ due to low-Mach-number expansion, then we have $\mathrm{Ma} = O(\delta_t^{1/3})$, which suggests how the Mach number should decrease as δ_t decreases under the acoustic scaling. The above results show that the LBE yields the stress $\boldsymbol{\Sigma}$ with a second-order accuracy [287,313]. Note that with the diffusive scaling, the term with the bulk viscosity, $\rho\zeta\,(\nabla \cdot \boldsymbol{u})\mathbf{I}$, disappears as it is an error term of the order $\delta_t O(\mathrm{Ma}^3)$, which is one-order smaller than truncation error of $O(\delta_t^2)$, and thus cannot be picked up in the analysis with the diffusive scaling of $\delta_t \sim \delta_x^2 \sim \varepsilon^2$.

5. Fourier-von Neumann analysis and equivalent equations

There are two types of errors in the LBE: (a) modeling error due to approximations such as linearization of collision term and the truncation of the low-Mach-number expansion, and (b) discretization error due to finite δ_x and δ_t. The LBE is inherently limited on available number of degrees of freedom (or the number of adjustable parameters). In the LBE, the intrinsic "scales" in the units of δ_x and δ_t include relaxation times $\tau_i := 1/s_i$ for the non-conserved moments and the speed of sound $c_s = O(c)$, $c := \delta_x/\delta_t$. In a simulation with the macroscopic characteristic length L, time T, and speed U, the macroscopic equations (4.11) are valid only in the limit of $L \gg \delta_x$, $T \gg \delta_t$, and $U \ll c_s$ for a continuum flow.

In addition to a very limited number of modes, the LBE does not have a vast separation between spatial-temporal scales of the macroscopic and "microscopic" modes, *i.e.*, the conserved and non-conserved modes, because the time scales of the modes are set by their relaxation times $\tau_i := 1/s_i$, and the ratios between s_i cannot be too large or numerical instability may be instigated. Given that the defects in the LBE are so conspicuous, it is imperative to quantify their numerical effects. In what follows we will discuss the *local* Fourier-von Neumann local analysis and the equivalent-equation analysis based on

the linearized LBE (4.16). It should be stressed again that the analysis in §4 only concerns the asymptotic behavior of the LBE in the diffusive limit of $\delta_t \sim \delta_x^2$ when $\delta_x \to 0$, whereas the local analysis presented in this section intends to analyze and hopefully minimize errors, whether due to discretization or modeling approximation, with a given set of parameters, including grid resolution and relaxation rates $\{s_i | 0 \le i \le b\}$.

It should be pointed out that the equivalent-equation analysis [315,316] and dispersion-equation analyses are fully equivalent to each other, except that the former is carried out in the real space $\boldsymbol{x}$ and uses spatial derivatives ordered in powers of δ_t, whereas the latter is in Fourier space $\boldsymbol{k}$ with terms ordered in powers of k. The equivalent-equation emphasizes the PDEs derived from the linearized LBE (4.16), whereas the dispersion equation stresses the small-scale effects in the LBE. The aim of these analyses is to expose, understand, and, hopefully, overcome, the artifacts and defects in the LBE algorithm.

5.1. Local Fourier-von Neumann analysis

For linear or linearized equations, the numerical and modeling defects can be analyzed via the Fourier-von Neumann analysis for the linearized LBE with $\boldsymbol{u} \neq \boldsymbol{0}$, which leads to the dispersion equation relating the wavevector $\boldsymbol{k}$ and the frequency ω. The *local* Fourier analysis seeks solutions in a uniform system in terms of plane waves, $\exp[-\imath \boldsymbol{k}\cdot\boldsymbol{x} + \imath\omega t]$. This can be illustrated *via* the Fourier analysis of the *linearized* compressible *athermal* Navier-Stokes equations derived from the MRT-LBE with a bulk viscosity ζ in d-dimensions (cf. Eq. (4.31) for the stress tensor):

$$\partial_t \rho + \boldsymbol{U}\cdot\nabla\rho + \nabla\cdot\boldsymbol{u} = 0, \tag{5.1a}$$

$$\partial_t \boldsymbol{u} + \boldsymbol{U}\cdot\nabla\boldsymbol{u} = -c_s^2\nabla\rho + \nu\nabla^2\boldsymbol{u} + \left(\frac{d-2}{d}\nu + \zeta\right)\nabla\nabla\cdot\boldsymbol{u}, \tag{5.1b}$$

where the unknowns ρ and $\boldsymbol{u}$ are assumed as small quantities, ρ is normalized by a constant density ρ_0, $\boldsymbol{U}$ is a constant flow velocity, and the equation of state $p = c_s^2\rho$ has been used. To study the system (5.1), we will decompose the velocity $\boldsymbol{u}$ into two parts: the longitudinal component $\boldsymbol{u}_\parallel$ along a given direction $\hat{\boldsymbol{k}}$ and the remaining transverse components $\boldsymbol{u}_\perp \perp \hat{\boldsymbol{k}}$ on the plane perpendicular to $\hat{\boldsymbol{k}}$, that is, $\boldsymbol{u} = \boldsymbol{u}_\parallel + \boldsymbol{u}_\perp = u_\parallel\hat{\boldsymbol{k}} + \boldsymbol{u}_\perp$, such that $\boldsymbol{u}_\parallel \in \mathbb{R}$ and $\boldsymbol{u}_\perp \in \mathbb{R}^{d-1}$. Here, by *isothermal* we mean that the energy is indeed a conserved quantity but also a constant in this case, so the energy equation (2.22c) disappears. This distinguishes from the *athermal* case, in which the energy is not conserved.

We will restrict ourselves in 2D space in the following analysis, *i.e.*, $d = 2$, so $\boldsymbol{u} = u_\parallel\hat{\boldsymbol{k}} + u_\perp\hat{\boldsymbol{k}}_\perp$, with $\hat{\boldsymbol{k}}_\perp \perp \hat{\boldsymbol{k}}$. By applying the Fourier transform of (5.1) in both space and time, (5.1) becomes the following set of homogeneous linear equations in 2D:

$$\begin{pmatrix} \omega' & k & 0 \\ c_s^2 k & \omega' - \imath\,(\nu+\zeta)k^2 & 0 \\ 0 & 0 & \omega' - \imath\,\nu k^2 \end{pmatrix} \begin{pmatrix} \rho \\ \tilde{u}_\parallel \\ \tilde{u}_\perp \end{pmatrix} = \begin{pmatrix} 0 \\ 0 \\ \boldsymbol{0} \end{pmatrix}, \tag{5.2}$$

where $\omega' := \omega + \boldsymbol{k}\cdot\boldsymbol{U}$. Nontrivial solutions exist if and only if the above 3×3 determinant (in general a $(d+1)\times(d+1)$ determinant) of the coefficient matrix in (5.2) is equal to zero, yielding the following solutions of ω's:

$$\omega_\perp = -\boldsymbol{U}\cdot\boldsymbol{k} + \imath k^2\nu, \tag{5.3a}$$

$$\omega_\pm = -\boldsymbol{U}\cdot\boldsymbol{k} \mp \frac{k}{2}\sqrt{4c_s^2 - k^2(\nu+\zeta)} + \frac{1}{2}\imath k^2(\nu+\zeta) \approx -(\boldsymbol{U}\cdot\boldsymbol{k} \pm c_s k) + \frac{1}{2}\imath k^2(\nu+\zeta), \tag{5.3b}$$

where the solution $\omega_\perp$ of (5.3a) comes from the bottom-right 1×1 block of the determinant in (5.2), which is decoupled from the other two modes in the system, and the solution $\omega_\pm$ of (5.3b) comes from the upper left 2×2 block. In general, the solution of the linearized Navier-Stokes equations includes two longitudinal acoustic waves ($\boldsymbol{u}_\parallel$ with $\omega_\pm$) and $(d-1)$ transverse shear waves ($\boldsymbol{u}_\perp$ with $\omega_\perp$). If the energy conservation is included, there is an additional mode for the heat diffusion, which is coupled to the acoustic modes. The dissipation affects the frequencies $\omega_\perp$ and $\omega_\parallel$, as shown in (5.3). If all the terms of k^2 or higher-order in terms of k in (5.3b) are neglected, the result reduces to the exact plane wave solutions corresponding to the linearized compressible Euler equations [269].

The solution of (5.3) shows that two acoustic modes propagate with the velocity $\boldsymbol{U}\cdot\hat{\boldsymbol{k}} \pm c_s$ along $\hat{\boldsymbol{k}}$ with the attenuation $\exp[-k^2(\nu+\zeta)t/2]$, and $(d-1)$ shear modes propagate with the speed $\boldsymbol{U}\cdot\hat{\boldsymbol{k}}$ with the attenuation $\exp(-k^2\nu t)$. Consistent with the order of accuracy of the LB method, the solutions (5.3) satisfy the Galilean invariance of the hydrodynamic equations, as evident in the term $\boldsymbol{U}\cdot\boldsymbol{k}$, and the rotational invariance (or isotropy), as evident in the fact that the speed of sound c_s and the attenuation are independent of the direction of $\boldsymbol{k}$ [149].

The above analysis can be applied to the discrete equation (4.16). The dispersion equation derived from the linearized LBE (4.16) differs from that of the linearized Navier-Stokes equations, and the differences can be analyzed to minimize the errors in the LBE. The Fourier transform of (4.16) is

$$\tilde{\mathbf{f}}(\boldsymbol{k}, t_n + \delta_t) = \mathbf{K}\cdot[\mathbf{I} + \mathbf{J}]\cdot\tilde{\mathbf{f}}(\boldsymbol{k}, t_n), \tag{5.4a}$$

$$\mathbf{K} := \mathrm{diag}\left(1,\ \exp(\imath\boldsymbol{k}\cdot\boldsymbol{\xi}_1),\ \exp(\imath\boldsymbol{k}\cdot\boldsymbol{\xi}_2),\ \ldots,\ \exp(\imath\boldsymbol{k}\cdot\boldsymbol{\xi}_b)\right), \tag{5.4b}$$

which can be recast as the following eigenvalue problem:

$$\mathbf{H}\tilde{\mathbf{f}}(\boldsymbol{k},\omega)=z\tilde{\mathbf{f}}(\boldsymbol{k},\omega),\quad \mathbf{H}:=\mathbf{K}[\mathbf{I}+\mathbf{J}],\quad z:=\exp(-\imath\omega\delta_t), \tag{5.5}$$

and the associated characteristic polynomial of degree q,

$$\det[\mathbf{H}-z\mathbf{I}]:=Z(z,\boldsymbol{k})=0, \tag{5.6}$$

determines the dispersion relation $\omega(\boldsymbol{k})=(\imath\ln z)/\delta_t$, which includes *all* possible parameters in the model. The LBE is linearly stable iff $|z_i|\le 1$, $\forall i$. In the case of the long wavelength limit of $\boldsymbol{k}\to\mathbf{0}$,

$$Z(z,\boldsymbol{k}=\mathbf{0})=(z-1)^{d_c}\textstyle\prod_{i=d_c+1}^{q}(z-1+s_i), \tag{5.7}$$

where d_c is the number of the conserved moments or the dimension of the null space of the collision operator $\mathbf{Q}$, thus $|Z(z,\mathbf{0})|\le 1$ naturally leads to $s_i\in[0,2]$ for the non-conserved moments, as discussed previously in §4. Another case worth noting is $k_x=k_y=\pi$ in 2D, *i.e.*, the shortest wavelength allowed, which corresponds to the so-called "checker-board" mode.

The dispersion-equation analysis must use the acoustic scaling, $\delta_x/\delta_t=1$, which is consistent with the compressible Navier-Stokes equations (5.1) to be analyzed. A technical reason for using the acoustic scaling is that, in the dispersion-equation analysis, the mass conservation equation has both derivatives of time and space, thus the time derivative ∂_t can be substituted by the gradient ∇ in the subsequent equations, as in the Chapman-Enskog analysis. However, with the diffusive scaling, the mass conservation equation reduces to $\nabla\cdot\boldsymbol{u}=0$, thus it cannot be used to replace ∂_t in the derivation.

The analytic solution of the dispersion equation (5.6) with perturbation expansion in $\boldsymbol{k}$ [149–151,317,318] is in principle straightforward but usually is tedious and even intractable. It is therefore useful to simplify (5.5) by using various approximations such as expansions of Chapman-Enskog, Hilbert, and Taylor, leading to equivalent equations.

5.2. Equivalent equation analysis

This section illustrates the equivalent-equation approach, which can be used to remove some defects in the LBE model and thus to optimize it [174,315,316,319–322].

To be concrete, we will consider the D2Q9 model which conserves the mass density ρ and the flow momentum $\rho\boldsymbol{u}:=\rho(u_x,u_y)$. For the *linearized* D2Q9 model with a constant $\boldsymbol{U}$, the first-order equivalent equation in terms of δ_t is:

$$\begin{pmatrix}\partial_t & \partial_x & \partial_y\\ \frac{1}{3}\partial_x-U_x\boldsymbol{U}\cdot\nabla & \bar{\mathcal{D}}_t+U_x\partial_x & U_x\partial_y\\ \frac{1}{3}\partial_y-U_y\boldsymbol{U}\cdot\nabla & U_y\partial_x & \bar{\mathcal{D}}_t+U_y\partial_y\end{pmatrix}\begin{pmatrix}\rho\\ \rho u_x\\ \rho u_y\end{pmatrix}=\begin{pmatrix}0\\0\\0\end{pmatrix}+O(\delta_t^2), \tag{5.8}$$

where $\nu:=(1/s_\nu-1/2)/3$, $\zeta:=(1/s_e-1/2)/3$, $\bar{\mathcal{D}}_t:=\partial_t+\boldsymbol{U}\cdot\nabla$, and s_ν is the relaxation rate for the second-order moments m_3 and m_4, and s_e is that for the second-order moment m_5 (cf. (3.26)). The propagation speed of sound waves in the frame of reference moving with the velocity $\boldsymbol{U}$ is $C_s=\pm c_s$ along the direction of $\boldsymbol{U}$, where $c_s:=(1/\sqrt{3})c$ is the speed of sound in the frame of reference at rest, for which the phase velocity of sound modes is $U\pm c_s$. The above equations are the compressible Euler equations plus some (undesirable) extra terms of $U\sim O(\mathrm{Ma})$ and $U^2\sim O(\mathrm{Ma}^2)$. The terms of $O(U^2)$ disappear with the "incompressible" LBE model (cf. the equilibria of (4.30)). The existence of these terms manifests the fact that the LBE model has a maximum speed, hence it cannot obey the Galilean invariance exactly. However, for the "incompressible" LBE model, which neglected the coupling between ρ and $\boldsymbol{u}$, the speed of sound is $C_s=U\pm c_s\sqrt{1+(U/c_s)^2}=U\pm c_s\sqrt{1+\mathrm{Ma}^2}$ [149]; that is, there is an error of $O(\mathrm{Ma}^2)$ in the speed of sound.

The second-order equivalent equation leads to the viscous term:

$$\begin{pmatrix}0 & 0 & 0\\ 0 & \nu\partial_{xx}+\zeta\Delta & \nu\partial_{xy}\\ 0 & \nu\partial_{xy} & \nu\partial_{yy}+\zeta\Delta\end{pmatrix}\begin{pmatrix}\rho\\ \rho u_x\\ \rho u_y\end{pmatrix}+O(\delta_t^3), \tag{5.9}$$

where $\Delta:=\nabla\cdot\nabla$ stands for the Laplacian. In the derivation, numerous terms of $O(U)$ have been neglected.

The equivalent equations up to $O(\delta_t^2)$ are consistent with the compressible Navier-Stokes equations as $U\to 0$. We also note that, in the equivalent equation of $O(\delta_t)$, the terms of $O(U)$ have no observable effect for finite values of U. A complete removal of these terms is impossible with the D2Q9 model.

The third-order equivalent equation affects the dispersion of sound waves. However, the result is too tedious to be included here.

The fourth order equation can be used to determine corrections to the shear viscosity as the shear mode relaxes at rate:

$$\omega=\nu k^2\left\{1-\left[\frac{1}{12}(1+36\nu(\nu-2\kappa'))+(1-54\nu\kappa')g(\theta)\right]k^2\right\}, \tag{5.10}$$

where $\kappa' := (1/s_q - 1/2)/3$, s_q is the relaxation rate for the third-order moments m_6 and m_7 (cf. (3.26)), and $g(\theta)$ is a function of the angle θ between $\boldsymbol{k}$ and the x axis (or $\boldsymbol{\xi}_1$). Removal of the angular (θ) dependence of the hyper-viscosity of the order $O(k^4)$ requires $\nu\kappa' = 1/54$, which leads to a relationship $s_q = s_q(s_\nu)$. As will be seen later in §6, the Dirichlet boundary condition for the velocity $\boldsymbol{u}$ requires a different s_ν-dependence of s_q. One can also set $\nu = 2\kappa = 1/(3\sqrt{3})$ so that the hyper-viscosity of $O(k^4)$ can be removed and the damping of the shear modes becomes fourth-order accurate [241].

The analysis based on the dispersion-equation reveals that the transport coefficients at small scales, *i.e.*, large wave-number k, are severely anisotropic and dispersive. This affects simulations at small scales. Therefore, one must be cautious about the validity and limitations of the LBE simulation at small scales comparable to the grid spacing.

The difference between the analysis based on the equivalent-equations and the dispersion-equation should be noted. The former is devised to derive macroscopic equations involving space derivatives beyond second-order so to identify the conditions to improve numerical *accuracy*. Whilst the latter, *i.e.*, the numerical determination of eigenvalues of the dispersion equation, is used to determine the numerical *stability* of the scheme, especially for the instabilities occurring at small scales comparable to the grid spacing δ_x which cannot be fully determined by the former approach alone.

In 3D, Eq. (5.8) is replaced by the following:

$$\begin{pmatrix} \partial_t & \partial_x & \partial_y & \partial_z \\ c_s\partial_x - U_x\boldsymbol{U}\cdot\nabla & \bar{\mathcal{D}}_t + U_x\partial_x & U_x\partial_y & U_x\partial_z \\ c_s\partial_y - U_y\boldsymbol{U}\cdot\nabla & U_y\partial_x & \bar{\mathcal{D}}_t + U_y\partial_y & U_y\partial_z \\ c_s\partial_z - U_z\boldsymbol{U}\cdot\nabla & U_z\partial_x & U_z\partial_y & \bar{\mathcal{D}}_t + U_z\partial_z \end{pmatrix} \begin{pmatrix} \rho \\ \rho u_x \\ \rho u_y \\ \rho u_z \end{pmatrix} = \begin{pmatrix} 0 \\ 0 \\ 0 \\ 0 \end{pmatrix} + O(\delta_t^2) \tag{5.11}$$

and the viscous term in 2D, (5.9), becomes

$$\begin{pmatrix} 0 & 0 & 0 & 0 \\ 0 & \eta\partial_{xx} + \nu\Delta & \eta\partial_{xy} & \eta\partial_{xz} \\ 0 & \eta\partial_{xy} & \eta\partial_{yy} + \nu\Delta & \eta\partial_{yz} \\ 0 & \eta\partial_{xz} & \eta\partial_{yz} & \eta\partial_{zz} + \nu\Delta \end{pmatrix} \begin{pmatrix} \rho \\ \rho u_x \\ \rho u_y \\ \rho u_z \end{pmatrix} + O(\delta_t^3), \tag{5.12}$$

where $\eta := \nu/3 + \zeta$. Note that for the D3Q19 model (cf. Fig. 2 and related discussion in §3.2), there exists a dispersion relation similar to (5.10), which can lead to the conditions for fourth-order accurate shear wave decay [241].

6. The forcing, boundary and initial conditions

This section discussed two issues: the forcing term and boundary and initial conditions. Appropriate boundary conditions (BCs) are perhaps the most important component of the hydrodynamic equations, and, correct implementation of various BCs are essential for the success of the LBE algorithm. In the previous sections, the stability and convergence are proved with the periodic boundary conditions. However, the proofs can be easily extended to a system with bounce-back boundary conditions. Therefore, the bounce-back boundary conditions are the most often studied boundary conditions for the LBE, and naturally, the most important ones, for the reasons that bounce-back BCs are the simplest and easiest to implement, and yet they yield second-order accuracy which is consistent with that of the LBE.

6.1. Implementation of the forcing term

With a force density $\boldsymbol{F} = \rho\boldsymbol{a}$ present in the Navier-Stokes equation, the LBE must include a forcing term $\mathbf{G}$:

$$\bar{\mathbf{f}}(\boldsymbol{x}_j + \boldsymbol{c}\delta_t,\, t_n + \delta_t) - \bar{\mathbf{f}}(\boldsymbol{x}_j,\, t_n) = \delta_t\left[\mathbf{Q}(\boldsymbol{x}_j,\, t_n) + \mathbf{G}(\boldsymbol{x}_j,\, t_n)\right], \tag{6.1}$$

$$\mathbf{G}(\boldsymbol{x}_j,\, t_n) := (G_0(\boldsymbol{x}_j,\, t_n),\, G_1(\boldsymbol{x}_j,\, t_n),\, \ldots,\, G_b(\boldsymbol{x}_j,\, t_n))^\dagger, \tag{6.2}$$

where G_i is given by (3.14) or otherwise provided. We will apply the acoustic scaling $\delta_x/\delta_t = 1$ to analyze the above equation. To implement the forcing correctly, the momentum $\boldsymbol{j} := \rho\boldsymbol{u}$ to be used in the equilibrium moments (3.26) must be modified to:

$$\boldsymbol{j}^{(0)} = \textstyle\sum_i f_i\boldsymbol{c}_i + \dfrac{1}{2}\boldsymbol{F}\delta_t := (j_x^{(0)},\, j_y^{(0)}), \tag{6.3}$$

and this modified linear momentum should be the output to compute the velocity field in simulations (cf. §3.3 and [141]). The collision step is applied after the momentum is modified according to (6.3). The momentum is further modified after collision as the following

$$\boldsymbol{j}^{(1)} = \boldsymbol{j}^{(0)} + \frac{1}{2}\boldsymbol{F} := (j_x^{(1)},\, j_y^{(1)}), \tag{6.4}$$

before applying $\mathbf{M}^{-1}$ to obtain the new post-collision value of the distributions, $\mathbf{f}^*$. The advection is applied to $\mathbf{f}^*$. This treatment of the forcing term can be generalized for any source terms in the Boltzmann equation. For example, a heat source in the advection-diffusion equation can be treated similarly.

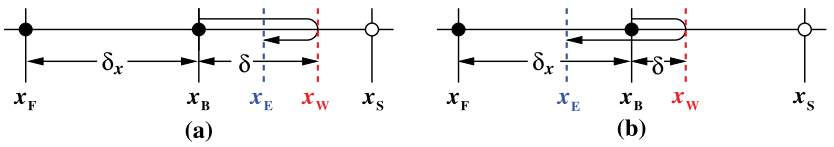

Fig. 3. Illustration of the bounce-back boundary conditions. The discs ($\bullet$, $\boldsymbol{x}_{\rm F}$ and $\boldsymbol{x}_{\rm B}$) and circles ($\circ$, $\boldsymbol{x}_{\rm S}$) mark the grid nodes inside and outside the flow domain Ω, respectively. The solid lines are the grid lines. $\boldsymbol{x}_{\rm W}$ is the location of a boundary, and $\boldsymbol{x}_{\rm E}$ is the position of the "particle" with the initial velocity $\boldsymbol{c}_1$ after advection. $\delta := \|\boldsymbol{x}_{\rm B} - \boldsymbol{x}_{\rm W}\|$. (a) $\delta > \delta_x/2$, (b) $\delta < \delta_x/2$.

The procedure to implement the LBE with a forcing term can be summarized as follows: (a) add $\boldsymbol{F}/2$ to $\boldsymbol{j} = \sum_i \boldsymbol{c}_i f_i$, *i.e.*, set $\boldsymbol{j}^{(0)} = \boldsymbol{j} + \boldsymbol{F}/2$; (b) use $\boldsymbol{j}^{(0)}$ to carry out the collision (relaxation); (c) add $\boldsymbol{F}/2$ to $\boldsymbol{j}^{(0)}$; (d) go back to the velocity space and perform the advection. This procedure is consistent with the analysis based on Strang splitting [141].

6.2. The bounce-back scheme for Dirichlet boundary conditions

The bounce-back boundary conditions are based on the picture that a moving particle reverses its momentum after colliding with a rigid wall at rest. For the sake of simplicity and without any loss of generality, we consider the situation in one dimension first, as illustrated in Fig. 3: $\boldsymbol{x}_{\rm F}$ and $\boldsymbol{x}_{\rm B}$ are two adjacent nodes in fluid domain Ω, whereas $\boldsymbol{x}_{\rm S}$ is a node outside fluid domain, the boundary is located at $\boldsymbol{x}_{\rm W}$, which is between nodes $\boldsymbol{x}_{\rm B}$ and $\boldsymbol{x}_{\rm S}$. Define $\delta := \|\boldsymbol{x}_{\rm W} - \boldsymbol{x}_{\rm B}\|$, and $\|\boldsymbol{x}_{\rm W} - \boldsymbol{x}_{\rm B}\| + \|\boldsymbol{x}_{\rm W} - \boldsymbol{x}_{\rm E}\| = \delta_x$ (cf. Fig. 3). Initially, the states (f_i's) are given at $\boldsymbol{x}_{\rm F}$ and $\boldsymbol{x}_{\rm B}$. The fluid-wall interaction occurs during the advection process: in one time step δ_t, a particle with velocity $\boldsymbol{c}_1$ moves to the wall at $\boldsymbol{x}_{\rm W}$, reverses its momentum to $\boldsymbol{c}_3 = -\boldsymbol{c}_1$, and arrives at $\boldsymbol{x}_{\rm E}$, which is *not* a grid node if $\delta \neq \delta_x/2$:

$$\begin{array}{cccc} t_n^+ & f_1^*(\boldsymbol{x}_{\rm F}) & f_3^*(\boldsymbol{x}_{\rm B}) & f_1^*(\boldsymbol{x}_{\rm B}) \\ & \Downarrow & \Downarrow & \Downarrow \\ t_{n+1}^- & f_1(\boldsymbol{x}_{\rm B}) & f_3(\boldsymbol{x}_{\rm F}) & f_3(\boldsymbol{x}_{\rm E}) \end{array} \quad \overset{\delta=\delta_x/2}{\Longrightarrow} \quad \begin{array}{cccc} t_n^+ & f_1^*(\boldsymbol{x}_{\rm F}) & f_3^*(\boldsymbol{x}_{\rm B}) & f_1^*(\boldsymbol{x}_{\rm B}) \\ & \Downarrow & \Downarrow & \Downarrow \\ t_{n+1}^- & f_1(\boldsymbol{x}_{\rm B}) & f_3(\boldsymbol{x}_{\rm F}) & f_3(\boldsymbol{x}_{\rm B}) \end{array}$$

where t_n^+ and t_{n+1}^- denote the time after and before collision, respectively, and f_i and f_i^* the pre- and post-collision states, respectively.

We will first discuss the case of $\delta = \delta_x/2$, in which $\boldsymbol{x}_{\rm E} = \boldsymbol{x}_{\rm B}$ (cf. Fig. 3), so the presence of a boundary does not affect the algorithmic simplicity of the LBE, which consists of collision and advection only. The following bounce-back scheme can be used to realize the Dirichlet boundary conditions $\boldsymbol{u}_{\rm w} = \boldsymbol{0}$:

$$f_{\bar{i}}(\boldsymbol{x}_{\rm B}, t_{n+1}^-) = f_i^*(\boldsymbol{x}_{\rm B}, t_n^+), \quad \boldsymbol{x}_{\rm B} \in \Omega,\ \boldsymbol{x}_{\rm B} + \boldsymbol{c}_i\delta_t \notin \Omega. \tag{6.5}$$

In this case the link-wise bounce-back scheme conserves mass, and the mass flux is zero at $\boldsymbol{x}_{\rm W}$ and $t = t_n + \delta_t/2$. This can be seen by using symmetry argument (or method of image): to achieve $\boldsymbol{u}_{\rm w} = \boldsymbol{0}$ when $\delta = 1/2$, the symmetry requires that $\boldsymbol{u}(\boldsymbol{x}_{\rm S}) = -\boldsymbol{u}(\boldsymbol{x}_{\rm B})$. This can also be shown by Chapman-Enskog analysis [323–325].

When $\boldsymbol{u}_{\rm w} \neq \boldsymbol{0}$, the bounce-back scheme (6.5) becomes

$$f_{\bar{i}}(\boldsymbol{x}_{\rm B}, t_{n+1}^-) = f_i^*(\boldsymbol{x}_{\rm B}, t_n^+) + 2w_i\rho\frac{\boldsymbol{c}_{\bar{i}}\cdot\boldsymbol{u}_{\rm w}}{c_s^2}, \quad \boldsymbol{x}_{\rm B} \in \Omega,\ \boldsymbol{x}_{\rm B} + \boldsymbol{c}_i\delta_t \notin \Omega, \tag{6.6}$$

that is, the particle bouncing back from a wall with the velocity $\boldsymbol{u}_{\rm w}$ should also gain a momentum $\rho\boldsymbol{u}_{\rm w}$ from the wall.

Similar to the bounce-back scheme for the Dirichlet BCs of $\boldsymbol{u}$, one can formulate a scheme to realize the Dirichlet BCs for the pressure $p = c_s^2\rho$, which is a scalar. Suppose the pressure gradient normal to the wall is zero or negligible, then it is expected that $\rho(\boldsymbol{x}_{\rm S}, t_n) = \rho(\boldsymbol{x}_{\rm B}, t_n)$ (cf. Fig. 3(a)). The boundary conditions for ρ must not affect the velocity at the boundary, $\boldsymbol{u}(\boldsymbol{x}_{\rm B})$. Hence, we have the so-called anti-bounce-back scheme [161,173,185,321,326]:

$$f_{\bar{i}}(\boldsymbol{x}_{\rm B}, t_{n_1}^-) = 2w_i\rho(\boldsymbol{x}_{\rm B}, t_n) - f_i(\boldsymbol{x}_{\rm B}, t_n^+), \tag{6.7}$$

which relies on the sum, $(f_{\bar{i}} + f_i)$, or the even-order moments, as opposed to the difference, $(f_{\bar{i}} - f_i)$, or the odd-order moments, in the bounce-back BCs, to achieve the desired BCs. Thus, the bounce-back scheme deals with the BCs for the odd-order moments (*e.g.*, $\boldsymbol{u}$), while the anti-bounce-back scheme deals with that for the even-order moments (*e.g.*, ρ or $\partial_x u$). Since $\boldsymbol{u}$ and ρ are odd and even functions about the boundary, hence can be approximated by linear and parabolic polynomials, respectively.

The bounce-back and anti-bounce-back schemes are simply based on the following expression of f_i:

$$f_i = w_i\rho\left[1 + \frac{\boldsymbol{c}_i\cdot\boldsymbol{u}}{c_s^2} + \frac{1}{2}\left(\frac{(\boldsymbol{c}_i\cdot\boldsymbol{u})^2}{c_s^4} - \frac{\boldsymbol{u}\cdot\boldsymbol{u}}{c_s^2}\right)\right] + f_i^{(1)}, \tag{6.8}$$

where the first part is the equilibrium given by (3.27) and $f_i^{(1)}$ contains $\boldsymbol{c}_i\cdot\nabla\boldsymbol{u}$ (cf. (4.10)). The terms $w_i\rho$ or $w_i\rho\boldsymbol{c}_i\cdot\boldsymbol{u}/c_s^2$ remain unchanged in the combination $(f_i + f_{\bar{i}})$ or $(f_i - f_{\bar{i}})$, respectively, as the leading-order term.

If there is only one conserved moment, say, ρ, then the model solves the convection-diffusion equation for ρ, and f_i becomes

$$f_i = w_i \rho + w_i \frac{\boldsymbol{c}_i \cdot \nabla \rho}{c_s^2} + \ldots. \tag{6.9}$$

Thus, to realize the Neumann or the flux BCs for ρ, the bounce-back scheme must be used.

Of course, for convection-diffusion equation of a scalar in 2D, one only needs the D2Q5 model [160–169], which has velocities $\{\boldsymbol{c}_i | i = 0, 1, \ldots, 4\}$ in (3.8). The D2Q5 model can be used to simulate the temperature equation in 2D, and the anti-bounce-back and bounce-back schemes are used to realize the constant temperature and adiabatic BCs [172,188].

When the intersection of a boundary and a grid line is not exactly $\delta_x/2$ away from the last fluid nodes (cf. Fig. 3), the simple bounce-back scheme is no longer accurate enough to capture the boundary location. One can use interpolations [166,327] to address this issue. Depending on the boundary location with respect to the last fluid node ($\boldsymbol{x}_B$ in Fig. 3) quantified by δ, the particle at $\boldsymbol{x}_B$ moving towards the boundary can end up outside (inside) of the flow domain if $\delta > \delta_x/2$ ($\delta < \delta_x/2$). Thus, $f_{\bar{i}}(\boldsymbol{x}_B)$ is obtained by interpolation *after* advection when $\delta > \delta_x/2$, and is obtained by computing $f_i(\boldsymbol{x}_E)$ with interpolation *before* advection. This approach is similar to cut-cell method [328–330]. The bounce-back scheme with interpolations can accurately handle boundaries of complicated geometries, such as realistic porous media [154,325,326,331–343], moving boundary problems [19,344–346], and flows with suspensions of rigid solid [266,347–358] and deformable particles [359–367].

6.3. The Poiseuille flow – an analytic solution

To elucidate the bounce-back boundary conditions, we use the Poiseuille flow as an example. Suppose the streamwise direction is along the x axis. Two parallel walls are placed at the bottom and top boundaries of the flow domain Ω. A constant body force along x direction, $\boldsymbol{F} = G\hat{\boldsymbol{x}}$, is applied to each node within Ω. Periodic boundary conditions are assumed in the x direction. There are N nodes in the flow domain in the spanwise direction. The LBE (3.17) for the D2Q9 model with the bounce-back boundary conditions has the following analytic solution in this case (cf., *e.g.*, [368]):

$$u(j) = \frac{4}{N^2}\left(j - \frac{1}{2}\right)\left(N + \frac{1}{2} - j\right) U_{\max} + U_s, \quad 1 \le j \le N, \tag{6.10a}$$

$$U_{\max} = \frac{GN^2}{8\nu}, \qquad U_s = \frac{1}{4}\left(\frac{8}{s_q} - \frac{8 - s_\nu}{2 - s_\nu}\right) U_{\max}, \tag{6.10b}$$

where $s_\nu = s_{4,5}$ and $s_q = s_{6,7}$. The above solution is obtained with a forcing splitting scheme [141], *i.e.*, with a forcing term $\boldsymbol{F}$ in the Navier-Stokes equation, after an advection, $\boldsymbol{F}\delta_t/2$ is added to the momentum $\rho\boldsymbol{u} = \rho(u_x, u_y)$ before the collision and $\boldsymbol{F}\delta_t/2$ is added after [141,151,172,188], and the output velocity $\boldsymbol{u}$ is obtained when only $\boldsymbol{F}/2$ is added after advection (cf. §6.1). Clearly, for the LBE solution of $u(j)$ to be consistent with the solution of the Navier-Stokes equation, we must have

$$u(j = 1/2) = u(j = N + 1/2) = 0, \quad U_s = 0 \iff s_q = 8\frac{(2 - s_\nu)}{(8 - s_\nu)}. \tag{6.11}$$

The analytic solution (6.10) reveals the following facts. First, the LBE with the bounce-back BCs is second-order *accurate* for the Poiseuille flow. Second, the Dirichlet BCs for the velocity $\boldsymbol{u}$ are satisfied at one-half grid spacing away from the fluid nodes next to the boundary, *i.e.*, $\delta = \delta_x/2$ (cf. Fig. 3). And third, it requires at least two relaxation rates, *i.e.*, s_ν (for the second-order moments m_3 and m_4) and s_q (for the third-order moments m_6 and m_7), to achieve this accuracy [323,325,326]. This immediately leads to the conclusion that the lattice BGK (LBGK) model with one relaxation parameter τ cannot achieve this accuracy unless τ is fixed at the special value of $\tau = (2 + \sqrt{3})/4 \approx 0.9330$ — for the LBGK model [369,370] with an arbitrary value of $\tau > 1/2$, the artificial slip velocity $U_s = (6\nu - 1/8\nu)$, $\nu = (\tau - 1/2)/3$. The viscosity-dependence of the location where the no-slip BCs are satisfied is a severe defect uniquely inherent to the LBGK model with bounce-back type [323,326,342,371–373] or other BCs based on direct manipulations of the distributions $\{f_i\}$ [368], but can be removed by using moment-based boundary conditions [374]. Also, the particular relationship (6.11) between s_q and s_ν depends on the choice of orthogonal moments (cf. §3.5) and the form of driving force [321].

There are limitations of the bounce-back scheme based on the analytic solution of the Poiseuille flow driven by a constant body force, in which both the nonlinear term and the pressure gradient are absent. It is only suitable for shear dominant flow near a no-slip boundary, nevertheless, its effectiveness has been tested for various flows [325,326,342,373].

6.4. Pressure boundary conditions at inlet and outlet

Often, the pressure boundary conditions are given in terms of a mean value, instead of a precise function $p(\boldsymbol{x})$, for $\boldsymbol{x} \in \partial\Omega$. For example, in a channel flow with streamwise direction along x axis or grid index i, the mean pressures are specified in both inlet ($j = 0$) and outlet ($j = N_x + 1$), and constant pressure BCs can be realized by the anti-bounce-back

scheme discussed in §6.2. However, a constant pressure is not a solution of the Navier-Stokes equations with no-slip BCs in this case. The following self-adaptive scheme can be used to improve the pressure boundary condition.

Suppose we have a 2D straight channel with two no-slip boundaries along x direction. Constant pressures p_{in} and p_{out} are specified at the inlet ($j=0$) and outlet ($j=N_x+1$), respectively. At the inlet nodes at $j=1$ (or outlet ones at $j=N_x$), the pressure p is no longer a constant along the y (or $\boldsymbol{k}$) direction, the averaged pressure at $j=1$ (or $j=N_x$) is

$$\bar{p}_1=\frac{1}{N_{\text{in}}}\sum_k p(j=1,\,k)\quad\text{or}\quad \bar{p}_{N_x}=\frac{1}{N_{\text{out}}}\sum_k p(j=N_x,\,k)$$

where N_{in} and N_{out} are the numbers of fluid nodes at the inlet $j=1$ and at the outlet $j=N_x$, respectively. Then the following boundary conditions are used [368,375]:

$$f_i(j=0,\,k)=\frac{p_{\text{in}}}{\bar{p}_1}f_i(j=1,\,k),\quad f_i(j=N_x+1,\,k)=\frac{p_{\text{out}}}{\bar{p}_{N_x}}f_i(j=N_x,\,k). \tag{6.12}$$

This procedure ensures the specified total mass flux, or the *averaged* pressure p_{in} (or p_{out}), at the boundary located at $j=0$ (or $j=N_x+1$).

It can be proven that the above iterative scheme yields the pressure p and velocity $\boldsymbol{u}$ which satisfy the following equation [376]:

$$\partial_t p=\kappa\left(\nabla^2 p+\nabla\nabla:\boldsymbol{jj}\right)-c_{\text{s}}^2\nabla\cdot\boldsymbol{j}, \tag{6.13}$$

where $\boldsymbol{j}:=\rho\boldsymbol{u}$, and $\boldsymbol{u}$ is the given velocity; κ is the diffusivity determined by the relaxation parameter for the momentum $\boldsymbol{j}$ (cf. (3.43) and related discussion). Thus, for a given divergence free velocity field, *i.e.*, $\nabla\cdot\boldsymbol{u}=0$, the steady pressure field so obtained satisfies the Poisson equation if the mean density $\bar{\rho}=1$ [376]:

$$\nabla^2 p=-\nabla\cdot(\boldsymbol{u}\cdot\nabla\boldsymbol{u}). \tag{6.14}$$

6.5. LBE and immersed boundary method

To handle flow-structure interaction with moving boundary, immersed-boundary method (IBM) is an effective and efficient approach [377–379]. The IBM can be easily implemented with the LBE [18,30,380]. In this approach, the LBE solves the flow equation on an Eulerian Cartesian mesh, while moving boundaries are tracked with Lagrangian markers. The *local* force due to the boundary conditions between flow and a moving object experienced at a marker point is distributed to surrounding Eulerian mesh points. This amounts to approximating the delta function by a smooth distribution on a compact support. This approach has been successfully applied to simulate particulate flows [18,381,382], moving boundary problems [344,346], and interfacial flows [380,383].

6.6. Initial conditions

As discussed in §3, an LBE model of q velocities has an equal number of *independent* moments, and all these moments require proper initial condition. Since the moments can be categorized as hydrodynamic *versus* non-hydrodynamic ones, their initial conditions will be discussed separately. Because the LBE is usually applied to simulate nearly incompressible flows, for which the only necessary initial condition is that of the velocity field $\boldsymbol{u}$ and the initial pressure is not given. Although the pressure can be obtained *via* the Poisson equation, this is usually not done. Thus the pressure p (or the density ρ) is the only hydrodynamic moment which may require proper initialization in the LBE. Secondly, the non-hydrodynamic moments also require proper initialization. For any athermal LBE model of q velocities in d dimensions, there are $q-(d+1)$ non-hydrodynamic moments which require initialization.

Improper initialization of the LBE, in terms of either the distribution functions $\{f_i\}$ or equivalently the moments $\{m_i\}$, induces unphysical relaxations of those improperly initialized moments, and this is the so-called "initial layer", which may linger for long times and affect the flow fields, severely degrading the quality of the simulation in some cases [158,312,376]. In particular, severe unphysical effects can be generated by the spurious relaxation of the initial pressure field inconsistent with a given initial velocity field, *i.e.*, the spurious acoustic waves. Among the non-hydrodynamic moments, the second-order ones, *i.e.*, the stresses and the divergence of the velocity field, and the third-order ones are directly coupled to the velocity, thus their relaxations due to the inconsistent initialization can affect the flow fields [158,376].

There are two approaches to initialize the LBE. First, one can freeze the velocity field with given initial conditions, and solve the remaining variables (or moments) numerically by iterating the LBE until it reaches a steady state [289,376]. A second approach is to use either Chapman-Enskog [312] or asymptotic expansions [289] to compute the moments without initial conditions based on those with given initial conditions, up to the required order of accuracy. The proper initialization is essential to the LBE simulations for flows which require accurate initialization, such as decaying turbulence [158].

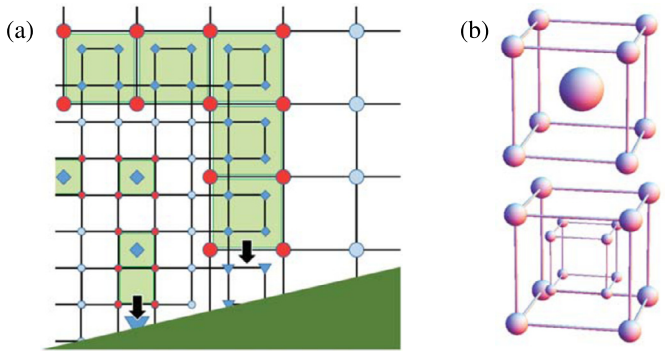

Fig. 4. (color online) Schematics of grid refinement in 2D (left) and 3D (right). In the left figure, large (small) discs, diamonds, and triangles are the nodes of coarse (fine) grid. The nodes of coarse and fine grid do not overlap. The information on the small (large) red discs of fine (coarse) grid are interpolated to the large (small) diamonds. The area in green is beyond flow domain. The information on the nodes marked by triangles has to be obtained by extrapolations from nearby nodes, as indicated by the arrows.

7. Grid refinement

Grid refinement is often necessary for computational efficiency. The LBE uses a Cartesian grid, for which the quad-tree (2D) or oct-tree (3D) mesh refinement is naturally suitable. The key technical issues are scalings and the interpolation coupling two meshes with different resolutions [384–387]. First of all, the convective (acoustic) scaling $\delta_t = O(\delta_x)$ is used, thus to maintain a constant viscosity ν across two meshes with different grid spacings δ_x^{coarse} and δ_x^{fine}, then the viscosity and the corresponding relaxation rate s_ν should be rescaled as δ_x varies according to

$$\nu^{\text{fine}} = \frac{\delta_x^{\text{coarse}}}{\delta_x^{\text{fine}}}\nu^{\text{coarse}}, \quad \left(\frac{1}{s_\nu^{\text{fine}}} - \frac{1}{2}\right) = \frac{\delta_x^{\text{coarse}}}{\delta_x^{\text{fine}}}\left(\frac{1}{s_\nu^{\text{coarse}}} - \frac{1}{2}\right), \tag{7.1}$$

and the relaxation rate for the third-order moments, s_q, obeys the relation (6.11) so the no-slip boundary conditions can be accurately realized. In most cases, other relaxation rates for higher-order moments may be set to 1 throughout the system. The dependence of ν on δ_x (7.1) means the coarser the mesh, the smaller the viscosity, the closer s_i is to its stability limit 2 from below. This can cause numerical instability with grid refinement. The cumulant LBE seems to be particularly robust and effective to deal with this situation [258].

Fig. 4 illustrates the interpolations for two meshes in 2D and 3D, in which the grid refinement factor is always 2. In the interface region between two meshes, the nodes on the meshes of different resolutions never overlap. The ratio of the time steps in two meshes is equal to that of the corresponding mesh sizes, so the speed of sound remains the same in two meshes of different grid spacings. In the interface region (or buffer zone), each unit cell of the fine mesh is inside a unit cell of the coarse mesh, and each node of the coarse mesh is inside a unit cell of the fine mesh (cf. Fig. 4).

Second, *all* interpolations are carried out using the moments $\{m_i\}$, *not* the distribution functions $\{f_i\}$. The pressure (or density) is computed with linear interpolation, and the velocity $\boldsymbol{u}$ and all second-order moments are computed by the compact quadratic interpolation using only the information on the eight vertices of a cell (cf. Fig. 4), the coefficients in the quadratic interpolation include the information of the first and second order derivatives of $\boldsymbol{u}$, which are computed from $\boldsymbol{u}$ by using finite-differencing and the nonequilibrium part of the second-order moments. The rest of moments of order higher than two are set to their equilibria during the interpolation, effectively setting the relaxation rates of these moments to 1.

Third, the interpolations are carried out on every time step on the coarse mesh. The overlapping region between two meshes should be wide enough in each dimension so the interpolation in time is not necessary.

Finally, in the case of two connected meshes with different mesh spacings intersecting with the boundary simultaneously, extrapolations must be used to compute the moments on nodes which do not have all neighboring nodes for interpolations (cf. Fig. 4). The grid refinement scheme has been validated in various flow simulations [52,159,388].

8. Numerical results

This section presents some numerical results to demonstrate the efficacy of the LBE method. The numerical results include (a) the Poiseuille flow and a double-shear layer flow in 2D; (b) direct numerical simulation (DNS) of decaying homogeneous isotropic turbulence in 3D, and (c) high-Reynolds-number flow past a sphere and a car.

8.1. 2D test cases

Two test cases in 2D are used to validate the LBE algorithm. The first is the Poiseuille flow with an inclined angle with respect to x axis, as illustrated in Fig. 5. No-slip boundary conditions are realized in three ways: the zig-zag bounce-back scheme, and the bounce-back scheme with linear and quadratic interpolations. The results are shown in Fig. 6.

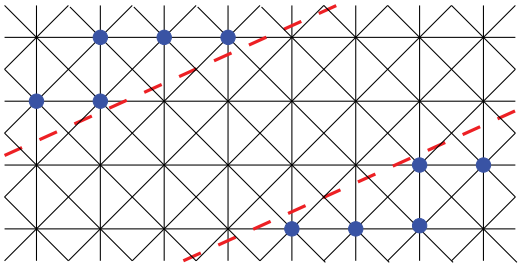

Fig. 5. The flow configuration of the Poiseuille flow with an inclined angle $\theta \approx 16.62^\circ$ ($\tan\theta = 20/67$) with respect to x axis. The solid lines are the grid lines, and the dashed lines are the no-slip walls. The solid discs indicate the boundary nodes in the zig-zag bounce-back scheme.

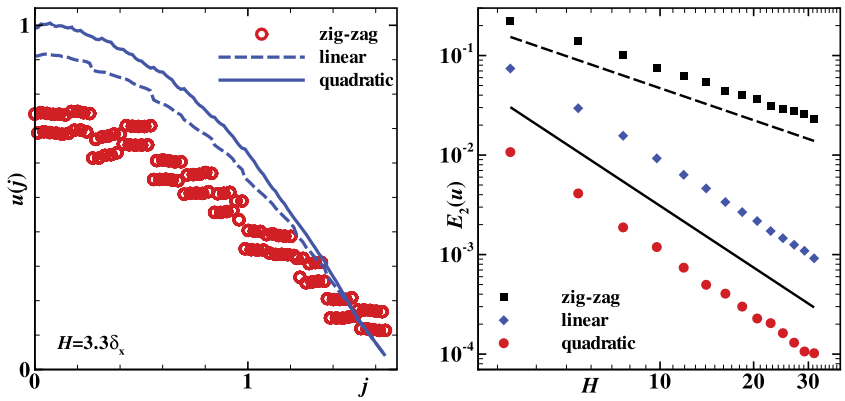

Fig. 6. The Poiseuille flow with an inclined angle $\theta \approx 16.62^\circ$ ($\tan\theta = 20/67$) with respect to x axis. Left: the velocity profile $u(j)$ with the zig-zag bounce-back, linear and quadratic interpolations at the walls. Right: the L^2 error of the velocity $u(y)$. The dashed and solid lines have the slope of -1 and -2, respectively.

First, the left panel in Fig. 6 shows the velocity profiles $u(j)$, $|j| \le 1.65\delta_x$, for a very narrow channel with the channel width $H = 3.3\delta_x$. The profile of $u(j)$ obtained with the zig-zag bounce-back scheme is the poorest and that obtained with the quadratic-interpolation bounce-back scheme is the best. The right panel of Fig. 6 for the L^2 error of the velocity $u(j)$ shows that the zig-zag bounce-back scheme leads to a first-order convergence, whereas the schemes with either linear or quadratic interpolations yield second-order convergence.

From Fig. 6 (left), it can be seen that the effect of inaccurate treatment at the boundary is a reduction of maximum velocity, or an increase of the effective viscosity ν. With $H = 3.3\delta_t$, the ratio between the measured velocity at the channel center, U_c and its theoretical value $U_{\max}$ given in (6.10) is 0.70254, 0.89965, and 0.99121 for the bounce-back scheme with the zig-zag, linear, and quadratic interpolations, respectively, and the corresponding relative L^2 error of $u(j)$ compared with the exact solution of (6.10) is 0.22224, 0.074077, and 0.010709. However, when compared with a parabola with its maximum equal to U_c, then the relative L^2 error becomes 0.067636, 0.012321, and 0.00865546. As the data show, the bounce-back scheme with the quadratic interpolations works extremely well in this case, even for a very narrow channel width.

The next simple test case is a double shear flow on a 2D periodic square with the following initial conditions [214,314,389]:

$$u = \begin{cases} U_0 \tanh[\beta(y - 1/4)], & 0 \le y < 1/2, \\ U_0 \tanh[\beta(3/4 - y)], & 1/2 \le y < 1, \end{cases} \tag{8.1a}$$

$$v = \delta U_0 \sin[2\pi(x + 1/4)], \qquad 0 \le x < 1. \tag{8.1b}$$

To eliminate the artificial initial layer due to inconsistent initial conditions, we iterate the LBE with the velocity fixed at the given initial conditions, until all other moments are consistent with the initial velocity field [376].

The number of grid points is $N \times N$. The D2Q13 model [145,151,214,390] is used. The simulation is carried out with a fixed Reynolds number at $\mathrm{Re} = U_0 N/\nu = 1000$, and $\beta = 80$. We use both acoustic and diffusive scalings. For the acoustic scaling, $U_0 = 0.01c$ is a constant, and $\delta = 0.05$, while the viscosity ν (in lattice units $\delta_x = \delta_t = 1$) increases linearly with N so to maintain a constant Re. For the diffusive scaling, $\nu = 0.0025c\delta_x$ is a constant, and $\delta = 0.01$, while U_0 decreases linearly with N to keep Re constant.

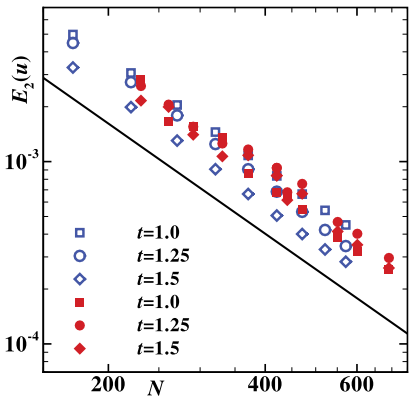

Fig. 7. The double shear layer flow on a 2D periodic square. The L^2 error of the velocity field at $t = 1.0$, 1.25, and 1.5. The solid and outlined symbols indicate the results obtained with the diffusive ($\delta_t = \delta_x^2$) and acoustic ($\delta_t = \delta_x$) scaling, respectively. The solid line has the slope of -2.

Fig. 7 shows the relative L^2 error of the velocity $\boldsymbol{u}(x, y)$ compared with the solution of incompressible Navier-Stokes equations obtained with a pseudo-spectral method with second-order accuracy in time. The spectral resolution used is $N^2 = 200^2$. Clearly, the simulations with both acoustic and diffusive scalings achieve a second-order spatial convergence with the mesh sizes shown in Fig. 7, before the error due to the Mach number becomes dominant [214]. That is, we do expect that the convergence of the simulations in the acoustic scaling should eventually deviate from the N^{-2} scaling once the spatial truncation error becomes comparable to the compressibility error. Of course, the simulation with the acoustic scaling is far more efficient than that with the diffusive scaling, because the number of time steps is $N_t \propto N$ for the acoustic scaling, and it is $N_t \propto N^2$ for the diffusive scaling.

8.2. Direct numerical simulation of homogeneous isotropic turbulence

The lattice Boltzmann method has been successfully used as a method of direct numerical simulation (DNS) [54,55,291,298,337,391–409] and a means for the large-eddy simulation (LES) based on the Smagorinsky model [291,293–298,303,410] to simulate turbulent flows. The numerical validity of the LBE for the LES based on the Smagorinsky model is discussed in Sec. 4.4. More details on the validity of the LBE-LES method can be found in a recent review by Löhner [411].

A detailed and direct comparison between the LBE and a pseudo-spectral method with a second-order accuracy in time has been made for the DNS of the decaying homogeneous isotropic turbulence in a 3D periodic cube [158]. The LBE model is D3Q19 [139]. The mesh size is $N^3 = 128^3$ for both the LBE and the pseudo-spectral method. The Taylor microscale Reynolds number Re_λ is in the range $24.35 \leq \mathrm{Re}_\lambda \leq 72.37$ [158]. In addition to the statistical quantities such as the total energy and the energy spectrum, the dissipation rate, the root-mean-square pressure fluctuation and the pressure spectrum, and the skewness and flatness of the velocity derivative, the instantaneous flows fields of $\boldsymbol{u}(\boldsymbol{x}, t)$ and $\boldsymbol{\omega}(\boldsymbol{x}, t)$ obtained with the LBE and the pseudo-spectral method for incompressible Navier-Stokes equations agree well with each other. Fig. 8 compares the vorticity field $\boldsymbol{\omega} := \nabla \times \boldsymbol{u}$ obtained by the LBE and pseudo-spectral method in three times. It shows that the LBE can accurately capture small vortexes of sizes of a few lattice spacings [158].

Some other results of DNS using the LBE method are worth mentioning here. It has been observed that the LBE can accurately capture detailed vortex motion and vortex-boundary interactions [412–420]. The LBE also yields accurate results for acoustics [237,239,241,242,421–424]. The accuracy of these LBE simulations supports the credibility of the DNS of turbulent flows carried out by using the LBE.

8.3. High Reynolds number flows in 3D

The D3Q27 cumulant LBE model [159] is used for the following two flows in 3D. The first case is the unsteady flow past a sphere with high Reynolds number. The flow domain size is $L \times W \times H = 11D \times 11D \times 11D$, where D is the diameter of the sphere. The sphere center is located at the streamwise centerline of the flow domain, $2D$ away from the upstream boundary. Constant velocity boundary conditions are used for the upstream and four side boundaries with the constant velocity $U = 0.0125c$, and non-reflective extrapolation boundary conditions are used for the downstream boundary. No-slip boundary conditions are imposed on the sphere surface. The mesh has six levels of binary refinement, *i.e.*, the ratio of the coarsest and the finest size of the grid spacing is $2^5 = 32$. The sphere diameter D is $512\delta_x$, where δ_x is the finest size of grid spacing. The total number of grid nodes is 73 855 051. The block ratio is 1/11. The simulation was carried out on four NVIDIA Tesla® C1060 GPUs with 4 GB memory each. The validation of the code can be found in [159].

Fig. 9 shows the Reynolds-number dependence of the drag coefficient C_D, compared with recent results obtained with finite-difference (FD) based large-eddy simulation [425], various fitting formulas for $C_\mathrm{D}(\mathrm{Re})$ [426,427], and experimental data [428]. The LBE results clearly show the "drag crisis".

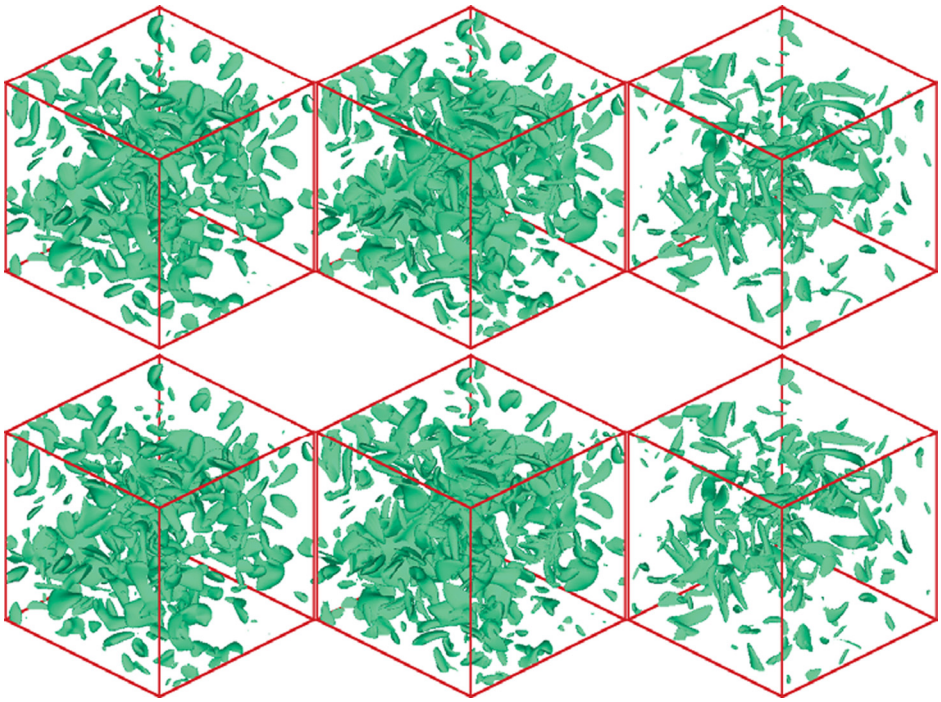

Fig. 8. DNS of homogeneous isotropic turbulence with $\mathrm{Re}_\lambda = 24.37$. Instantaneous vorticity iso-surface $|\boldsymbol{\omega}|$: LBE results (top row) vs. pseudo-spectral results. From left to right: $t' = 0.1348$, 0.2359, and 0.573.

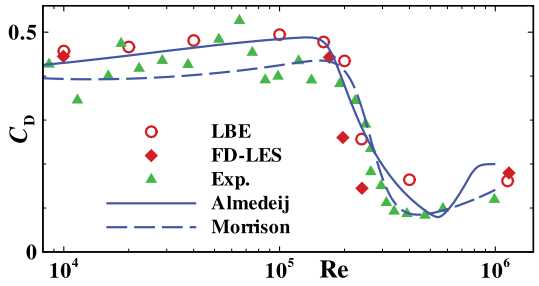

Fig. 9. Flow past a sphere. The drag coefficient C_D depends on Re. The LBE results (∘) are compared with the data obtained by FD-LES [425], fitting formulas [426,427], and experimental data [428].

Fig. 10 shows the magnitude of the velocity field $|\boldsymbol{u}(\boldsymbol{x})|$ on the vertical symmetric plane of the flow domain (xy plane) in color with $\mathrm{Re} = 10^5$ and 4.0×10^5, before and after the drag crisis, respectively. On the surface of the sphere, the value of the pressure fluctuation $\delta p(\boldsymbol{x})$ is shown in color.

The flow past the DrivAer car is the second test case of high-Reynolds-number flow in 3D [52]. The flow domain is $L \times W \times H = 70\mathrm{m} \times 20\mathrm{m} \times 13\mathrm{m}$, and the car size is $L_c \times W_c \times H_c = 4.61\mathrm{m} \times 2.03\mathrm{m} \times 1.42\mathrm{m}$, thus the blockage ratio is about 0.8%. No-slip boundary conditions are imposed on the car surface and the floor which is moving with a constant velocity, a constant velocity is imposed on the inlet, two side and the top walls, and a constant pressure is imposed at the outlet by using extrapolations. The wheels rotate with a given constant angular velocity. The mesh has six levels of refinements. The Reynolds number is set to 4.87×10^6, and no explicit turbulence modeling is used in the simulation. The size of the finest grid spacing is 3.125 mm. The number of grid points of the largest mesh is about 125.6×10^6. The geometry of the car is described with great details [52]. The simulations were carried out on two NVIDIA Tesla® K40C GPUs with 12 GB memory each.

The measured quantities include the drag coefficient C_D and the pressure coefficients C_p on the top and bottom of the car. With the largest mesh, C_D obtained with the LBE is 0.274, compared to the experimental value of 0.275. The results of C_p are shown in Fig. 11. Details of the simulation, including a convergence study, can be found in [52].

The LBE algorithm implemented on general-purpose graphic processing units (GPGPUs) has achieved a great parallel efficiency [386,429,430]. The powerful combination of the LBE and GPGPUs has significantly extended our capability to simulate realistic flows, as shown above. It is also worth to note that the high-Reynolds-number simulations were carried out with single-precision (32 bit) accuracy as the performance of GPGPUs is essentially doubled for this data type. The

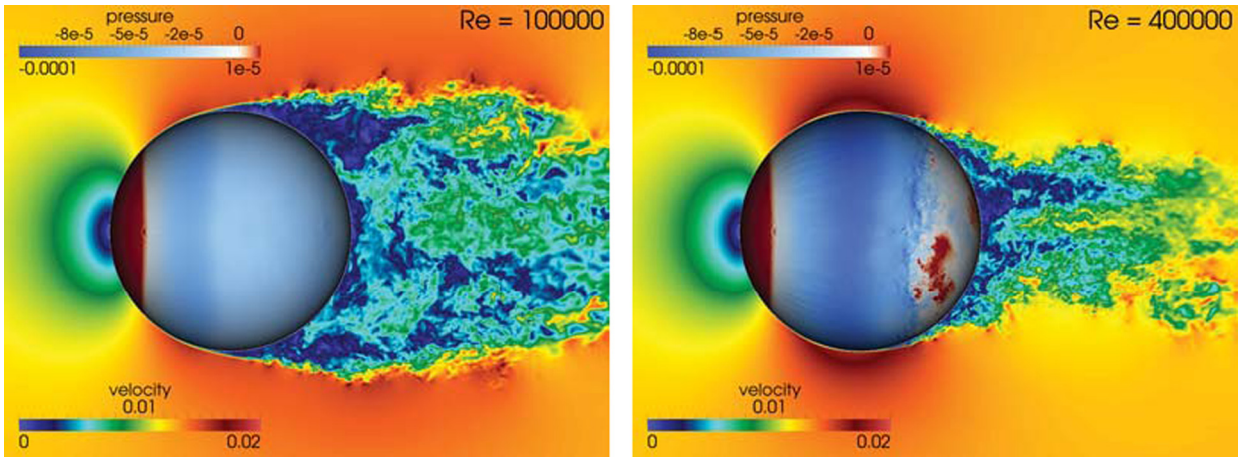

Fig. 10. Flow past a sphere with $\mathrm{Re} = 10^5$ before the drag crisis (left) and 4×10^5 after the drag crisis (right). The velocity magnitude $|\boldsymbol{u}(\boldsymbol{x})|$ on the symmetric xy plane. The pressure fluctuation δp is shown on the sphere surface.

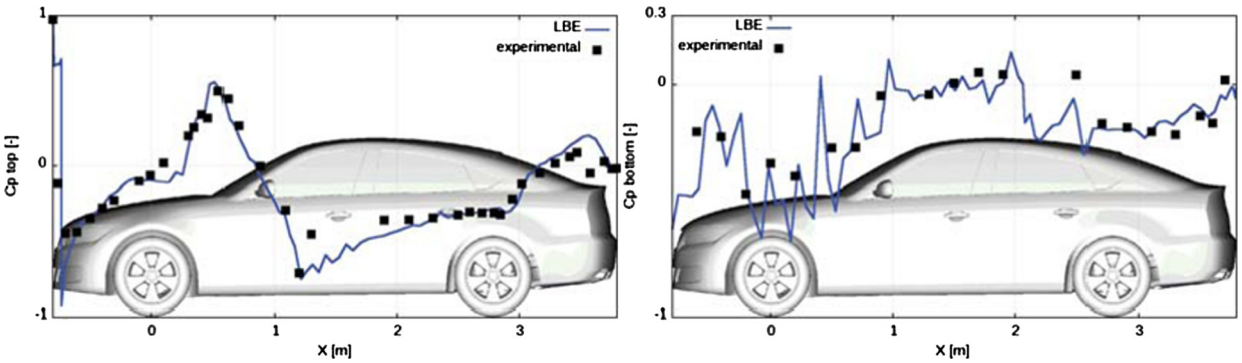

Fig. 11. C_P at the top (left) and bottom (right) of the DrivAer car model.

numerical stability and robustness of single-precision computations critically depend on the implementation of the collision operator and boundary conditions. Because the order of magnitude of different moments (or cumulants) and their non-equilibrium parts differ significantly, especially for higher-order moments, therefore considerable care must be taken to minimize round-off errors when these quantities are only stored in single-precision during the computation, such as using only the fluctuating part of the density in the LB simulations (cf. Sec. 4.4 and [312]).

9. Discussion and conclusions

This article reviews the fundamental theory and analysis about the lattice Boltzmann equation as an explicit solver for nearly incompressible Navier-Stokes equations — from its kinetic origin to its numerical analysis. We have chosen to *narrowly* focus on the LBE models for *simple* fluids, and leave the LBE models for *complex* fluids for a future review. The reason for this choice is that the rigorous theory and analysis on the LBE models for complex fluids are not as mature as that for simple fluids, although this is one of the fastest growing and most promising areas of research. We would like to conclude this review with a discussion on some outstanding issues of the LBE and an outlook.

In spite of its kinetic origin, perhaps the most fundamentally challenging issue the LBE faces is whether a simple kinetic scheme such as the LBE can be used to approximate kinetic equations effectively and efficiently, and to what extent. While there have been numerous claims that the LBE can be used to solve rarefied gas problems in a wide range of the Knudsen number effectively from continuum to free-molecule regime [218,272,273,431–441], there is no rigorous analysis to substantiate these claims, and these claims have been refuted to a certain extent (cf., *e.g.*, [368,442,443]). It should be noted (cf., *e.g.*, [444]) that while the discrete velocity sets of the LBE are similar to that of the discrete velocity models (DVMs) [445–452], which are indeed kinetic solvers [453–456]. The characteristics of the two methods are, however, fundamentally different — the DVMs, which by design are kinetic solvers, do not have the coherent discretization which ties discretized phase space and discretized time together as in the LBE (cf. §3). It should also be noted that the solutions of a single DVM do not converge to anything; the DVM solutions would converge to a solution of the Boltzmann equation only under suitable refinement of the number of discrete velocities. In addition, a typical DVM solution will not converge to a Navier-Stokes

solution even for small Knudsen number because the necessary moment relations will not hold (cf., *e.g.*, [444] and refs. therein). Although there exists some discrete evidence that the LBE can be applied to simulate the slip flows [368,374] and flows with moderate Knudsen numbers [279,372,457,458], rigorous analysis of the convergence of the LBE to the Boltzmann equation remains to be seen.

A second category of issues in the LBE is more of a pragmatic nature and it is most related to the numerical analysis and improvement of the numerical efficiency of the LBE. As shown in this review, many advanced and well developed techniques for numerical solutions of various PDEs have yet to be fully adopted by the populace in the LBE community. For example, the multigrid technique for solving the steady state problems [459,460] has yet to fully realize its potential efficiency with the LBE, although there have been some promising preliminary efforts [461–463]. Similarly, efficient and accurate implicit LBE schemes for time-stepping to break the CFL barrier have yet to be well formulated [464–468]; and a systematic method to develop high-order LBE schemes is still lacking (cf., [174,241,316,321]). For Stokes flows, there has been progress to enhance efficiency by reducing the LBE simulation in a d dimensional volume to a boundary-value problem on a $(d-1)$ dimensional surface [469–472]. We can expect significant advances to be made in these areas in the near future.

One of the most active area of research involving the LBE is multi-phase and multi-component flows with liquid-gas or liquid-liquid interfaces [43,92,93,95–98,380,430,473,474]. The LBE models for multi-phase and multi-component flows are mostly diffusive interface capturing schemes which employ the techniques based on the immersed-boundary method [381,475,476], phase-field method [16,43,96,98,477–479], level-set method [20,480,481], or some similar techniques. While the LBE is widely used for interfacial dynamics, very little rigorous analysis has been done [482]. This is another area of active research which deserves attention.

Finally, we would like to give a summary of the LBE method. The LBE with uniform Cartesian meshes is indeed a very simple algorithm to simulate nearly incompressible Navier-Stokes equations with a second-order accuracy. The LBE method has a broad range of applications, including generalized Newtonian fluids. The versatility of the LBE is partly due to its kinetic origin — it is relatively easy to construct a collision operator in terms of *linear* relaxation process in kinetic theory to mimic certain physical phenomena. A relatively simple linear relaxation process at the kinetic level can lead to some complicated PDEs at the macroscopic level, and viscoelastic fluids serve as a good example. While the LBE is a drastically simplified kinetic model designed to simulate hydrodynamic equations, it in fact retains most essential features of the Boltzmann equation, including the conservation laws and dissipative property. A key feature which benefits the LBE is the linearity of the advection term with constant coefficients in the kinetic equation, while the nonlinearity resides in the *local* collision term. As we have shown, the LBE can be seen as a method to simulate first-order PDEs derived from the linearized Boltzmann equation (cf. (2.21) in §2); first-order PDEs with *linear* advection terms enjoy certain computational advantages [483], including

- Requirement of the smallest possible stencil for accurate discretization, reducing the need for inter-nodal data communication;
- The stiffness due to the local nonlinear collision term can be overcome by local techniques;
- Discretized first-order systems may be easier to converge than equivalent higher-order systems;
- First-order PDEs yield the highest potential for discretization accuracy on non-smooth, adaptively refined grids;
- Systems of 1st-order PDEs are better suited for functional decomposition, thus easier to parallelize.

In addition, the over-relaxation property of the LBE allows it to use small viscosity thus making it an efficient method (cf. §3.6). These are perhaps the very reasons that the LBE is an effective and efficient explicit scheme for the simulation of nearly incompressible flows. However, to systematically improve the accuracy and efficiency of the LBE while retaining its simplicity remains a challenge. It should be noted that once the mathematics of the kinetic methods is understood, the above advantages can be immediately adopted into traditional methods. In fact, there is an explicit connection between the LBE and some finite-difference schemes [86,87,89,91,484] which can be directly applied to discretize the Navier-Stokes equations. Also, the Navier-Stokes equations can be recast to a system of first-order relaxation equations [485,486]; and some kinetic schemes can be directly derived without explicit reference to kinetic theory [487,488].

Undoubtedly, the LBE is a new variety in the colorful garden of CFD. It opens up a new avenue for new thoughts and methods. The LBE and other kinetic methods are intellectually interesting for several reasons. Simple LBE models can serve as minimalist models in kinetic theory, which may exhibit the kinetic origin and features of fluid systems. They may also serve as the connection between macroscopic flow theory and its underlying microscopic physics, *i.e.*, the route to multiscale physics. At the least, kinetic methods add spices to our lives. If this review could arouse some interests in kinetic methods, that would be most rewarding to the authors' effort.

Declaration of competing interest

The authors declare that they have no known competing financial interests or personal relationships that could have appeared to influence the work reported in this paper.

Acknowledgements

This work is supported by the National Natural Science Foundation of China (NSFC) under the Grants U1530401 and U1930409 and the Deutsche Forschungsgemeinschaft (DFG, German Research Foundation) under the Project ID 414265976–TRR–277.

The authors are grateful to Dr. Lizhen Chen at Computational Science Research Center (CSRC, www.csrc.ac.cn), Beijing, China, for providing the data obtained by the spectral method for the double-shear layer flow; to Prof. Martin Geier, Dr. Martin Schönherr, and Dr. Andrea Pasquali at iRMB, TU Braunschweig, Germany, for providing the data and figures for the flows past a sphere and car; and to Prof. Weidong Li of Wuhan University of Technology, China, for providing Fig. 1.

The authors would also like to thank the following colleagues for their reading and incisive and insightful comments: Dr. Paul J. Dellar of Oxford, UK, Dr. Robert Rubinstein of Hampton, Virginia, USA, Prof. Zhaoli Guo of Huazhong University of Science and Technology, China, Prof. Victor E. Ambruş of West University of Timişoara, Romania, Prof. Remi Abgrall of University of Zurich, Switzerland, Prof. Weidong Li of Wuhan University of Technology, China, and Mr. Charles Armstrong of Old Dominion University, USA. The authors are particularly grateful to three anonymous referees for their constructive and critical reviews, which have helped us improve this manuscript significantly.

List of symbols

Different fonts are used for different quantities:

italic font for scalars, *e.g.*, u, V, ϵ
bold-italic for a d dimensional vector with $d = 2$ or 3, *e.g.*, $\boldsymbol{r}$, $\boldsymbol{u}$, $\boldsymbol{x}$, $\boldsymbol{F}$
bold-upright for an n dimensional vector with arbitrary $n \geq 2$, *e.g.*, $\mathbf{f}$, $\mathbf{m}$, $\mathbf{G}$, $\mathbf{Q}$
bold sans serif for tensors in general, *e.g.*, p, B, M, S, $\boldsymbol{\Sigma}$, $\mathsf{\Sigma}$, $\boldsymbol{\sigma}$, …
calligraphic for operators, *e.g.*, $\mathcal{I}$, $\mathcal{L}$, Q
math blackboard font for spaces or sets, *e.g.*, $\mathbb{\Gamma}$, $\mathbb{R}^n$, $\mathbb{X}_q$, $\mathbb{Z}_d$.
Superscript † transpose operator

In what follows, the equation number or the section number indicates when the symbol is first appeared or defined.

- $\boldsymbol{A} := A(\vartheta, \bar{\boldsymbol{c}})\bar{\boldsymbol{c}}$ [(2.38)]
- $\boldsymbol{a} := \mathrm{d}\boldsymbol{\xi}/\mathrm{d}t$: particle acceleration due to an external force $\boldsymbol{F}$ [(2.1a)]
- $\mathsf{B} := B(\vartheta, \bar{\boldsymbol{c}})\widehat{\mathbf{C}}$ [(2.38)]
- $B(\Theta, \boldsymbol{\xi}, \boldsymbol{\xi}_*)$: collision kernel [(2.1b), (2.4)]
- $b := q - 1$: the number of non-zero discrete velocities [(3.17)]
- $\widehat{\mathbf{C}} := \bar{\boldsymbol{c}}\bar{\boldsymbol{c}} - \frac{1}{d}\bar{c}^2\mathbf{I}$: the traceless part of the tensor $\bar{\boldsymbol{c}}\bar{\boldsymbol{c}}$ [(2.38)]
- $C_{lmn}(\boldsymbol{x}, t)$: the cumulant computed from the generating function $F(\boldsymbol{x}, \boldsymbol{K}, t)$, *i.e.*, $C_{lmn} := c^{-(l+m+n)}\partial^l\partial^m\partial^n \ln F/\partial K_x^l \partial K_y^m \partial K_z^n$ at $\boldsymbol{K} = \mathbf{0}$ [(3.57)
- $\boldsymbol{c} := \boldsymbol{\xi} - \boldsymbol{u}$: the peculiar velocity [(2.10a)]
- $\bar{\boldsymbol{c}} := \boldsymbol{c}/c_\mathrm{s}$: the dimensionless peculiar velocity, normalized by the speed of sound c_s [(2.38)]
- $c_\mathrm{s} := \sqrt{\gamma\vartheta}$: the speed of sound [(3.29)]
- $c_{\mathrm{s}0} := \sqrt{\gamma\vartheta_0}$: the reference or initial speed of sound based on a reference/initial thermal energy per unit mass and per degree of freedom ϑ_0 [§2.2]
- $\bar{\mathcal{D}}_t := \partial_t + \boldsymbol{U}\cdot\nabla$ [(5.8)]
- $\mathbf{D} := \mathrm{diag}\left(\varepsilon^2\partial_t, \varepsilon^2\partial_t + \varepsilon\boldsymbol{\xi}_1\cdot\nabla, \ldots, \varepsilon^2\partial_t + \varepsilon\boldsymbol{\xi}_b\cdot\nabla\right)$ [(4.8)]
- d: the spatial dimension, *i.e.*, $\boldsymbol{r} \in \mathbb{R}^d$ [(2.10)]
- d_c: the number of conserved moments [§3.1]
- E: the total energy per unit mass, $\rho E = \rho(d\vartheta + u^2)/2$ [(3.48), (3.49)]
- $\mathbf{E} := \partial\mathbf{W}^{-1}\mathbf{f}^{(0)}/\partial\mathbf{f}$ [(4.17)]
- $\mathrm{E}_{ij} := (1/w_i)\partial f_i^{(0)}/\partial f_j$ [(4.17)]
- e: the total internal energy per unit mass $e := d\vartheta/2$ [(2.22c)]
- $\boldsymbol{F}$: external force [(2.1)]
- $\mathrm{Fr} := V_0/\sqrt{LG}$: the Froude number [(2.17)]
- $f := f(\boldsymbol{x}, \boldsymbol{\xi}, t)$: the single particle velocity distribution function with pre-collision velocity $\boldsymbol{\xi}$ [(2.1a)]
- $f_* := f(\boldsymbol{x}, \boldsymbol{\xi}_*, t)$: the single particle velocity distribution function with pre-collision velocity $\boldsymbol{\xi}_*$ [(2.1a)]
- $f^{(0)} := f^{(0)}(\rho, \boldsymbol{u}, \vartheta)$: the Maxwellian equilibrium distribution function [(2.11)]
- $f^{(n)}$: the n-th order coefficient in the Chapman-Enskog expansion of f [(2.23)]
- $\mathbf{f}_\mathrm{L}^{(0)}$, $\mathbf{f}_\mathrm{Q}^{(0)}$: the parts of the local equilibrium that are linear and quadratic in $\boldsymbol{u}$, respectively. [(4.7)]
- $\mathbf{f} := (f_0, f_1, \ldots, f_{q-1})^\dagger$: the distribution functions correspond to the discrete velocities $\{\boldsymbol{\xi}_0, \boldsymbol{\xi}_1, \ldots, \boldsymbol{\xi}_{q-1}\}$ [(3.17)]
- G: a constant acceleration [(2.17)]
- G_i: the forcing density along the direction of the velocity $\boldsymbol{\xi}_i$ [(3.1), (3.14)]

- $\mathbf{H} := \mathbf{K}[\mathbf{I} + \mathbf{J}]$: the evolution operator for the linearized LBE in Fourier space $\boldsymbol{k}$ [(5.4)]
- $\mathbf{H}^{(n)}$: the n-th order tensorial Hermite polynomial [(2.44), (2.45), (2.46)]
- $H(\boldsymbol{r}, t)$: the local H function $H(\boldsymbol{r}, t) := \int f \ln f \mathrm{d}\boldsymbol{\xi}$ [(2.12)]
- $\bar{H}(t)$: the global H function $\bar{H}(t) := \int H(\boldsymbol{r}, t)\mathrm{d}\boldsymbol{r}$ [(2.12)]
- $\mathbf{I}$: the identify tensor (matrix) [(2.29), (2.38), (2.39), (2.47)]
- $\mathcal{I}[\phi(\boldsymbol{\xi})]$: an integral operator of $\phi(\boldsymbol{\xi})$ w.r.t. $Q[f, f_*]$, $\mathcal{I}[\phi(\boldsymbol{\xi})] := \langle \phi(\boldsymbol{\xi}) Q[f, f_*] \rangle$ [(2.6)]
- $\mathbf{J}$: Jacobian derived from the LBE [(4.17)]
- $\mathbf{K}$: $q \times q$ diagonal matrix with diagonal elements $\exp(\imath \boldsymbol{k} \cdot \boldsymbol{\xi}_i)$ [(5.4)]
- $\boldsymbol{j}_i^{(n)}$: The n-th order flux vector corresponding to collisional invariance φ_i and $f^{(n)}$ in the Hilbert expansion [(2.29)]
- $\mathrm{Kn} := \ell / L$: the Knudsen number [(2.17), (2.18)]
- k_B: the Boltzmann constant [(2.10b)]
- $\boldsymbol{K}$: the wave-vector in Fourier space corresponding to the velocity coordinates $\boldsymbol{\xi}$ [(3.57)]
- $\boldsymbol{k}$: the wave-vector in Fourier space corresponding to the spatial coordinates $\boldsymbol{r}$ [§5.1]
- LBE: lattice Boltzmann equation
- L: macroscopic characteristic length [(2.16)]
- $\mathcal{L}$: the linearized collision operator [(2.27)]
- $\mathcal{L}_N$: the mutilated linearized collision operator with N eigenvalues [(2.51)]
- ℓ: the molecular mean-free path [§2.2]
- $\mathbf{M}$: the transform matrix mapping the distribution functions $\mathbf{f}$ to the moments $\mathbf{m}$ [(3.24), (3.25), (3.23)]
- $\mathbf{M}^{(n)}$: the n-th order velocity moment tensor [(2.19)]
- Ma: the local Mach number $|\boldsymbol{u}|/c_\mathrm{s}$ or the characteristic Mach number V_0/c_s [(2.17)]
- $M(t)$: the central moment generating function of the distribution $f(x)$ [(3.55)]
- $m(t)$: the moment generating function of the distribution $f(x)$ [(3.53)]
- m: particle mass, $m = 1$ unless otherwise stated [(2.1b)]
- m_i: the i-th moment [§3.5]
- $m_i^{(0)}$: the equilibrium of the moment m_i [§3.5]
- $\delta\mathbf{m} := (\mathbf{m} - \mathbf{m}^{(0)})$: the nonequilibrium parts of the moments [(3.30)]
- NSF: Navier-Stokes-Fourier
- N: the total number of particles [§2.2]
- $n := n(\boldsymbol{r}, t) = \rho/m$: particle number density [(2.2)]
- $\mathbf{P}$: projection operator [(4.18)]
- $\mathbf{p} := \boldsymbol{\Pi} - p\mathbf{I}$ [(2.47)]
- $p := \rho\vartheta$: the pressure [(2.29)]
- $Q[f, f_*]$: the collision operator [(2.1b)]
- q: the number of discrete velocities [§3]
- $\boldsymbol{q}$: the heat (energy) flux vector [(2.22c)]
- $\boldsymbol{q}^{(n)}$: the n-th order heat flux vector corresponding to $f^{(n)}$ [(2.33b)]
- R the gas constant [§2.6]
- $\mathbf{R} := \mathbf{f}(\boldsymbol{x}_j + \boldsymbol{\xi}\varepsilon, t_n + \varepsilon^2) - \mathbf{f}(\boldsymbol{x}_j, t_n) - \mathbf{Q}(\boldsymbol{x}_j, t_n)$: the residual for the LBE [(4.6), (4.7)]
- $\boldsymbol{r}$: the spatial position in d dimensions, *i.e.*, $\boldsymbol{r} \in \mathbb{R}^d$ [(2.1a)]
- $r_{21} := |\boldsymbol{r}_2 - \boldsymbol{r}_1|$: the spatial distance between two points $\boldsymbol{r}_2$ and $\boldsymbol{r}_1$ [(2.3)]
- $\mathbf{S}$: diagonal matrix of relaxation rates $\{s_i | 0 \le i \le q-1\}$ [(3.25)]
- $\hat{\mathbf{S}} := \mathbf{M}^{-1}\mathbf{S}\mathbf{M}$ [§3.5]
- $\mathrm{St} := L/\tau_0 \bar{c}_\mathrm{s}$: the kinetic Strouhal number [(2.17)]
- s_i: the i-th relaxation rate [(3.25)]
- $U(\boldsymbol{r}_1, \boldsymbol{r}_2)$: two-body potential [(2.2)]
- $\boldsymbol{u} := \boldsymbol{u}(\boldsymbol{x}, t)$: the flow velocity [(2.10b)]
- $\boldsymbol{u}^{(n)}$: the coefficient in the expansion of $\boldsymbol{u}$ corresponding to $f^{(n)}$ [(4.4)]
- $\boldsymbol{u}_\varepsilon$: the flow velocity corresponding to $\mathbf{f}(\boldsymbol{x}_j, t_n; \varepsilon)$ [(4.4)]
- $u_\parallel$: the component of $\boldsymbol{u}$ along a given direction $\hat{\boldsymbol{k}}$ [(5.2)]
- $\boldsymbol{u}_\perp$: the component of $\boldsymbol{u}$ perpendicular to a given direction $\hat{\boldsymbol{k}}$ [(5.2)]
- $\boldsymbol{V} := \boldsymbol{\xi}_* - \boldsymbol{\xi}$: the difference between the incidental velocities [(2.1)]
- V_0: characteristic macroscopic flow speed [2.2]
- $\mathbf{W}$: the $q \times q$ diagonal matrix $\mathbf{W} := \mathrm{diag}(w_0, w_1, \ldots, w_b)$ [(4.17)]
- w_i: the weight corresponding to the discrete velocity $\boldsymbol{\xi}_i$ [§3, §3.2]
- $\mathbb{X}_q$: the set of q discrete velocities $\{\boldsymbol{\xi}_i | 0 \le i \le q-1\}$ [§3, (3.2)]
- $Z(z, \boldsymbol{k})$: the characteristic polynomial associate with $\mathbf{H}$ [(5.5)]

Greek symbols:

- α: accommodation coefficient [(2.52)]

- γ: the adiabatic exponent or the ratio of specific heats [(3.49)]
- ϵ: the polar angle on the plane perpendicular to $\boldsymbol{V} := \boldsymbol{\xi}_* - \boldsymbol{\xi}$ [(2.1)]
- ε: a small parameter, in the Hilbert and Chapman-Enskog expansions in §2, $\varepsilon \sim \mathrm{Kn}$; in the Taylor expansions in §4, $\varepsilon \sim \delta_x$, δ_x is the grid spacing.
- Θ: the angle between the apse line and $\boldsymbol{V} := \boldsymbol{\xi}_* - \boldsymbol{\xi}$ in the plane of particle trajectory, as depicted in Fig. 1 [(2.1b), (2.4)]
- $\theta := \pi - 2\Theta$: deflection angle in binary elastic collision [(2.5)]
- $\vartheta := k_B T/m$: internal energy per unit mass and per degree of freedom [(2.10b), §2.2]
- $\vartheta_0 := k_B T_0/m$: reference or initial internal energy per unit mass and per degree of freedom [§2.2]
- κ: heat diffusivity or diffusivity [(2.39b), (3.42), (3.43)]
- $\kappa(t) := \ln m(t)$: the cumulant generating function [(3.56)]
- κ_n: the n-th order cumulant [(3.56)]
- $\boldsymbol{\Lambda}$: diagonal matrix with the elements of relaxation rates $\{s_i\}$ [(4.18)]
- μ: the dynamic viscosity [(2.39a), (2.40a)]
- μ_n: the n-th order moment of a distribution function $f(x)$ [(3.52)]
- $\nu := \mu/\rho$: the kinematic (or shear) viscosity [(2.42), (4.11)]
- $\boldsymbol{\xi}$: molecular velocity [(2.1)]
- $\boldsymbol{\xi}_i$: the i-th discrete velocity [(3.2), (3.7), (3.8)]
- $\boldsymbol{\xi}_{\bar{i}} := -\boldsymbol{\xi}_i$ [(4.9)]
- $\boldsymbol{\Pi}$: the pressure tensor [(2.22b)]
- $\boldsymbol{\Pi}^{(n)}$: the n-th order pressure tensor corresponding to $f^{(n)}$ [(2.33a)]
- $\rho = \rho(\boldsymbol{x}, t)$: flow mass density [(2.10b)]
- $\rho^{(n)}$: the coefficient in the expansion of ρ corresponding to $f^{(n)}$ [(4.4)]
- ρ_ε: the density corresponding to $\mathbf{f}(\boldsymbol{x}_j, t_n; \varepsilon)$ [(4.4)]
- $\varrho = \varrho(\boldsymbol{x}, t)$: conserved moments [(2.10)]
- $\boldsymbol{\Sigma}$: strain-rate tensor [(2.39a)]
- $\widehat{\boldsymbol{\Sigma}}$: the traceless part of $\boldsymbol{\Sigma}$, $\widehat{\boldsymbol{\Sigma}} := \boldsymbol{\Sigma} - \frac{1}{d}(\nabla \cdot \boldsymbol{u})\mathbf{I}$ [(2.39)]
- $\boldsymbol{\sigma}$: the shear stress tensor [(2.39), (4.31)]
- $\widehat{\boldsymbol{\sigma}}$: the traceless part of the shear stress tensor [(2.39)]
- $\sigma(\chi, V)$: the differential collision cross section [(2.5)]
- ς: the effective particle radius or interaction range [§2.2]
- ζ: the bulk viscosity [(4.31), (4.32)]
- τ: the mean-free time [§2.2]
- τ_ν: the relaxation time for the continuous BGK model [(3.35)]
- τ_0: the macroscopic characteristic temporal scale [§2.2, (2.16)]
- $\phi^{(n)}$: $\phi^{(n)} := f^{(n)}/f^{(0)}$, $f^{(n)}$ is the coefficient of the n-th order term in the Hilbert expansion [(2.23)]
- $\phi(\boldsymbol{\xi})$: a collisional invariant [(2.8)]
- φ_i: $\{\varphi_i | 0 \le i \le d+1\}$ collisional invariants [(2.10a)]
- $\varphi^{(n)}$: the coefficient in the n-th order Hilbert expansion (2.24)
- $\boldsymbol{\Psi}$: the $q \times q$ diagonal matrix whose diagonal elements are $|\boldsymbol{\Psi}_i|^2$, $0 \le i \le q-1$ [(3.30), (3.31)]
- $\boldsymbol{\Psi}_i \in \mathbb{R}^q$: eigenvector of the LBE collision operator whose elements are $\psi_i(\boldsymbol{\xi}_k)$, $0 \le k \le (q-1)$ [(3.18)]
- $\psi_i(\boldsymbol{\xi})$: the orthogonal polynomials on the discrete velocity set $\{\boldsymbol{\xi}_i\}$ [(3.18)]
- χ_n: the n-th order moment about the mean, *i.e.*, the n-th central moment [(3.54)]

References

[1] O.B. Usta, J.E. Butler, A.J.C. Ladd, Transverse migration of a confined polymer driven by an external force, Phys. Rev. Lett. 98 (9) (2007) 098301, https://doi.org/10.1103/PhysRevLett.98.098301.

[2] A.J.C. Ladd, R. Kekre, J.E. Butler, Comparison of the static and dynamic properties of a semiflexible polymer using lattice Boltzmann and Brownian-dynamics simulations, Phys. Rev. E 80 (3) (2009) 036704, https://doi.org/10.1103/PhysRevE.80.036704.

[3] Y. Zhang, A. Donev, T. Weisgraber, B.J. Alder, M.D. Graham, J.J. de Pablo, Tethered DNA dynamics in shear flow, J. Chem. Phys. 130 (23) (2009) 234902, https://doi.org/10.1063/1.3149860.

[4] O.A. Hickey, C. Holm, J.L. Harden, G.W. Slater, Implicit method for simulating electrohydrodynamics of polyelectrolytes, Phys. Rev. Lett. 105 (14) (2010) 148301, https://doi.org/10.1103/PhysRevLett.105.148301.

[5] A. Hammack, Y.-L. Chen, J.K. Pearce, Role of dissolved salts in thermophoresis of DNA: lattice-Boltzmann-based simulations, Phys. Rev. E 83 (3, 1) (2011) 031915, https://doi.org/10.1103/PhysRevE.83.031915.

[6] F. Farahpour, A. Maleknejad, F. Varnik, M.R. Ejtehadi, Chain deformation in translocation phenomena, Soft Matter 9 (9) (2013) 2750–2759, https://doi.org/10.1039/c2sm27416g.

[7] O.A. Hickey, C. Holm, J. Smiatek, Lattice-Boltzmann simulations of the electrophoretic stretching of polyelectrolytes: the importance of hydrodynamic interactions, J. Chem. Phys. 140 (16) (2014) 164904, https://doi.org/10.1063/1.4872366.

[8] Y.-L. Chen, H. Ma, M.D. Graham, J.J. de Pablo, Modeling DNA in confinement: a comparison between the Brownian dynamics and lattice Boltzmann method, Macromolecules 40 (16) (2007) 5978–5984, https://doi.org/10.1021/ma070729t.

[9] A. Izmitli, D.C. Schwartz, M.D. Graham, J.J. de Pablo, The effect of hydrodynamic interactions on the dynamics of DNA translocation through pores, J. Chem. Phys. 128 (8) (2008) 085102, https://doi.org/10.1063/1.2831777.

[10] J. Hall, N. Clarke, The mechanics of cilium beating: quantifying the relationship between metachronal wavelength and fluid flow rate, J. Fluid Mech. 891 (2020) A20, https://doi.org/10.1017/jfm.2020.161.
[11] X. Frank, D. Funfschilling, N. Midoux, H. Li, Bubbles in a viscous liquid: lattice Boltzmann simulation and experimental validation, J. Fluid Mech. 546 (2006) 113–122, https://doi.org/10.1017/S0022112005007135.
[12] K. Connington, T. Lee, Lattice Boltzmann simulations of forced wetting transitions of drops on superhydrophobic surfaces, J. Comput. Phys. 250 (2013) 601–615, https://doi.org/10.1016/j.jcp.2013.05.012.
[13] J.-Y. Delenne, V. Richefeu, F. Radjai, Liquid clustering and capillary pressure in granular media, J. Fluid Mech. 762 (2015) R5, https://doi.org/10.1017/jfm.2014.676.
[14] J.E. McClure, M.A. Berrill, W.G. Gray, C.T. Miller, Tracking interface and common curve dynamics for two-fluid flow in porous media, J. Fluid Mech. 796 (2016) 211–232, https://doi.org/10.1017/jfm.2016.212.
[15] A. Fakhari, D. Bolster, L.-S. Luo, A weighted multiple-relaxation-time lattice Boltzmann method for multiphase flows and its application to partial coalescence cascades, J. Comput. Phys. 341 (2017) 22–43, https://doi.org/10.1016/j.jcp.2017.03.062.
[16] R.H.H. Abadi, M.H. Rahimian, A. Fakhari, Conservative phase-field lattice-Boltzmann model for ternary fluids, J. Comput. Phys. 374 (2018) 668–691, https://doi.org/10.1016/j.jcp.2018.07.045.
[17] L. Rego, F. Avallone, D. Ragni, D. Casalino, Jet-installation noise and near-field characteristics of jet-surface interaction, J. Fluid Mech. 895 (2020), https://doi.org/10.1017/jfm.2020.294.
[18] Z. Feng, E.E. Michaelides, The immersed boundary-lattice Boltzmann method for solving fluid-particles interaction problems, J. Comput. Phys. 195 (2) (2004) 602–628, https://doi.org/10.1016/j.jcp.2003.10.013.
[19] F.-B. Tian, H. Luo, L. Zhu, J.C. Liao, X.-Y. Lu, An efficient immersed boundary-lattice Boltzmann method for the hydrodynamic interaction of elastic filaments, J. Comput. Phys. 230 (19) (2011) 7266–7283, https://doi.org/10.1016/j.jcp.2011.05.028.
[20] F. Dugast, Y. Favennec, C. Josset, Reactive fluid flow topology optimization with the multi-relaxation time lattice Boltzmann method and a level-set function, J. Comput. Phys. 409 (2020) 109252, https://doi.org/10.1016/j.jcp.2020.109252.
[21] P. Lallemand, L.-S. Luo, Lattice Boltzmann equation with overset method for moving objects in two-dimensional flows, J. Comput. Phys. 407 (2020), https://doi.org/10.1016/j.jcp.2019.109223.
[22] C. Sun, C. Migliorini, L.L. Munn, Red blood cells initiate leukocyte rolling in postcapillary expansions: a lattice Boltzmann analysis, Biophys. J. 85 (1) (2003) 208–222.
[23] J. Zhang, P.C. Johnson, A.S. Popel, Red blood cell aggregation and dissociation in shear flows simulated by lattice Boltzmann method, J. Biomech. 41 (1) (2008) 47–55, https://doi.org/10.1016/j.jbiomech.2007.07.020.
[24] S. Melchionna, A model for red blood cells in simulations of large-scale blood flows, Macromol. Theory Simul. 20 (7, SI) (2011) 548–561, https://doi.org/10.1002/mats.201100012.
[25] D.A. Reasor Jr., M. Mehrabadi, D.N. Ku, C.K. Aidun, Determination of critical parameters in platelet margination, Ann. Biomed. Eng. 41 (2) (2013) 238–249, https://doi.org/10.1007/s10439-012-0648-7.
[26] J. Wylie, D. Koch, A. Ladd, Rheology of suspensions with high particle inertia and moderate fluid inertia, J. Fluid Mech. 480 (2003) 95–118, https://doi.org/10.1017/S0022112002003531.
[27] P. Poesio, G. Ooms, A. Ten Cate, J.C.R. Hunt, Interaction and collisions between particles in a linear shear flow near a wall at low Reynolds number, J. Fluid Mech. 555 (2006) 113–130, https://doi.org/10.1017/S0022112006008780.
[28] C.K. Aidun, J.R. Clausen, Lattice-Boltzmann method for complex flows, Annu. Rev. Fluid Mech. 42 (2010) 439–472.
[29] M. Masaeli, E. Sollier, H. Amini, W. Mao, K. Camacho, N. Doshi, S. Mitragotri, A. Alexeev, D. Di Carlo, Continuous inertial focusing and separation of particles by shape, Phys. Rev. X 2 (3) (2012) 031017, https://doi.org/10.1103/PhysRevX.2.031017.
[30] K.W. Connington, T. Lee, J.F. Morris, Interaction of fluid interfaces with immersed solid particles using the lattice Boltzmann method for liquid-gas-particle systems, J. Comput. Phys. 283 (2015) 453–477, https://doi.org/10.1016/j.jcp.2014.11.044.
[31] D. Nie, J. Lin, Simulation of sedimentation of two spheres with different densities in a square tube, J. Fluid Mech. 896 (2020), https://doi.org/10.1017/jfm.2020.291.
[32] N. Wang, C. Semprebon, H. Liu, C. Zhang, H. Kusumaatmaja, Modelling double emulsion formation in planar flow-focusing microchannels, J. Fluid Mech. 895 (2020), https://doi.org/10.1017/jfm.2020.299.
[33] B. Ferreol, D. Rothman, Lattice-Boltzmann simulations of flow-through Fontainebleau sandstone, Transp. Porous Media 20 (1–2) (1995) 3–20, https://doi.org/10.1007/BF00616923.
[34] M. Spaid, F. Phelan, Lattice Boltzmann methods for modeling microscale flow in fibrous porous media, Phys. Fluids 9 (9) (1997) 2468–2474, https://doi.org/10.1063/1.869392.
[35] A. Koponen, D. Kandhai, E. Hellen, M. Alava, A. Hoekstra, M. Kataja, K. Niskanen, P. Sloot, J. Timonen, Permeability of three-dimensional random fiber webs, Phys. Rev. Lett. 80 (4) (1998) 716–719, https://doi.org/10.1103/PhysRevLett.80.716.
[36] B. Manz, L. Gladden, P. Warren, Flow and dispersion in porous media: lattice-Boltzmann and NMR studies, AIChE J. 45 (9) (1999) 1845–1854, https://doi.org/10.1002/aic.690450902.
[37] R. Hill, D. Koch, A. Ladd, The first effects of fluid inertia on flows in ordered and random arrays of spheres, J. Fluid Mech. 448 (2001) 213–241.
[38] R. Hill, D. Koch, A. Ladd, Moderate-Reynolds-number flows in ordered and random arrays of spheres, J. Fluid Mech. 448 (2001) 243–278.
[39] B. Ahrenholz, J. Tölke, P. Lehmann, A. Peters, A. Kaestner, M. Krafczyk, W. Durner, Prediction of capillary hysteresis in a porous material using lattice-Boltzmann methods and comparison to experimental data and a morphological pore network model, Adv. Water Resour. 31 (9) (2008) 1151–1173.
[40] V. Pot, S. Peth, O. Monga, L.E. Vogel, A. Genty, P. Garnier, L. Vieuble-Gonod, M. Ogurreck, F. Beckmann, P.C. Baveye, Three-dimensional distribution of water and air in soil pores: Comparison of two-phase two-relaxation-times lattice-Boltzmann and morphological model outputs with synchrotron X-ray computed tomography data, Adv. Water Resour. 84 (2015) 87–102, https://doi.org/10.1016/j.advwatres.2015.08.006.
[41] X. Yang, Y. Mehmani, W.A. Perkins, A. Pasquali, M. Schönherr, K. Kim, M. Perego, M.L. Parks, N. Trask, M.T. Balhoff, M.C. Richmond, M. Geier, M. Krafczyk, L.-S. Luo, A.M. Tartakovsky, T.D. Scheibe, Intercomparison of 3D pore-scale flow and solute transport simulation methods, Adv. Water Resour. 95 (2016) 176–189.
[42] G.J. Rubinstein, J.J. Derksen, S. Sundaresan, Lattice Boltzmann simulations of low-Reynolds-number flow past fluidized spheres: effect of Stokes number on drag force, J. Fluid Mech. 788 (2016) 576–601, https://doi.org/10.1017/jfm.2015.679.
[43] A. Fakhari, Y. Li, D. Bolster, K.T. Christensen, A phase-field lattice Boltzmann model for simulating multiphase flows in porous media: application and comparison to experiments of CO_2 sequestration at pore scale, Adv. Water Resour. 114 (2018) 119–134, https://doi.org/10.1016/j.advwatres.2018.02.005.
[44] D. Maggiolo, F. Picano, F. Zanini, S. Carmignato, M. Guarnieri, S. Sasic, H. Strom, Solute transport and reaction in porous electrodes at high Schmidt numbers, J. Fluid Mech. 896 (2020) A13, https://doi.org/10.1017/jfm.2020.344.
[45] A. Parmigiani, S. Faroughi, C. Huber, O. Bachmann, Y. Su, Bubble accumulation and its role in the evolution of magma reservoirs in the upper crust, Nature 532 (7600) (2016) 492, https://doi.org/10.1038/nature17401.
[46] T. Gao, X.-Y. Lu, Insect normal hovering flight in ground effect, Phys. Fluids 20 (8) (2008) 087101, https://doi.org/10.1063/1.2958318.
[47] G.-J. Li, X.-Y. Lu, Force and power of flapping plates in a fluid, J. Fluid Mech. 712 (2012) 598–613, https://doi.org/10.1017/jfm.2012.443.

[48] D. Qi, G. He, Y. Liu, Lattice Boltzmann simulations of a pitch-up and pitch-down maneuver of a chord-wise flexible wing in a free stream flow, Phys. Fluids 26 (2) (2014) 021902, https://doi.org/10.1063/1.4866182.
[49] K. Suzuki, K. Minami, T. Inamuro, Lift and thrust generation by a butterfly-like flapping wing-body model: immersed boundary-lattice Boltzmann simulations, J. Fluid Mech. 767 (2015) 659–695, https://doi.org/10.1017/jfm.2015.57.
[50] M. Rouméas, P. Gilliéron, A. Kourta, Separated flows around the rear window of a simplified car geometry, Trans. ASME, J. Fluids Eng. 130 (2) (2008) 021101, https://doi.org/10.1115/1.2829566.
[51] M. Rouméas, P. Gilliéron, A. Kourta, Drag reduction by flow separation control on a car after body, Int. J. Numer. Methods Fluids 60 (11) (2009) 1222–1240, https://doi.org/10.1002/fld.1930.
[52] A. Pasquali, M. Schönherr, M. Geier, M. Krafczyk, Simulation of external aerodynamics of the DrivAer model with the LBM on GPGPUs, in: G.R. Joubert, H. Leather, M. Parsons, F. Peters, M. Sawyer (Eds.), Parallel Computing: on the Road to Exascale, in: Advances in Parallel Computing, vol. 27, IOS Press, Amsterdam, 2016, pp. 391–400.
[53] D.M. Holman, R.M. Brionnaud, M. Chavez Modena, E. Valero Sanchez, Lattice Boltzmann method contribution to the second high-lift prediction workshop, J. Aircr. 52 (4) (2015) 1122–1135, https://doi.org/10.2514/1.C033219.
[54] L. Djenidi, Lattice-Boltzmann simulation of grid-generated turbulence, J. Fluid Mech. 552 (2006) 13–35, https://doi.org/10.1017/S002211200600869X.
[55] D. Yu, S.S. Girimaji, Direct numerical simulations of homogeneous turbulence subject to periodic shear, J. Fluid Mech. 566 (2006) 117–151, https://doi.org/10.1017/S0022112006001832.
[56] O. Ertunc, N. Oezyilmaz, H. Lienhart, F. Durst, K. Beronov, Homogeneity of turbulence generated by static-grid structures, J. Fluid Mech. 654 (2010) 473–500, https://doi.org/10.1017/S0022112010000479.
[57] S.S. Chikatamarla, C.E. Frouzakis, I.V. Karlin, A.G. Tomboulides, K.B. Boulouchos, Lattice Boltzmann method for direct numerical simulation of turbulent flows, J. Fluid Mech. 656 (2010) 298–308, https://doi.org/10.1017/S0022112010002740.
[58] Z. Li, A. Banaeizadeh, F.A. Jaberi, Two-phase filtered mass density function for LES of turbulent reacting flows, J. Fluid Mech. 760 (2014) 243–277, https://doi.org/10.1017/jfm.2014.573.
[59] Y. Jin, M.F. Uth, A.V. Kuznetsov, H. Herwig, Numerical investigation of the possibility of macroscopic turbulence in porous media: a direct numerical simulation study, J. Fluid Mech. 766 (2015) 76–103, https://doi.org/10.1017/jfm.2015.9.
[60] A. Scagliarini, H. Einarsson, A. Gylfason, F. Toschi, Law of the wall in an unstably stratified turbulent channel flow, J. Fluid Mech. 781 (2015) R5, https://doi.org/10.1017/jfm.2015.498.
[61] R. Benzi, S. Succi, M. Vergassola, The lattice Boltzmann-equation: theory and applications, Phys. Rep. 222 (3) (1992) 145–197.
[62] S. Chen, G.D. Doolen, Lattice Boltzmann method for fluid flows, Annu. Rev. Fluid Mech. 30 (1998) 329–364.
[63] S. Succi, I.V. Karlin, H. Chen, Role of the *H* theorem in lattice Boltzmann hydrodynamic simulations, Rev. Mod. Phys. 74 (2002) 1203–1220.
[64] D. Yu, R. Mei, L.-S. Luo, W. Shyy, Viscous flow computations with the method of lattice Boltzmann equation, Prog. Aerosp. Sci. 39 (5) (2003) 329–367.
[65] D.H. Rothman, S. Zaleski, Lattice-Gas Cellular Automata: Simple Models of Complex Hydrodynamics, Cambridge University Press, Cambridge, UK, 1997.
[66] D.A. Wolf-Gladrow, Lattice-Gas Cellular Automata and Lattice Boltzmann Models, Lecture Notes in Mathematics, vol. 1725, Springer, New York, 2000.
[67] J. Zhou, Lattice Boltzmann Methods for Shallow Water Flows, Springer, Berlin, 2004.
[68] B. Chopard, M. Droz, Cellular Automata Modeling of Physical Systems, Cambridge University Press, Cambridge, UK, 2005.
[69] J.-P. Rivet, J. Boon, Lattice Gas Hydrodynamics, Cambridge University Press, Cambridge, UK, 2005.
[70] T. Krüger, H. Kusumaatmaja, A.K.O. Shardt, G. Silva, E.M. Viggen, The Lattice Boltzmann Method, Springer, Berlin, 2017.
[71] S. Succi, The Lattice Boltzmann Equation, Oxford University Press, New York, 2018.
[72] G.R. McNamara, G. Zanetti, Use of the lattice Boltzmann to simulate lattice-gas automata, Phys. Rev. Lett. 61 (1988) 2332–2335.
[73] F.J. Higuera, S. Succi, R. Benzi, Lattice gas dynamics with enhanced collisions, Europhys. Lett. 9 (4) (1989) 345–349.
[74] F.J. Higuera, J. Jiménez, Boltzmann approach to lattice gas simulations, Europhys. Lett. 9 (7) (1989) 663–668.
[75] M. Vergassola, R. Benzi, S. Succi, On the hydrodynamic behavior of the lattice Boltzmann-equation, Europhys. Lett. 13 (5) (1990) 411–416, https://doi.org/10.1209/0295-5075/13/5/006.
[76] U. Frisch, Relation between the lattice Boltzmann-equation and the Navier-Stokes equations, Physica D 47 (1–2) (1991) 231–232, https://doi.org/10.1016/0167-2789(91)90293-I.
[77] U. Frisch, B. Hasslacher, Y. Pomeau, Lattice-gas automata for the Navier-Stokes equation, Phys. Rev. Lett. 56 (1986) 1505–1508.
[78] D. d'Humières, P. Lallemand, U. Frisch, Lattice gas models for 3D hydrodynamics, Europhys. Lett. 2 (4) (1986) 291–297, https://doi.org/10.1209/0295-5075/2/4/006.
[79] S. Wolfram, Cellular automaton fluids 1: basic theory, J. Stat. Phys. 45 (1986) 471–526.
[80] U. Frisch, D. d'Humières, B. Hasslacher, P. Lallemand, Y. Pomeau, J.-P. Rivet, Lattice gas hydrodynamics in two and three dimensions, Complex Syst. 1 (1987) 649–707.
[81] D. d'Humières, Generalized lattice-Boltzmann equations, in: B.D. Shizgal, D.P. Weave (Eds.), Rarefied Gas Dynamics: Theory and Simulations, in: Prog. Astronaut. Aeronaut., vol. 159, AIAA, Washington, DC, 1992, pp. 450–458.
[82] T. Abe, Derivation of the lattice Boltzmann method by means of the discrete ordinate method for the Boltzmann equation, J. Comput. Phys. 131 (1) (1997) 241–246, https://doi.org/10.1006/jcph.1996.5595.
[83] X. He, L.-S. Luo, A priori derivation of the lattice Boltzmann equation, Phys. Rev. E 55 (6) (1997) R6333–R6336.
[84] X. He, L.-S. Luo, Theory of lattice Boltzmann method: from the Boltzmann equation to the lattice Boltzmann equation, Phys. Rev. E 56 (6) (1997) 6811–6817.
[85] P.J. Dellar, Nonhydrodynamic modes and a priori construction of shallow water lattice Boltzmann equations, Phys. Rev. E 65 (3, 2B) (2002) 036309, https://doi.org/10.1103/PhysRevE.65.036309.
[86] M. Junk, A. Klar, Discretizations for the incompressible Navier-Stokes equations based on the lattice Boltzmann method, SIAM J. Sci. Comput. 22 (1) (2000) 1–19, https://doi.org/10.1137/S1064827599357188.
[87] M. Junk, A finite difference interpretation of the lattice Boltzmann method, Numer. Methods Partial Differ. Equ. 17 (2001) 383–402.
[88] F. Dubois, P. Lallemand, C. Obrecht, M.M. Tekitek, Lattice Boltzmann model approximated with finite difference expressions, Comput. Fluids 155 (SI) (2017) 3–8, https://doi.org/10.1016/j.compfluid.2016.04.013.
[89] P. Asinari, T. Ohwada, Connection between kinetic methods for fluid-dynamic equations and macroscopic finite-difference schemes, Comput. Math. Appl. 58 (5) (2009) 841–861.
[90] T. Ohwada, P. Asinari, Artificial compressibility method revisited: asymptotic numerical method for incompressible Navier-Stokes equations, J. Comput. Phys. 229 (5) (2010) 1698–1723, https://doi.org/10.1016/j.jcp.2009.11.003.
[91] P. Asinari, T. Ohwada, E. Chiavazzo, A.F. Di Rienzo, Link-wise artificial compressibility method, J. Comput. Phys. 231 (15) (2012) 5109–5143, https://doi.org/10.1016/j.jcp.2012.04.027.
[92] A. Gunstensen, D. Rothman, S. Zaleski, G. Zanetti, Lattice Boltzmann model of immiscible fluids, Phys. Rev. A 43 (8) (1991) 4320–4327, https://doi.org/10.1103/PhysRevA.43.4320.
[93] A. Gunstensen, D. Rothman, Microscopic modeling of immiscible fluids in 3 dimensions by a lattice Boltzmann method, Europhys. Lett. 18 (2BIS) (1992) 157–161, https://doi.org/10.1209/0295-5075/18/2/012.

[94] X. He, S. Chen, R. Zhang, A lattice Boltzmann scheme for incompressible multiphase flow and its application in simulation of Rayleigh-Taylor instability, J. Comput. Phys. 146 (1999) 232–300.
[95] J. Tölke, M. Krafczyk, M. Schulz, E. Rank, Lattice Boltzmann simulations of binary fluid flow through porous media, Philos. Trans. R. Soc. Lond. Ser. A 360 (1792) (2002) 535–545.
[96] M. Geier, A. Fakhari, T. Lee, Conservative phase-field lattice Boltzmann model for interface tracking equation, Phys. Rev. E 91 (6) (2015), https://doi.org/10.1103/PhysRevE.91.063309.
[97] A. Fakhari, M. Geier, T. Lee, A mass-conserving lattice Boltzmann method with dynamic grid refinement for immiscible two-phase flows, J. Comput. Phys. 315 (2016) 434–457, https://doi.org/10.1016/j.jcp.2016.03.058.
[98] T. Mitchell, C. Leonardi, A. Fakhari, Development of a three-dimensional phase-field lattice Boltzmann method for the study of immiscible fluids at high density ratios, Int. J. Multiph. Flow 107 (2018) 1–15, https://doi.org/10.1016/j.ijmultiphaseflow.2018.05.004.
[99] S. Chapman, T.G. Cowling, The Mathematical Theory of Nonuniform Gases, Cambridge University Press, Cambridge, UK, 1952.
[100] J.O. Hirschfelder, C.F. Curtiss, R.B. Bird, Molecular Theory of Gases and Liquids, Wiley, New York, 1954.
[101] S. Harris, An Introduction to the Theory of Boltzmann Equation, Holt, Rinehart and Winston, New York, 1971, reprinted by Dover, 2004.
[102] C. Cercignani, The Boltzmann Equation and Its Applications, Springer, New York, 1988.
[103] C. Cercignani, R. Illner, M. Pulvirenti, The Mathematical Theory of Dilute Gases, Springer, New York, 1994.
[104] Y. Sone, Kinetic Theory and Fluid Dynamics, Birkhäuser, Boston, 2002.
[105] R.L. Liboff, Kinetic Theory: Classical, Quantum, and Relativistic Description, 3rd edition, Springer, New York, 2003.
[106] F. Golse, The Boltzmann equation and its hydrodynamic limits, in: C. Dafermos, E. Feireisl (Eds.), Evolutionary Equations, Vol. II of Handbooks of Differential Equations, Elsevier, Amsterdam, 2005, pp. 159–301, Ch. 3.
[107] Y. Sone, Molecular Gas Dynamics: Theory, Techniques, and Applications, Birkhäuser, Boston, 2007.
[108] L. Saint-Raymond, Hydrodynamic Limits of the Boltzmann Equation, Lecture Notes in Mathematics, vol. 1971, Springer, Heidelberg, Germany, 2009.
[109] H. Grad, Principles of the kinetic theory of gases, in: S. Flügge (Ed.), Thermodynamik der Gase, Vol. XII of Handbuch der Physik, Springer, Berlin, 1958, pp. 205–294, Ch. 26.
[110] L. Boltzmann, Lectures on Gas Theory, Dover, New York, 1995.
[111] C. Bardos, F. Golse, C.D. Levermore, Fluid dynamic limits of kinetic equations II convergence proofs for the Boltzmann equation, Commun. Pure Appl. Math. 46 (5) (1993) 667–753.
[112] J.C. Maxwell, On the dynamical theory of gases, Philos. Trans. R. Soc. Lond. 157 (1867) 49–88, reprinted in The Scientific Papers of James Clerk Maxwell, vol. 2, Cambridge University Press, Cambridge, 1890, pp. 26–78.
[113] E. Ikenberry, C. Truesdell, On the pressures and the flux of energy in a gas according to Maxwell kinetic theory 1, J. Ration. Mech. Anal. 5 (1) (1956) 1–54.
[114] C. Truesdell, R.G. Muncaster, Fundamentals of Maxwell's Kinetic Theory of a Simple Monatomic Gas: Treated as a Branch of Rational Mechanics, Pure and Applied Mathematics, vol. 83, Academic Press, New York, 1980.
[115] A.C. Pipkin, A Course on Integral Equations, Springer, New York, 1991.
[116] R. Kress, Linear Integral Equations, 3rd edition, Applied Mathematics Sciences, vol. 82, Springer, New York, 2014.
[117] C. Cercignani, Mathematical Methods in Kinetic Theory, 2nd edition, Plunum Press, New York, 1990.
[118] H. Grad, Note on n-dimensional Hermite polynomials, Commun. Pure Appl. Math. 2 (4) (1949) 325–330.
[119] H. Grad, On the kinetic theory of rarefied gases, Commun. Pure Appl. Math. 2 (4) (1949) 331–407.
[120] H. Struchtrup, Microscopic Transport Equations for Rarefied Gas Flows — Approximation Methods in Kinetic Theory, Interaction of Mechanics and Mathematics, Springer, Berlin, 2005.
[121] I. Müller, T. Ruggeri, Rational Extended Thermodynamics, Springer Tracts in Natural Philosophy, vol. 37, Springer, Heidelberg, 1998.
[122] Z. Cai, Y. Fan, R. Li, On hyperbolicity of 13-moment system, Kinet. Relat. Models 7 (3) (2014) 415–432, https://doi.org/10.3934/krm.2014.7.415.
[123] Z. Cai, Y. Fan, R. Li, Globally hyperbolic regularization of Grad's moment system, Commun. Pure Appl. Math. 67 (3) (2014) 464–518, https://doi.org/10.1002/cpa.21472.
[124] Z. Cai, Y. Fan, R. Li, A framework on moment model reduction for kinetic equation, SIAM J. Appl. Math. 75 (5) (2015) 2001–2023, https://doi.org/10.1137/14100110X.
[125] W. Zhao, W.-A. Yong, L.-S. Luo, Stability analysis of a class of globally hyperbolic moment system, Commun. Math. Sci. 15 (3) (2017) 609–633.
[126] E.P. Gross, E.A. Jackson, Kinetic models and the linearized Boltzmann equation, Phys. Fluids 2 (4) (1959) 432–441.
[127] P.L. Bhatnagar, E.P. Gross, M. Krook, A model for collision processes in gases. I. Small amplitude processes in charged and neutral one-component systems, Phys. Rev. 94 (3) (1954) 511–525.
[128] E.M. Shakhov, Generalization of the Krook kinetic relaxation equation, Fluid Dyn. 3 (5) (1968) 95–96.
[129] L. Sirovich, Kinetic modeling of gas mixtures, Phys. Fluids 5 (8) (1962) 908–918, https://doi.org/10.1063/1.1706706.
[130] C. Cercignani, M. Lampis, Kinetic model for gas-surface interaction, Transp. Theory Stat. Phys. 1 (2) (1971) 101–114, https://doi.org/10.1080/00411457108231440.
[131] F. Sharipov, Rarefied Gas Dynamics – Fundamentals for Research and Practice, Wiley-VCH, Berlin, Germany, 2016.
[132] F.R.W. McCourt, J.J.M. Beenakker, W.E. Köhler, I. Kuscer, Nonequilibrium Phenomena in Polyatomic Gases: Volume 1: Dilute Gases, Oxford University Press, Oxford, UK, 1990.
[133] R.B. Bird, C.F. Curtis, R.C. Amstrong, O. Hassager, Dynamics of Polymeric Liquids, Volume 2: Kinetic Theory, 2nd edition, Wiley, New York, 1987.
[134] M. Doi, S.F. Edwards, The Theory of Polymer Dynamics, Clarendon Press, Oxford, UK, 1986.
[135] X. Shan, X. He, Discretization of the velocity space in the solution of the Boltzmann equation, Phys. Rev. Lett. 80 (1998) 65–68.
[136] R. Rubinstein, L.-S. Luo, Theory of the lattice Boltzmann equation: symmetry properties of discrete velocity sets, Phys. Rev. E 77 (3) (2008) 036709.
[137] Y.H. Qian, S.A. Orszag, Lattice BGK models for the Navier-Stokes equation: nonlinear deviation in compressible regimes, Europhys. Lett. 21 (3) (1993) 255–259, https://doi.org/10.1209/0295-5075/21/3/001.
[138] D. d'Humières, M. Bouzidi, P. Lallemand, Thirteen-velocity three-dimensional lattice Boltzmann model, Phys. Rev. E 63 (2001) 066702.
[139] D. d'Humières, I. Ginzburg, M. Krafczyk, P. Lallemand, L.-S. Luo, Multiple-relaxation-time lattice Boltzmann models in three-dimensions, Philos. Trans. R. Soc. Lond. Ser. A 360 (1792) (2002) 437–451.
[140] X. He, S. Chen, G.D. Doolen, A novel thermal model for the lattice Boltzmann method in incompressible limit, J. Comput. Phys. 146 (1) (1998) 282–300.
[141] P.J. Dellar, An interpretation and derivation of the lattice Boltzmann method using Strang splitting, Comput. Math. Appl. 65 (2013) 129–141.
[142] S. Dellacherie, Construction and analysis of lattice Boltzmann methods applied to a 1D convection-diffusion equation, Acta Appl. Math. 131 (2014) 69–140.
[143] L.-S. Luo, Unified theory of the lattice Boltzmann models for nonideal gases, Phys. Rev. Lett. 81 (1998) 1618–1621.
[144] L.-S. Luo, Theory of lattice Boltzmann method: lattice Boltzmann models for nonideal gases, Phys. Rev. E 62 (4) (2000) 4982–4996.
[145] J.R. Weimar, J.P. Boon, Nonlinear reactions advected by a flow, Physica A 224 (1–2) (1996) 207–215, https://doi.org/10.1016/0378-4371(95)00355-X.
[146] Y.H. Qian, Y. Zhou, Complete Galilean-invariant lattice BGK models for the Navier-Stokes equation, Europhys. Lett. 42 (4) (1998) 359–364, https://doi.org/10.1209/epl/i1998-00255-3.

[147] G. Silva, V. Semiao, Truncation errors and the rotational invariance of three-dimensional lattice models in the lattice Boltzmann method, J. Comput. Phys. 269 (2014) 259–279, https://doi.org/10.1016/j.jcp.2014.03.027.
[148] K. Suga, Y. Kuwata, K. Takashima, R. Chikasue, A D3Q27 multiple-relaxation-time lattice Boltzmann method for turbulent flows, Comput. Math. Appl. 69 (6) (2015) 518–529, https://doi.org/10.1016/j.camwa.2015.01.010.
[149] P. Lallemand, L.-S. Luo, Theory of the lattice Boltzmann method: dispersion, dissipation, isotropy, Galilean invariance, and stability, Phys. Rev. E 61 (6) (2000) 6546–6562.
[150] P. Lallemand, D. d'Humières, L.-S. Luo, R. Rubinstein, Theory of the lattice Boltzmann method: three-dimensional model for linear viscoelastic fluids, Phys. Rev. E 67 (2003) 021203.
[151] P. Lallemand, L.-S. Luo, Theory of the lattice Boltzmann method: acoustic and thermal properties in two and three dimensions, Phys. Rev. E 68 (3) (2003) 036706.
[152] A.J.C. Ladd, Short-time motion of colloidal particles — numerical-simulation via a fluctuating lattice-Boltzmann equation, Phys. Rev. Lett. 70 (9) (1993) 1339–1342, https://doi.org/10.1103/PhysRevLett.70.1339.
[153] R. Adhikari, K. Stratford, M.E. Cates, A.J. Wagner, Fluctuating lattice Boltzmann, Europhys. Lett. 71 (3) (2005) 473–479, https://doi.org/10.1209/epl/i2004-10542-5.
[154] B. Chun, A.J.C. Ladd, Interpolated boundary condition for lattice Boltzmann simulations of flows in narrow gaps, Phys. Rev. E 75 (6) (2007) 066705, https://doi.org/10.1103/PhysRevE.75.066705.
[155] B. Dünweg, U.D. Schiller, A.J.C. Ladd, Statistical mechanics of the fluctuating lattice Boltzmann equation, Phys. Rev. E 76 (3) (2007) 036704, https://doi.org/10.1103/PhysRevE.76.036704.
[156] I.V. Karlin, S. Ansumali, C.E. Frouzakis, S.S. Chikatamarla, Elements of the lattice Boltzmann method I: linear advection equation, Commun. Comput. Phys. 1 (4) (2006) 616–655.
[157] F. Drui, E. Franck, P. Helluy, L. Navoret, An analysis of over-relaxation in a kinetic approximation of systems of conservation laws, C. R. Mecanique 347 (3) (2019) 259–269, https://doi.org/10.1016/j.crme.2018.12.001.
[158] Y. Peng, W. Liao, L.-S. Luo, L.-P. Wang, Comparison of the lattice Boltzmann and pseudo-spectral methods for decaying turbulence: low order statistics, Comput. Fluids 39 (4) (2010) 568–591.
[159] M. Geier, M. Schönherr, A. Pasquali, M. Krafczyk, The cumulant lattice Boltzmann equation in three dimensions: theory and validation, Comput. Math. Appl. 70 (4) (2015) 507–547.
[160] I. Ginzburg, Equilibrium-type and link-type lattice Boltzmann models for generic advection and anisotropic-dispersion equation, Adv. Water Resour. 28 (11) (2005) 1171–1195.
[161] I. Ginzburg, Generic boundary conditions for lattice Boltzmann models and their application to advection and anisotropic dispersion equations, Adv. Water Resour. 28 (11) (2005) 1196–1216.
[162] I. Ginzburg, Variably saturated flow described with the anisotropic lattice Boltzmann methods, Comput. Fluids 35 (8–9) (2006) 831–848.
[163] I. Ginzburg, D. d'Humières, Lattice Boltzmann and analytical modeling of flow processes in anisotropic and heterogeneous stratified aquifers, Adv. Water Resour. 30 (11) (2007) 2202–2234.
[164] I. Ginzburg, Lattice Boltzmann modeling with discontinuous collision components: hydrodynamic and advection-diffusion equations, J. Stat. Phys. 126 (1) (2007) 157–206.
[165] I. Ginzburg, F. Verhaeghe, D. d'Humières, Two-relaxation-time lattice Boltzmann scheme: about parametrization, velocity, pressure and mixed boundary conditions, Commun. Comput. Phys. 3 (2) (2008) 427–478.
[166] I. Ginzburg, F. Verhaeghe, D. d'Humières, Study of simple hydrodynamic solutions with the two-relaxation-times lattice Boltzmann scheme, Commun. Comput. Phys. 3 (3) (2008) 519–581.
[167] I. Ginzburg, D. d'Humières, A. Kuzmin, Optimal stability of advection-diffusion lattice Boltzmann models with two relaxation times for positive/negative equilibrium, J. Stat. Phys. 139 (6) (2010) 1090–1143.
[168] I. Ginzburg, Truncation errors, exact and heuristic stability analysis of two-relaxation-times lattice Boltzmann schemes for anisotropic advection-diffusion equation, Commun. Comput. Phys. 11 (5) (2012) 1439–1502.
[169] I. Ginzburg, L. Roux, Truncation effect on Taylor-Aris dispersion in lattice Boltzmann schemes: accuracy towards stability, J. Comput. Phys. 299 (2015) 974–1003, https://doi.org/10.1016/j.jcp.2015.07.017.
[170] M. Zhang, W. Zhao, P. Lin, Lattice Boltzmann method for general convection-diffusion equations: MRT model and boundary schemes, J. Comput. Phys. 389 (2019) 147–163, https://doi.org/10.1016/j.jcp.2019.03.045.
[171] M. Hénon, Viscosity of a lattice gas, Complex Syst. 1 (1987) 763–789.
[172] J. Wang, D. Wang, P. Lallemand, L.-S. Luo, Lattice Boltzmann simulations of thermal convective flows in two dimensions, Comput. Math. Appl. 65 (2) (2013) 262–286.
[173] F. Dubois, P. Lallemand, M.M. Tekitek, On anti-bounce back boundary condition for lattice Boltzmann schemes, Comput. Math. Appl. 79 (3) (2020) 555–575.
[174] F. Dubois, P. Lallemand, Towards higher order lattice Boltzmann schemes, J. Stat. Mech. Theory Exp. 2009 (2009) P06006.
[175] F. Dubois, C.-A. Lin, M.M. Tekitek, Anisotropic thermal lattice Boltzmann simulation of 2D natural convection in a square cavity, Comput. Fluids 124 (2016) 278–287, https://doi.org/10.1016/j.compfluid.2015.10.015.
[176] J.D. Anderson Jr., Hypersonic and High Temperature Gas Dynamics, McGraw-Hill, New York, 1989, reprinted by AIAA, 2000.
[177] F. Alexander, S. Chen, J. Sterling, Lattice Boltzmann thermohydrodynamics, Phys. Rev. E 47 (4) (1993) R2249–R2252.
[178] G. McNamara, A. Garcia, B. Alder, A hydrodynamically correct thermal lattice Boltzmann model, J. Stat. Phys. 87 (5/6) (1997) 1111–1121.
[179] P.J. Dellar, Two routes from the Boltzmann equation to compressible flow of polyatomic gases, Prog. Comput. Fluid Dyn. 8 (1–4) (2008) 84–96, https://doi.org/10.1504/PCFD.2008.018081.
[180] G. McNamara, B. Alder, Analysis of the lattice Boltzmann treatment of hydrodynamics, Physica A 194 (1993) 218–228.
[181] Y. Chen, H. Ohashi, M. Akiyama, Heat-transfer in lattice BGK modeled fluid, J. Stat. Phys. 81 (1–2) (1995) 71–85.
[182] G. McNamara, A. Garcia, B. Alder, Stabilization of thermal lattice Boltzmann models, J. Stat. Phys. 81 (1/2) (1995) 395–408.
[183] P.J. Dellar, Lattice and discrete Boltzmann equations for fully compressible flow, in: K.-J. Bathe (Ed.), Computational Fluid and Solid Mechanics 2005, Elsevier, Amsterdam, the Netherlands, 2005, pp. 632–635.
[184] P. Lallemand, L.-S. Luo, Hybrid finite-difference thermal lattice Boltzmann equation, Int. J. Mod. Phys. B 17 (1/2) (2003) 41–47.
[185] P. Lallemand, F. Dubois, Comparison of simulations of convective flows, Commun. Comput. Phys. 17 (5) (2015) 1169–1184, https://doi.org/10.4208/cicp.2014.m400.
[186] J.G.M. Eggels, J.A. Somers, Numerical-simulation of free convective flow using the lattice-Boltzmann scheme, Int. J. Heat Fluid Flow 16 (5) (1995) 357–364.
[187] Z. Guo, B. Shi, C. Zheng, A coupled lattice BGK model for the Boussinesq equations, Int. J. Numer. Methods Fluids 39 (4) (2002) 325–342.
[188] D. Contrino, P. Lallemand, P. Asinari, L.-S. Luo, Lattice-Boltzmann simulations of the thermally driven 2D square cavity at high Rayleigh numbers, J. Comput. Phys. 275 (2014) 257–272.
[189] B. Trouette, Lattice Boltzmann simulations of a time-dependent natural convection problem, Comput. Math. Appl. 66 (8) (2013) 1360–1371, https://doi.org/10.1016/j.camwa.2013.07.024.

[190] B.T. Nadiga, D.I. Pullin, A method for near-equilibrium discrete-velocity gas-flows, J. Comput. Phys. 112 (1) (1994) 162–172, https://doi.org/10.1006/jcph.1994.1089.
[191] B.T. Nadiga, An Euler solver based on locally adaptive discrete velocities, J. Stat. Phys. 81 (1–2) (1995) 129–146, https://doi.org/10.1007/BF02179972.
[192] G. Yan, Y. Chen, S. Hu, Simple lattice Boltzmann model for simulating flows with shock wave, Phys. Rev. E 59 (1, A) (1999) 454–459.
[193] F. Hinton, M. Rosenbluth, S. Wong, Y. Lin-Liu, R. Miller, Modified lattice Boltzmann method for compressible fluid simulations, Phys. Rev. E 63 (6, 1) (2001) 061212, https://doi.org/10.1103/PhysRevE.63.061212.
[194] W. Shi, W. Shyy, R. Mei, Finite-difference-based lattice Boltzmann method for inviscid compressible flows, Numer. Heat Transf. B 40 (1) (2001) 1–21, https://doi.org/10.1080/104077901300233578.
[195] P. Dellar, Compound waves in a thermohydrodynamic lattice BGK scheme using non-perturbative equilibria, Europhys. Lett. 57 (5) (2002) 690–696, https://doi.org/10.1209/epl/i2002-00518-y.
[196] R. Mason, A multi-speed compressible lattice-Boltzmann model, J. Stat. Phys. 107 (1–2) (2002) 385–400.
[197] T. Kataoka, M. Tsutahara, Lattice Boltzmann method for the compressible Euler equations, Phys. Rev. E 69 (5, 2) (2004) 056702, https://doi.org/10.1103/PhysRevE.69.056702.
[198] K. Hejranfar, A. Ghaffarian, A spectral difference lattice Boltzmann method for solution of inviscid compressible flows on structured grids, Comput. Math. Appl. 72 (5) (2016) 1341–1368, https://doi.org/10.1016/j.camwa.2016.06.043.
[199] K. Hejranfar, A. Ghaffarian, A high-order accurate unstructured spectral difference lattice Boltzmann method for computing inviscid and viscous compressible flows, Aerosp. Sci. Technol. 98 (2020) UNSP 105661, https://doi.org/10.1016/j.ast.2019.105661.
[200] Y. Chen, H. Ohashi, M. Akiyama, Thermal lattice Bhatnagar-Gross-Krook model without nonlinear deviations in macrodynamic equations, Phys. Rev. E 50 (4) (1994) 2776–2783, https://doi.org/10.1103/PhysRevE.50.2776.
[201] J. Huang, F. Xu, M. Vallieres, D. Feng, Y. Qian, B. Fryxell, M. Strayer, A thermal LBGK model for large density and temperature differences, Int. J. Mod. Phys. C 8 (4) (1997) 827–841, https://doi.org/10.1142/S0129183197000710.
[202] P. Pavlo, G. Vahala, L. Vahala, Higher order isotropic velocity grids in lattice methods, Phys. Rev. Lett. 80 (18) (1998) 3960–3963, https://doi.org/10.1103/PhysRevLett.80.3960.
[203] M. Soe, G. Vahala, P. Pavlo, L. Vahala, H. Chen, Thermal lattice Boltzmann simulations of variable Prandtl number turbulent flows, Phys. Rev. E 57 (1998) 4227–4237, https://doi.org/10.1103/PhysRevE.57.4227.
[204] A. Renda, G. Bella, S. Succi, I. Karlin, Thermohydrodynamic lattice BGK schemes with non-perturbative equilibria, Europhys. Lett. 41 (3) (1998) 279–283.
[205] C. Sun, Lattice-Boltzmann models for high speed flows, Phys. Rev. E 58 (6, A) (1998) 7283–7287, https://doi.org/10.1103/PhysRevE.58.7283.
[206] C. Sun, Adaptive lattice Boltzmann model for compressible flows: viscous and conductive properties, Phys. Rev. E 61 (2000) 2645–2653.
[207] C. Sun, Simulations of compressible flows with strong shocks by an adaptive lattice Boltzmann model, J. Comput. Phys. 161 (2000) 70–84.
[208] T. Kataoka, M. Tsutahara, Lattice Boltzmann model for the compressible Navier-Stokes equations with flexible specific-heat ratio, Phys. Rev. E 69 (3, 2) (2004), https://doi.org/10.1103/PhysRevE.69.035701.
[209] T. Kataoka, M. Tsutahara, Accuracy of the lattice Boltzmann method for describing the behavior of a gas in the continuum limit, Phys. Rev. E 82 (2010) 056709, https://doi.org/10.1103/PhysRevE.82.056709.
[210] M.H. Saadat, F. Bosch, I.V. Karlin, Lattice Boltzmann model for compressible flows on standard lattices: variable Prandtl number and adiabatic exponent, Phys. Rev. E 99 (1) (2019) 013306, https://doi.org/10.1103/PhysRevE.99.013306.
[211] G. Zanetti, Counting hydrodynamic modes in lattice gas automata models, Physica D 47 (1) (1991) 30–35, https://doi.org/10.1016/0167-2789(91)90276-F.
[212] G. Hazi, P. Kavran, On the cubic velocity deviations in lattice Boltzmann methods, J. Phys. A 39 (12) (2006) 3127–3136.
[213] X. Nie, X. Shan, H. Chen, Galilean invariance of lattice Boltzmann models, Europhys. Lett. 81 (3) (2008) 34005.
[214] P.J. Dellar, Lattice Boltzmann algorithms without cubic defects in Galilean invariance on standard lattices, J. Comput. Phys. 259 (2014) 270–283, https://doi.org/10.1016/j.jcp.2013.11.021.
[215] F. Hajabdollahi, K.N. Premnath, Galilean-invariant preconditioned central-moment lattice Boltzmann method without cubic velocity errors for efficient steady flow simulations, Phys. Rev. E 97 (5) (2018) 053303, https://doi.org/10.1103/PhysRevE.97.053303.
[216] R. Huang, H. Wu, N.A. Adams, Eliminating cubic terms in the pseudopotential lattice Boltzmann model for multiphase flow, Phys. Rev. E 97 (2018) 053308, https://doi.org/10.1103/PhysRevE.97.053308.
[217] M. Namburi, S. Krithivasan, S. Ansumali, Crystallographic lattice Boltzmann method, Sci. Rep. 6 (2016) 27172, https://doi.org/10.1038/srep27172.
[218] X. Shan, X. Yuan, H. Chen, Kinetic theory representation of hydrodynamics: a way beyond the Navier-Stokes equation, J. Fluid Mech. 550 (2006) 413–441.
[219] S.S. Chikatamarla, I.V. Karlin, Entropy and Galilean invariance of lattice Boltzmann theories, Phys. Rev. Lett. 97 (19) (2006).
[220] G. Hazi, C. Jimenez, Simulation of two-dimensional decaying turbulence using the “incompressible” extensions of the lattice Boltzmann method, Comput. Fluids 35 (3) (2006) 280–303, https://doi.org/10.1016/j.compfluid.2004.12.003.
[221] M.R. Swift, W.R. Osborn, J.M. Yeomans, Lattice Boltzmann simulation of nonideal fluids, Phys. Rev. Lett. 75 (1995) 830–833.
[222] M. Banda, M. Junk, A. Klar, Kinetic derivation of a finite difference scheme for the incompressible Navier-Stokes equation, J. Comput. Appl. Math. 154 (2) (2003) 341–354, https://doi.org/10.1016/S0377-0427(02)00857-9.
[223] E.F. Toro, Riemann Solvers and Numerical Methods for Fluid Dynamics, 2nd edition, Springer, Berlin, 1999.
[224] M. Stiebler, J. Tölke, M. Krafczyk, An upwind discretization scheme for the finite volume lattice Boltzmann method, Comput. Fluids 35 (8–9) (2006) 814–819, https://doi.org/10.1016/j.compfluid.2005.09.002.
[225] B. Mondal, S.C. Mishra, P. Asinari, R. Borchiellini, Analysis of a localized fire in a 3-D tunnel using a hybrid solver: lattice Boltzmann method, finite-volume method, and fully explicit upwind scheme, Numer. Heat Transf. A 53 (4) (2008) 392–417, https://doi.org/10.1080/10407780701634052.
[226] K. Li, C.-W. Zhong, A multiple-relaxation-time lattice Boltzmann method for high-speed compressible flows, Chin. Phys. B 24 (5) (2015) 050501, https://doi.org/10.1088/1674-1056/24/5/050501.
[227] R.-F. Qiu, Y.-C. You, C.-X. Zhu, R.-Q. Chen, Lattice Boltzmann simulation for high-speed compressible viscous flows with a boundary layer, Appl. Math. Model. 48 (2017) 567–583, https://doi.org/10.1016/j.apm.2017.03.016.
[228] R. Qiu, R. Chen, Y. You, An implicit-explicit finite-difference lattice Boltzmann subgrid method on nonuniform meshes, Int. J. Mod. Phys. C 28 (4) (2017) 1750045, https://doi.org/10.1142/S0129183117500450.
[229] F. Yang, H. Yang, Y. Yan, X. Guo, R. Dai, C. Liu, Simulation of natural convection in an inclined polar cavity using a finite-difference lattice Boltzmann method, J. Mech. Sci. Technol. 31 (6) (2017) 3053–3065, https://doi.org/10.1007/s12206-017-0549-7.
[230] Y. Li, H.-Z. Yuan, X.-D. Niu, Y.-Y. Yang, S. Shu, WENO scheme-based lattice Boltzmann flux solver for simulation of compressible flows, Comput. Phys. Commun. 23 (4, SI) (2018) 1012–1036, https://doi.org/10.4208/cicp.OA-2016-0210.
[231] M. Watari, M. Tsutahara, Supersonic flow simulations by a three-dimensional multispeed thermal model of the finite difference lattice Boltzmann method, Physica A 364 (2006) 129–144, https://doi.org/10.1016/j.physa.2005.06.103.
[232] M. Watari, Finite difference lattice Boltzmann method with arbitrary specific heat ratio applicable to supersonic flow simulations, Physica A 382 (2) (2007) 502–522, https://doi.org/10.1016/j.physa.2007.03.037.

[233] R. Qiu, R. Chen, C. Zhu, Y. You, A Hermite-based lattice Boltzmann model with artificial viscosity for compressible viscous flows, Int. J. Mod. Phys. B 32 (13) (2018), https://doi.org/10.1142/S0217979218501576.
[234] D. Wilde, A. Kramer, D. Reith, H. Foysi, Semi-Lagrangian lattice Boltzmann method for compressible flows, Phys. Rev. E 101 (5) (2020) 053306, https://doi.org/10.1103/PhysRevE.101.053306.
[235] M.H. Saadat, F. Boesch, I.V. Karlin, Semi-Lagrangian lattice Boltzmann model for compressible flows on unstructured meshes, Phys. Rev. E 101 (2) (2020) 023311, https://doi.org/10.1103/PhysRevE.101.023311.
[236] M.H. Saadat, I.V. Karlin, Arbitrary Lagrangian-Eulerian formulation of lattice Boltzmann model for compressible flows on unstructured moving meshes, Phys. Fluids 32 (4) (2020) 046105, https://doi.org/10.1063/5.0004024.
[237] K. Schladitz, S. Peters, D. Reinel-Bitzer, A. Wiegmann, J. Ohser, Design of acoustic trim based on geometric modeling and flow simulation for non-woven, Comput. Mater. Sci. 38 (1) (2006) 56–66, https://doi.org/10.1016/j.commatsci.2006.01.018.
[238] M. Tsutahara, T. Kataoka, K. Shikata, N. Takada, New model and scheme for compressible fluids of the finite difference lattice Boltzmann method and direct simulations of aerodynamic sound, Comput. Fluids 37 (1) (2008) 79–89, https://doi.org/10.1016/j.compfluid.2005.12.002.
[239] S. Maríe, D. Ricot, P. Sagaut, Comparison between lattice Boltzmann method and Navier-Stokes high-order schemes for computational aeroacoustics, J. Comput. Phys. 228 (4) (2009) 1056–1070.
[240] A. Tamura, M. Tsutahara, Direct simulation of Aeolian tones emitted from a circular cylinder in transonic flows using the finite difference lattice Boltzmann method, Fluid Dyn. Res. 42 (1) (2010) 015007, https://doi.org/10.1088/0169-5983/42/1/015007.
[241] F. Dubois, P. Lallemand, Quartic parameters for acoustic applications of lattice Boltzmann scheme, Comput. Math. Appl. 61 (12) (2011) 3404–3416, https://doi.org/10.1016/j.camwa.2011.01.011.
[242] H. Xu, P. Sagaut, Optimal low-dispersion low-dissipation LBM schemes for computational aeroacoustics, J. Comput. Phys. 230 (13) (2011) 5353–5382.
[243] A. Augier, F. Dubois, L. Gouarin, B. Graille, Linear lattice Boltzmann schemes for acoustic: parameter choices and isotropy properties, Comput. Math. Appl. 65 (6) (2013) 845–863, https://doi.org/10.1016/j.camwa.2012.06.025.
[244] D. Casalino, A.F.P. Ribeiro, E. Fares, S. Noelting, Lattice-Boltzmann aeroacoustic analysis of the LAGOON landing-gear configuration, AIAA J. 52 (6) (2014) 1232–1248, https://doi.org/10.2514/1.J052365.
[245] D. Lallier-Daniels, M. Piellard, B. Coutty, S. Moreau, Aeroacoustic study of an axial engine cooling module using lattice-Boltzmann simulations and the Ffowcs Williams and Hawkings' analogy, Eur. J. Mech. B, Fluids 61 (2, SI) (2017) 244–254, https://doi.org/10.1016/j.euromechflu.2016.10.008.
[246] D. Casalino, A. Hazir, A. Mann, Turbofan broadband noise prediction using the lattice Boltzmann method, AIAA J. 56 (2) (2018) 609–628, https://doi.org/10.2514/1.J055674.
[247] F. Avallone, D. Casalino, D. Ragni, Impingement of a propeller-slipstream on a leading edge with a flow-permeable insert: a computational aeroacoustic study, Int. J. Aeroacoust. 17 (6–8, SI) (2018) 687–711, https://doi.org/10.1177/1475472X18788961.
[248] S. Uphoff, M. Krafczyk, K. Kutscher, K. Rurkowska, S. Langer, N. Lippitz, B. Fassmann, A hierarchical approach to determining acoustic absorption properties of porous media combining pore-resolved and macroscopic models, J. Porous Media 21 (1) (2018) 83–100, https://doi.org/10.1615/JPorMedia.v21.i1.50.
[249] D. Casalino, F. Avallone, I. Gonzalez-Martino, D. Ragni, Aeroacoustic study of a wavy stator leading edge in a realistic fan/OGV stage, J. Sound Vib. 442 (2019) 138–154, https://doi.org/10.1016/j.jsv.2018.10.057.
[250] W. Shao, J. Li, Review of lattice Boltzmann method applied to computational aeroacoustics, Arch. Acoust. 44 (2) (2019) 215–238, https://doi.org/10.24425/aoa.2019.128486.
[251] C. Teruna, F. Manegar, F. Avallone, D. Ragni, D. Casalino, T. Carolus, Noise reduction mechanisms of an open-cell metal-foam trailing edge, J. Fluid Mech. 898 (2020) A18, https://doi.org/10.1017/jfm.2020.363.
[252] C.W. Gardiner, Handbook of Stochastic Methods, 2nd edition, Springer, New York, 1985.
[253] M. Geier, Ab initio derivation of the cascaded lattice Boltzmann automaton, Ph.D. thesis, University of Freiburg, Germany, 2006, available at http://www.imtek.de.
[254] M. Geier, A. Greiner, J.G. Korvink, Cascaded digital lattice Boltzmann automata for high Reynolds number flow, Phys. Rev. E 73 (6) (2006) 066705.
[255] M. Geier, A. Greiner, J.G. Korvink, Properties of the cascaded lattice Boltzmann automaton, Int. J. Mod. Phys. C 18 (4) (2007) 455–462.
[256] M. Geier, De-aliasing and stabilization formalism of the cascaded lattice Boltzmann automaton for under-resolved high Reynolds number flow, Int. J. Numer. Methods Fluids 56 (8) (2008) 1249–1254.
[257] P. Asinari, Generalized local equilibrium in the cascaded lattice Boltzmann method, Phys. Rev. E 78 (2008) 016701, https://doi.org/10.1103/PhysRevE.78.016701.
[258] F. Dubois, T. Février, B. Graille, On the stability of a relative velocity lattice Boltzmann scheme for compressible Navier–Stokes equations, C. R. Mecanique 343 (10–11) (2015) 599–610, https://doi.org/10.1016/j.crme.2015.07.010.
[259] L. Giraud, D. d'Humières, P. Lallemand, A lattice Boltzmann model for visco-elasticity, Int. J. Mod. Phys. C 8 (1997) 805–815.
[260] L. Giraud, D. d'Humières, P. Lallemand, A lattice Boltzmann model for Jeffreys viscoelastic fluid, Europhys. Lett. 42 (1998) 625–630.
[261] P.J. Dellar, Lattice Boltzmann formulation for linear viscoelastic fluids using an abstract second stress, SIAM J. Sci. Comput. 36 (6) (2014) A2507–A2532, https://doi.org/10.1137/130940372.
[262] S. Chen, H. Chen, D. Martinez, W. Matthaeus, Lattice Boltzmann model for simulation of magnetohydrodynamics, Phys. Rev. Lett. 67 (27) (1991) 3776–3779, https://doi.org/10.1103/PhysRevLett.67.3776.
[263] P.J. Dellar, Lattice kinetic schemes for magnetohydrodynamics, J. Comput. Phys. 179 (1) (2002) 95–126, https://doi.org/10.1006/jcph.2002.7044.
[264] G. Breyiannis, D. Valougeorgis, Lattice kinetic simulations of 3-D MHD turbulence, Comput. Fluids 35 (8–9) (2006) 920–924, https://doi.org/10.1016/j.compfluid.2005.07.016.
[265] P.J. Dellar, Lattice Boltzmann magnetohydrodynamics with current-dependent resistivity, J. Comput. Phys. 237 (2013) 115–131, https://doi.org/10.1016/j.jcp.2012.11.021.
[266] A.J.C. Ladd, Numerical simulations of particulate suspensions via a discretized Boltzmann equation. Part 2. Numerical results, J. Fluid Mech. 271 (1994) 311–339.
[267] J.W. Dufty, M. Ernst, Lattice Boltzmann-Langevin equations, in: A.T. Lawniczak, R. Kapral (Eds.), Pattern Formation and Lattice Gas Automata, in: Fields Institute Communications, vol. 6, AMS and Fields Institute, 1996, pp. 99–107.
[268] B. Dünweg, A.J.C. Ladd, Lattice Boltzmann simulations of soft matter systems, in: C. Holm, K. Kremer (Eds.), Advanced Computer Simulation Approaches for Soft Matter Sciences III, in: Advances in Polymer Science, vol. 221, Springer, Berlin, 2008, pp. 89–166.
[269] L. Landau, E. Lifschitz, Fluid Mechanics, 2nd edition, Course of Theoretical Physics, vol. 6, Pergamon, Oxford, UK, 1987.
[270] M. Junk, W.-A. Yong, Weighted $\mathbb{L}^2$-stability of the lattice Boltzmann method, SIAM J. Numer. Anal. 47 (3) (2009) 1651–1665.
[271] M. Junk, Kinetic schemes in the case of low Mach numbers, J. Comput. Phys. 151 (2) (1999) 947–968, https://doi.org/10.1006/jcph.1999.6228.
[272] S. Ansumali, I.V. Karlin, S. Arcidiacono, A. Abbas, N.I. Prasianakis, Hydrodynamics beyond Navier-Stokes: exact solution to the lattice Boltzmann hierarchy, Phys. Rev. Lett. 98 (2007) 124502.
[273] A. Montessori, P. Prestininzi, M. La Rocca, S. Succi, Lattice Boltzmann approach for complex nonequilibrium flows, Phys. Rev. E 92 (4) (2015), https://doi.org/10.1103/PhysRevE.92.043308.
[274] E.P. Gross, E.A. Jackson, S. Ziering, Boundary value problems in kinetic theory of gases, Ann. Phys. 1 (1957) 141–167.

[275] E.P. Gross, S. Ziering, Kinetic theory of linear shear flow, Phys. Fluids 1 (1958) 215–224.
[276] B. Shizgal, Spectral Methods in Chemistry and Physics: Applications to Kinetic Theory and Quantum Mechanics, Scientific Computation, Springer, New York, 2015.
[277] V.E. Ambruş, V. Sofonea, Implementation of diffuse-reflection boundary conditions using lattice Boltzmann models based on half-space Gauss-Laguerre quadratures, Phys. Rev. E 89 (2014) 041301(R), https://doi.org/10.1103/PhysRevE.89.041301.
[278] G.P. Ghiroldi, L. Gibelli, A finite-difference lattice Boltzmann approach for gas microflows, Commun. Comput. Phys. 17 (2015) 1007–1018.
[279] V.E. Ambruş, V. Sofonea, Lattice Boltzmann models based on half-range Gauss-Hermite quadratures, J. Comput. Phys. 316 (2016) 760–788, https://doi.org/10.1016/j.jcp.2016.04.010.
[280] C. Feuchter, W. Schleifenbaum, High-order lattice Boltzmann models for wall-bounded flows at finite Knudsen numbers, Phys. Rev. E 94 (2016), https://doi.org/10.1103/PhysRevE.94.013304.
[281] M. Watari, Is the lattice Boltzmann method applicable to rarefied gas flows? Comprehensive evaluation of the higher-order models, Trans. ASME: J. Fluids Eng. 138 (1) (2016) 011202, https://doi.org/10.1115/1.4031000.
[282] M. Junk, W.-A. Yong, Rigorous Navier-Stokes limit of the lattice Boltzmann equation, Asymptot. Anal. 35 (2003) 165–185.
[283] M. Junk, A. Klar, L.-S. Luo, Asymptotic analysis of the lattice Boltzmann equation, J. Comput. Phys. 210 (2) (2005) 676–704, https://doi.org/10.1016/j.jcp.2005.05.003.
[284] M.K. Banda, W.-A. Yong, A. Klar, A stability notion for lattice Boltzmann equations, SIAM J. Sci. Comput. 27 (6) (2006) 2098–2111.
[285] M. Junk, Z. Yang, Convergence of lattice Boltzmann methods for Navier-Stokes flows in periodic and bounded domains, Numer. Math. 112 (1) (2009) 65–87.
[286] W.-A. Yong, An Onsager-like relation for the lattice Boltzmann method, Comput. Math. Appl. 58 (5) (2009) 862–866.
[287] W.-A. Yong, L.-S. Luo, Accuracy of the viscous stress in the lattice Boltzmann equation with simple boundary conditions, Phys. Rev. E 86 (2012) 065701R.
[288] G. Strang, On construction and comparison of difference schemes, SIAM J. Numer. Anal. 5 (3) (1968) 506–517, https://doi.org/10.1137/0705041.
[289] J. Huang, H. Wu, W.-A. Yong, On initial conditions for the lattice Boltzmann method, Commun. Comput. Phys. 18 (2) (2015) 450–468, https://doi.org/10.4208/cicp.040913.220115a.
[290] Z. Yang, W.-A. Yong, Asymptotic analysis of the lattice Boltzmann method for generalized Newtonian fluid flows, SIAM Multiscale Model. Simul. 12 (3) (2014) 1028–1045.
[291] J.G.M. Eggels, Direct and large-eddy simulation of turbulent flow using the lattice-Boltzmann scheme, Int. J. Heat Fluid Flow 17 (3) (1996) 307–323.
[292] S.L. Hou, J.D. Sterling, S. Chen, G.D. Doolen, A lattice Boltzmann subgrid model for high Reynolds number flows, in: A.T. Lawniczak, R. Kapral (Eds.), Pattern Formation and Lattice Gas Automata, in: Fields Institute Communications, vol. 6, AMS and Fields Institute, 1996, pp. 151–166.
[293] J.J. Derksen, H.E.A. van den Akker, Large eddy simulations on the flow driven by a Rushton turbine, AIChE J. 45 (1999) 209–221.
[294] M. Krafczyk, J. Tölke, L.-S. Luo, Large-eddy simulations with a multiple-relaxation-time LBE model, Int. J. Mod. Phys. B 17 (1/2) (2003) 33–39.
[295] H. Yu, L.-S. Luo, S.S. Girimaji, LES of turbulent square jet flow using an MRT lattice Boltzmann model, Comput. Fluids 35 (8/9) (2006) 957–965.
[296] P. Sagaut, Toward advanced subgrid models for lattice-Boltzmann-based large-eddy simulation: theoretical formulations, Comput. Math. Appl. 59 (7) (2010) 2194–2199.
[297] O. Malaspinas, P. Sagaut, Advanced large-eddy simulation for lattice Boltzmann methods: the approximate deconvolution model, Phys. Fluids 23 (10) (2011) 105103.
[298] M. Krafczyk, K. Kucher, Y. Wang, M. Geier, DNS/LES studies of turbulent flows based on the cumulant lattice Boltzmann approach, in: High Performance Computing in Science and Engineering '14: Transactions of the High Performance Computing Center, Stuttgart (HLRS) 2014, Springer, Heidelberg, 2015, pp. 519–532.
[299] E. Flekkøy, H. Herrmann, Lattice Boltzmann models for complex fluids, Physica A 199 (1) (1993) 1–11, https://doi.org/10.1016/0378-4371(93)90091-H.
[300] S. Gabbanelli, G. Drazer, J. Koplik, Lattice Boltzmann method for non-Newtonian (power-law) fluids, Phys. Rev. E 72 (4, 2) (2005) 046312, https://doi.org/10.1103/PhysRevE.72.046312.
[301] D. Kehrwald, Lattice Boltzmann simulation of shear-thinning fluids, J. Stat. Phys. 121 (1–2) (2005) 223–237, https://doi.org/10.1007/s10955-005-5963-z.
[302] J. Boyd, J. Buick, S. Green, A second-order accurate lattice Boltzmann non-Newtonian flow model, J. Phys. A 39 (46) (2006) 14241–14247, https://doi.org/10.1088/0305-4470/39/46/001.
[303] S.S. Girimaji, Boltzmann kinetic equation for filtered fluid turbulence, Phys. Rev. Lett. 99 (3) (2007) 034501, https://doi.org/10.1103/PhysRevLett.99.034501.
[304] Y. Yan, J. Koplik, Flow of power-law fluids in self-affine fracture channels, Phys. Rev. E 77 (3, 2) (2008) 036315, https://doi.org/10.1103/PhysRevE.77.036315.
[305] J.J. Derksen, Drag on random assemblies of spheres in shear-thinning and thixotropic liquids, Phys. Fluids 21 (8) (2009) 083302, https://doi.org/10.1063/1.3200946.
[306] K.N. Premnath, M.J. Pattison, S. Banerjee, Dynamic subgrid scale modeling of turbulent flows using lattice-Boltzmann method, Physica A 388 (13) (2009) 2640–2658, https://doi.org/10.1016/j.physa.2009.02.041.
[307] R. Sungkorn, J.J. Derksen, J.G. Khinast, Modeling of aerated stirred tanks with shear-thinning power law liquids, Int. J. Heat Fluid Flow 36 (2012) 153–166, https://doi.org/10.1016/j.ijheatfluidflow.2012.04.006.
[308] S. Geller, S. Uphoff, M. Krafczyk, Turbulent jet computations based on MRT and cascaded lattice Boltzmann models, Comput. Math. Appl. 65 (12) (2013) 1956–1966.
[309] W.-A. Yong, L.-S. Luo, Nonexistence of H theorems for the athermal lattice Boltzmann models with polynomial equilibria, Phys. Rev. E 67 (2003) 051105.
[310] W.-A. Yong, L.-S. Luo, Nonexistence of H theorem for some lattice Boltzmann models, J. Stat. Phys. 121 (1/2) (2005) 91–103.
[311] X. He, L.-S. Luo, Lattice Boltzmann model for the incompressible Navier-Stokes equation, J. Stat. Phys. 88 (3/4) (1997) 927–944.
[312] P.A. Skordos, Initial and boundary conditions for the lattice Boltzmann method, Phys. Rev. E 48 (6) (1993) 4823–4842.
[313] W.-A. Yong, W. Zhao, L.-S. Luo, Theory of the lattice Boltzmann method: derivation of macroscopic equations via the Maxwell iteration, Phys. Rev. E 93 (3) (2016) 033310, https://doi.org/10.1103/PhysRevE.93.033310.
[314] P.J. Dellar, Bulk and shear viscosities in lattice Boltzmann equations, Phys. Rev. E 64 (3) (2001) 031203.
[315] F. Dubois, Equivalent partial differential equations of a lattice Boltzmann scheme, Comput. Math. Appl. 55 (7) (2008) 1441–1449.
[316] F. Dubois, Third order equivalent equation of lattice Boltzmann scheme, Discrete Contin. Dyn. Syst., Ser. A 23 (1–2) (2009) 221–248.
[317] L.-S. Luo, Lattice-gas automata and lattice Boltzmann equations for two-dimensional hydrodynamics, Ph.D. thesis, Georgia Institute of Technology, Atlanta, 1993, available at http://www.lions.odu.edu/~lluo.
[318] Z. Guo, T. Zhao, Y. Shi, Preconditioned lattice-Boltzmann method for steady flows, Phys. Rev. E 70 (6) (2004), https://doi.org/10.1103/PhysRevE.70.066706.
[319] M.M. Tekitek, M. Bouzidi, F. Dubois, P. Lallemand, On numerical reflected waves in lattice Boltzmann schemes, Prog. Comput. Fluid Dyn. 8 (1–4) (2008) 49–55, https://doi.org/10.1504/PCFD.2008.018078.

[320] M.M. Tekitek, M. Bouzidi, F. Dubois, P. Lallemand, Towards perfectly matching layers for lattice Boltzmann equation, Comput. Math. Appl. 58 (5) (2009) 903–913, https://doi.org/10.1016/j.camwa.2009.02.013.
[321] F. Dubois, P. Lallemand, M. Tekitek, On a superconvergent lattice Boltzmann boundary scheme, Comput. Math. Appl. 59 (7) (2010) 2141–2149.
[322] F. Dubois, P. Lallemand, M.M. Tekitek, Taylor expansion method for linear lattice Boltzmann schemes with an external force: application to boundary conditions, in: R. Abgrall, H. Beaugendre, P.M. Congedo, C. Dobrzynski, V. Perrier, M. Ricchiuto (Eds.), High Order Nonlinear Numerical Schemes for Evolutionary PDEs, in: Lecture Notes in Computational Science and Engineering, vol. 99, Springer International Publishing, Cham, Switzerland, 2014, pp. 89–107, Ch. 6.
[323] I. Ginzbourg, P.M. Adler, Boundary flow condition analysis for the three-dimensional lattice Boltzmann model, J. Phys. II 4 (2) (1994) 191–214.
[324] I. Ginzbourg, D. d'Humières, Local second-order boundary methods for lattice Boltzmann models, J. Stat. Phys. 84 (5/6) (1996) 927–971.
[325] I. Ginzburg, D. d'Humières, Multireflection boundary conditions for lattice Boltzmann models, Phys. Rev. E 68 (6) (2003) 066614.
[326] D. d'Humières, I. Ginzburg, Viscosity independent numerical errors for lattice Boltzmann models: from recurrence equations to "magic" collision numbers, Comput. Math. Appl. 58 (5) (2009) 823–840.
[327] M. Bouzidi, M. Firdaouss, P. Lallemand, Momentum transfer of Boltzmann-lattice fluid with boundaries, Phys. Fluids 13 (11) (2001) 3452–3459.
[328] P. Tucker, Z. Pan, A Cartesian cut cell method for incompressible viscous flow, Appl. Math. Model. 24 (8–9) (2000) 591–606, https://doi.org/10.1016/S0307-904X(00)00005-6.
[329] M. Meinke, L. Schneiders, C. Guenther, W. Schroeder, A cut-cell method for sharp moving boundaries in Cartesian grids, in: International Workshop on Future of CFD and Aerospace Sciences, RIKEN Adv. Inst. Computat. Sci., Kobe, Japan, Apr 23–25, 2012, Comput. Fluids 85 (SI) (2013) 135–142, https://doi.org/10.1016/j.compfluid.2012.11.010.
[330] Y.-F. Peng, R. Mittal, A. Sau, R.R. Hwang, Nested Cartesian grid method in incompressible viscous fluid flow, J. Comput. Phys. 229 (19) (2010) 7072–7101, https://doi.org/10.1016/j.jcp.2010.05.041.
[331] N.S. Martys, H. Chen, Simulations of multicomponent fluids in complex three-dimensional geometries by the lattice Boltzmann method, Phys. Rev. E 53 (1996) 743–750.
[332] D.L. Koch, A.J.C. Ladd, Moderate Reynolds number flows through periodic and random arrays of aligned cylinders, J. Fluid Mech. 349 (1997) 31–66.
[333] R.S. Maier, D.M. Kroll, Y.E. Kutsovsky, H.T. Davis, R.S. Bernard, Simulation of flow through bead packs using the lattice Boltzmann method, Phys. Fluids 10 (1) (1998) 60–74, https://doi.org/10.1063/1.869550.
[334] R.S. Maier, D.M. Kroll, R.S. Bernard, S.E. Howington, J.F. Peters, H.T. Davis, Pore-scale simulation of dispersion, Phys. Fluids 12 (8) (2000) 2065–2079, https://doi.org/10.1063/1.870452.
[335] D. Zhang, R. Zhang, S. Chen, V.E. Soll, Pore scale study of flow in porous media: scale dependency, REV, and statistical REV, Geophys. Res. Lett. 27 (8) (2000) 1195–1198, https://doi.org/10.1029/1999GL011101.
[336] R.J. Hill, D.L. Koch, Moderate-Reynolds-number flow in wall-bounded porous medium, J. Fluid Mech. 453 (2002) 315–344.
[337] R.J. Hill, D.L. Koch, The transition from steady to weakly turbulent flow in a close-packed ordered array of spheres, J. Fluid Mech. 465 (2002) 59–97.
[338] Y. Keehm, T. Mukerji, A. Nur, Permeability prediction from thin sections: 3D reconstruction and lattice-Boltzmann flow simulation, Geophys. Res. Lett. 31 (2004) L04606.
[339] B. Porter, R. Zauel, H. Stockman, R. Guldberg, D. Fyhrie, 3-D computational modeling of media flow through scaffolds in a perfusion bioreactor, J. Biomech. 38 (3) (2005) 543–549, https://doi.org/10.1016/j.jbiomech.2004.04.011.
[340] M.A. van der Hoef, R. Beetstra, J.A.M. Kuipers, Lattice-Boltzmann simulations of low-Reynolds-number flow past mono- and bidisperse arrays of spheres: results for the permeability and drag force, J. Fluid Mech. 528 (2005) 233–254, https://doi.org/10.1017/S0022112004003295.
[341] H. Vogel, J. Tölke, V. Schulz, M. Krafczyk, K. Roth, Comparison of a lattice-Boltzmann model, a full-morphology model, and a pore network model for determining capillary pressure-saturation relationships, Vadose Zone J. 4 (2) (2005) 380–388, https://doi.org/10.2136/vzj2004.0114.
[342] C. Pan, L.-S. Luo, C. Miller, An evaluation of lattice Boltzmann schemes for porous medium flow simulation, Comput. Fluids 35 (8/9) (2006) 898–909.
[343] M.J. Blunt, B. Bijeljic, H. Dong, O. Gharbi, S. Iglauer, P. Mostaghimi, A. Paluszny, C. Pentland, Pore-scale imaging and modelling, Adv. Water Resour. 51 (2013) 197–216, https://doi.org/10.1016/j.advwatres.2012.03.003.
[344] P. Lallemand, L.-S. Luo, Lattice Boltzmann method for moving boundaries, J. Comput. Phys. 184 (2) (2003) 406–421.
[345] J. Zhang, N.-S. Liu, X.-Y. Lu, Locomotion of a passively flapping flat plate, J. Fluid Mech. 659 (2010) 43–68, https://doi.org/10.1017/S0022112010002387.
[346] J. Favier, A. Revell, A. Pinelli, A lattice Boltzmann-immersed boundary method to simulate the fluid interaction with moving and slender flexible objects, J. Comput. Phys. 261 (2014) 145–161, https://doi.org/10.1016/j.jcp.2013.12.052.
[347] A.J.C. Ladd, Numerical simulations of particulate suspensions via a discretized Boltzmann equation. Part 1. Theoretical foundation, J. Fluid Mech. 271 (1994) 285–309.
[348] C.K. Aidun, Y. Lu, E. Ding, Direct analysis of particulate suspensions with inertia using the discrete Boltzmann equation, J. Fluid Mech. 373 (1998) 287–311, https://doi.org/10.1017/S0022112098002493.
[349] D. Qi, Lattice-Boltzmann simulations of particles in non-zero-Reynolds-number flows, J. Fluid Mech. 385 (1999) 41–62, https://doi.org/10.1017/S0022112099004401.
[350] A.J.C. Ladd, R. Verberg, Lattice-Boltzmann simulations of particle-fluid suspensions, J. Stat. Phys. 104 (5–6) (2001) 1191–1251.
[351] D. Qi, L.-S. Luo, Transitions in rotations of a nonspherical particle in a three-dimensional moderate Reynolds number Couette flow, Phys. Fluids 14 (12) (2002) 4440–4443.
[352] D. Qi, L.-S. Luo, Rotational and orientational behaviour of a three-dimensional spheroidal particles in Couette flow, J. Fluid Mech. 477 (2003) 201–213.
[353] D. Qi, L.-S. Luo, R. Aravamuthan, W. Strieder, Lateral migration and orientation of elliptical particles in Poiseuille flows, J. Stat. Phys. 107 (1/2) (2002) 102–120.
[354] H. Huang, X. Yang, M. Krafczyk, X.-Y. Lu, Rotation of spheroidal particles in Couette flows, J. Fluid Mech. 692 (2012) 369–394.
[355] B. Metzger, O. Rahli, X. Yin, Heat transfer across sheared suspensions: role of the shear-induced diffusion, J. Fluid Mech. 724 (2013) 527–552, https://doi.org/10.1017/jfm.2013.173.
[356] H. Haddadi, J.F. Morris, Microstructure and rheology of finite inertia neutrally buoyant suspensions, J. Fluid Mech. 749 (2014) 431–459, https://doi.org/10.1017/jfm.2014.238.
[357] H. Haddadi, S. Shojaei-Zadeh, K. Connington, J.F. Morris, Suspension flow past a cylinder: particle interactions with recirculating wakes, J. Fluid Mech. 760 (2014) R2, https://doi.org/10.1017/jfm.2014.613.
[358] W. Mao, A. Alexeev, Motion of spheriod particles in shear flow with inertia, J. Fluid Mech. 749 (2014) 145–166, https://doi.org/10.1017/jfm.2014.224.
[359] Y. Sui, H.T. Low, Y.T. Chew, P. Roy, Tank-treading, swinging, and tumbling of liquid-filled elastic capsules in shear flow, Phys. Rev. E 77 (1, 2) (2008) 016310, https://doi.org/10.1103/PhysRevE.77.016310.
[360] R.M. MacMeccan, J.R. Clausen, G.P. Neitzel, C.K. Aidun, Simulating deformable particle suspensions using a coupled lattice-Boltzmann and finite-element method, J. Fluid Mech. 618 (2009) 13–39, https://doi.org/10.1017/S0022112008004011.
[361] J. Wu, C.K. Aidun, A numerical study of the effect of fibre stiffness on the rheology of sheared flexible fibre suspensions, J. Fluid Mech. 662 (2010) 123–133, https://doi.org/10.1017/S0022112010003885.
[362] J.R. Clausen, D.A. Reasor Jr., C.K. Aidun, The rheology and microstructure of concentrated non-colloidal suspensions of deformable capsules, J. Fluid Mech. 685 (2011) 202–234, https://doi.org/10.1017/jfm.2011.307.

[363] A. Salahuddin, J. Wu, C.K. Aidun, Numerical study of rotational diffusion in sheared semidilute fibre suspension, J. Fluid Mech. 692 (2012) 153–182, https://doi.org/10.1017/jfm.2011.501.
[364] J. Gounley, Y. Peng, Shape recovery of elastic capsules from shear flow induced deformation, Commun. Comput. Phys. 16 (1) (2014) 56–74, https://doi.org/10.4208/cicp.220513.151113a.
[365] T. Krüger, B. Kaoui, J. Harting, Interplay of inertia and deformability on rheological properties of a suspension of capsules, J. Fluid Mech. 751 (2014) 725–745, https://doi.org/10.1017/jfm.2014.315.
[366] J. Gounley, Y. Peng, Computational modeling of membrane viscosity of red blood cells, Commun. Comput. Phys. 17 (4) (2015) 1073–1087, https://doi.org/10.4208/cicp.2014.m355.
[367] T. Rosen, M. Do-Quang, C.K. Aidun, F. Lundell, The dynamical states of a prolate spheroidal particle suspended in shear flow as a consequence of particle and fluid inertia, J. Fluid Mech. 771 (2015) 115–158, https://doi.org/10.1017/jfm.2015.127.
[368] F. Verhaeghe, L.-S. Luo, B. Blanpain, Lattice Boltzmann modeling of microchannel flow in slip flow regime, J. Comput. Phys. 228 (1) (2009) 147–157, https://doi.org/10.1016/j.jcp.2008.09.004.
[369] H. Chen, S. Chen, H.W. Matthaeus, Recovery of the Navier-Stokes equations using a lattice-gas Boltzmann method, Phys. Rev. A 45 (8) (1992) R5339–R5342.
[370] Y. Qian, D. d'Humières, P. Lallemand, Lattice BGK models for Navier-Stokes equation, Europhys. Lett. 17 (6) (1992) 479–484.
[371] X. He, Q. Zou, L.-S. Luo, M. Dembo, Analytic solutions and analysis on non-slip boundary condition for the lattice Boltzmann BGK model, J. Stat. Phys. 87 (1/2) (1997) 115–136.
[372] Z. Guo, C. Zheng, B. Shi, Lattice Boltzmann equation with multiple effective relaxation times for gaseous microscale flow, Phys. Rev. E 77 (3) (2008) 036707.
[373] L.-S. Luo, W. Liao, X. Chen, Y. Peng, W. Zhang, Numerics of the lattice Boltzmann method: effects of collision models on the lattice Boltzmann simulations, Phys. Rev. E 83 (5) (2011) 056710.
[374] T. Reis, P.J. Dellar, Lattice Boltzmann simulations of pressure-driven flows in micro channels using Navier-Maxwell slip boundary conditions, Phys. Fluids 24 (11) (2012) 112001, https://doi.org/10.1063/1.4764514.
[375] Z. Guo, C. Zheng, B. Shi, An extrapolation method for boundary conditions in lattice Boltzmann method, Phys. Fluids 14 (6) (2002) 2007–2010, https://doi.org/10.1063/1.1471914.
[376] R. Mei, L.-S. Luo, P. Lallemand, D. d'Humières, Consistent initial conditions for lattice Boltzmann simulations, Comput. Fluids 35 (2006) 855–862.
[377] M. Lai, C. Peskin, An immersed boundary method with formal second-order accuracy and reduced numerical viscosity, J. Comput. Phys. 160 (2) (2000) 705–719, https://doi.org/10.1006/jcph.2000.6483.
[378] C.S. Peskin, The immersed boundary method, Acta Numer. 11 (2002) 479–517.
[379] L. Zhu, C. Peskin, Simulation of a flapping flexible filament in a flowing soap film by the immersed boundary method, J. Comput. Phys. 179 (2) (2002) 452–468, https://doi.org/10.1006/jcph.2002.7066.
[380] P. Lallemand, L.-S. Luo, Y. Peng, A lattice Boltzmann front-tracking method for interface dynamics with surface tension in two dimensions, J. Comput. Phys. 226 (2) (2007) 1367–1384.
[381] Y. Peng, L.-S. Luo, A comparative study of immersed-boundary and interpolated bounce-back methods in LBE, Prog. Comput. Fluid Dyn. 8 (1–4) (2008) 156–167.
[382] Q. Zhou, L.-S. Fan, A second-order accurate immersed boundary-lattice Boltzmann method for particle-laden flows, J. Comput. Phys. 268 (2014) 269–301, https://doi.org/10.1016/j.jcp.2014.02.038.
[383] Z. Li, J. Favier, U. D'Ortona, S. Poncet, An immersed boundary-lattice Boltzmann method for single- and multi-component fluid flows, J. Comput. Phys. 304 (2016) 424–440, https://doi.org/10.1016/j.jcp.2015.10.026.
[384] O. Filippova, D. Hänel, Grid refinement for lattice-BGK models, J. Comput. Phys. 147 (1) (1998) 219–228, https://doi.org/10.1006/jcph.1998.6089.
[385] M. Geier, A. Greiner, J.G. Korvink, Bubble functions for the lattice Boltzmann method and their application to grid refinement, Eur. Phys. J. Spec. Top. 171 (1) (2009) 173–179.
[386] M. Schönherr, K. Kucher, M. Geier, M. Stiebler, S. Freudiger, M. Krafczyk, Multi-thread implementations of the lattice Boltzmann method on non-uniform grids for CPUs and GPUs, Comput. Math. Appl. 61 (12) (2011) 3730–3743, https://doi.org/10.1016/j.camwa.2011.04.012.
[387] M. Schönherr, Towards reliable LES-CFD computations based on advanced LBM models utilizing (multi-) GPGPU hardware, Ph.D. thesis, Technische Universität Braunschweig, Germany, 2015.
[388] E. Kian Far, M. Geier, K. Kutscher, M. Krafczyk, Distributed cumulant lattice Boltzmann simulation of the dispersion process of ceramic agglomerates, J. Comput. Methods Sci. Eng. 16 (2) (2016) 231–252.
[389] M.L. Minion, D.L. Brown, Performance of under-resolved two-dimensional incompressible flow simulations, II, J. Comput. Phys. 138 (2) (1997) 734–765, https://doi.org/10.1006/jcph.1997.5843.
[390] A. Augier, F. Dubois, B. Graille, P. Lallemand, On rotational invariance of lattice Boltzmann schemes, Comput. Math. Appl. 67 (2) (2014) 239–255, https://doi.org/10.1016/j.camwa.2013.06.009.
[391] J.A. Somers, Direct simulation of fluid flow with cellular automata and the lattice-Boltzmann equation, Appl. Sci. Res. 51 (1993) 127–133.
[392] D. Martinez, W. Matthaeus, S. Chen, D. Montgomery, Comparison of spectral method and lattice Boltzmann simulations of 2-dimensional hydrodynamics, Phys. Fluids 6 (3) (1994) 1285–1298.
[393] R. Benzi, M.V. Struglia, R. Tripiccione, Extended self-similarity in numerical simulations of three-dimensional anisotropic turbulence, Phys. Rev. E 53 (1996) R5565–R5568.
[394] A. ten Cate, J. Derksen, L. Portela, H. van den Akker, Fully resolved simulations of colliding monodisperse spheres in forced isotropic turbulence, J. Fluid Mech. 519 (2004) 233–271, https://doi.org/10.1017/s0022112004001326.
[395] H. Yu, S.S. Girimaji, L.-S. Luo, DNS and LES of decaying isotropic turbulence with and without frame rotation using lattice Boltzmann method, J. Comput. Phys. 209 (2) (2005) 599–616.
[396] H. Yu, S.S. Girimaji, Near-field turbulent simulations of rectangular jets using lattice Boltzmann method, Phys. Fluids 17 (12) (2005) 125106, https://doi.org/10.1063/1.2140021.
[397] H. Yu, S. Girimaji, L.-S. Luo, Lattice Boltzmann simulations of decaying homogeneous isotropic turbulence, Phys. Rev. E 71 (1) (2005) 016708.
[398] D. Yu, S. Girimaji, Direct numerical simulations of homogeneous turbulence subject to periodic shear, Phys. Rev. E 71 (1) (2005) 016708.
[399] D. Yu, S.S. Girimaji, DNS of homogeneous shear turbulence revisited with the lattice Boltzmann method, J. Turbul. 6 (2005) N6, https://doi.org/10.1080/14685240500103200.
[400] P. Burattini, P. Lavoie, A. Agrawal, L. Djenidi, R.A. Antonia, Power law of decaying homogeneous isotropic turbulence at low Reynolds number, Phys. Rev. E 73 (6) (2006) 066304.
[401] L. Djenidi, B. Moghtaderi, Numerical investigation of laminar mixing in a coaxial microreactor, J. Fluid Mech. 568 (2006) 223–242, https://doi.org/10.1017/S0022112006002035.
[402] W.A.K.S. Izawa, A.K. Xiong, Y. Fukunishi, Identification of multi-scale coherent eddy structures in a homogeneous isotropic turbulence, Prog. Comput. Fluid Dyn. 6 (7) (2006) 402–408.
[403] A. ten Cate, E. van Vliet, J. Derksen, H. van den Akker, Application of spectral forcing in lattice-Boltzmann simulations of homogeneous turbulence, Comput. Fluids 35 (10) (2006) 1239–1251, https://doi.org/10.1017/S0022112006008652.

[404] Y.-H. Dong, P. Sagaut, S. Marie, Inertial consistent subgrid model for large-eddy simulation based on the lattice Boltzmann method, Phys. Fluids 20 (3) (2008) 035104, https://doi.org/10.1063/1.2842379.
[405] Y.-H. Dong, P. Sagaut, A study of time correlations in lattice Boltzmann-based large-eddy simulation of isotropic turbulence, Phys. Fluids 20 (3) (2008) 035105, https://doi.org/10.1063/1.2842381.
[406] L. Djenidi, S.F. Tardu, On the anisotropy of a low-Reynolds-number grid turbulence, J. Fluid Mech. 702 (2012) 332–353, https://doi.org/10.1017/jfm.2012.179.
[407] L. Djenidi, S.F. Tardu, R.A. Antonia, Relationship between temporal and spatial averages in grid turbulence, J. Fluid Mech. 730 (2013) 593–606, https://doi.org/10.1017/jfm.2013.351.
[408] L. Djenidi, R.A. Antonia, Transport equation for the mean turbulent energy dissipation rate in low-R-lambda grid turbulence, J. Fluid Mech. 747 (2014) 288–315, https://doi.org/10.1017/jfm.2014.157.
[409] N. Lefeuvre, F. Thiesset, L. Djenidi, R.A. Antonia, Statistics of the turbulent kinetic energy dissipation rate and its surrogates in a square cylinder wake flow, Phys. Fluids 26 (9) (2014) 095104, https://doi.org/10.1063/1.4895637.
[410] S. Menon, J. Soo, Simulation of vortex dynamics in three-dimensional synthetic and free jets using the large-eddy lattice Boltzmann method, J. Turbul. 5 (2004) 032.
[411] R. Löhner, Towards overcoming the LES crisis, Int. J. Comput. Fluid Dyn. 33 (3) (2019) 87–97, https://doi.org/10.1080/10618562.2019.1612052.
[412] J.J. Derksen, H.E.A. van den Akker, Simulation of vortex core precession in a reverse-flow cyclone, AIChE J. 46 (2000) 1317–1331.
[413] M. Cheng, L.-S. Luo, Characteristics of two-dimensional flow around a rotating circular cylinder near a plane wall, Phys. Fluids 19 (6) (2007) 063601, https://doi.org/10.1063/1.2738608.
[414] M. Cheng, J. Lou, T.T. Lim, Motion of a vortex ring in a simple shear flow, Phys. Fluids 21 (8) (2009) 081701, https://doi.org/10.1063/1.3196903.
[415] M. Cheng, J. Lou, L.-S. Luo, Numerical study of a vortex ring impacting a flat wall, J. Fluid Mech. 660 (2010) 430–455, https://doi.org/10.1017/S0022112010002727.
[416] M. Cheng, J. Lou, T.T. Lim, Vortex ring with swirl: a numerical study, Phys. Fluids 22 (9) (2010) 097101, https://doi.org/10.1063/1.3478976.
[417] F.L. Ponta, Vortex decay in the Kármán eddy street, Phys. Fluids 22 (9) (2010) 093601, https://doi.org/10.1063/1.3478976.
[418] G. Toth, G. Hazi, Merging of shielded Gaussian vortices and formation of a tripole at low Reynolds numbers, Phys. Fluids 22 (5) (2010) 053101, https://doi.org/10.1063/1.3428539.
[419] M. Cheng, J. Lou, T.T. Lim, A numerical study of a vortex ring impacting a permeable wall, Phys. Fluids 26 (10) (2014) 103602, https://doi.org/10.1063/1.4897519.
[420] M. Cheng, J. Lou, T.T. Lim, Leapfrogging of multiple coaxial viscous vortex rings, Phys. Fluids 27 (3) (2015) 031702, https://doi.org/10.1063/1.4915890.
[421] J. Buick, C. Greated, D. Campbell, Lattice BGK simulation of sound waves, Europhys. Lett. 43 (3) (1998) 235–240, https://doi.org/10.1209/epl/i1998-00346-7.
[422] A. Wilde, Calculation of sound generation and radiation from instationary flows, Comput. Fluids 35 (8/9) (2006) 986–993.
[423] G. Barrios, R. Rechtman, Dynamics of an acoustically levitated particle using the lattice Boltzmann method, J. Fluid Mech. 596 (2008) 191–200, https://doi.org/10.1017/S0022112007009548.
[424] D. Ricot, S. Maríe, P. Sagaut, C. Bailly, Lattice Boltzmann method with selective viscosity filter, J. Comput. Phys. 228 (12) (2009) 4478–4490.
[425] M. Muto, M. Tsubokura, N. Oshima, Negative Magnus lift on a rotating sphere at around the critical Reynolds number, Phys. Fluids 24 (1) (2012) 014102, https://doi.org/10.1063/1.3673571.
[426] J. Almedeij, Drag coefficient of flow around a sphere: matching asymptotically the wide trend, Powder Technol. 186 (3) (2008) 218–223, https://doi.org/10.1016/j.powtec.2007.12.006.
[427] F.A. Morrison, An Introduction to Fluid Mechanics, Cambridge University Press, Cambridge, 2013.
[428] E. Loth, Compressibility and rarefaction effects on drag of a spherical particle, AIAA J. 46 (9) (2008) 2219–2228.
[429] Q. Xiong, B. Li, J. Xu, X. Wang, L. Wang, W. Ge, Efficient 3D DNS of gas-solid flows on Fermi GPGPU, Comput. Fluids 70 (2012) 86–94, https://doi.org/10.1016/j.compfluid.2012.08.026.
[430] A. Banari, C. Janssen, S.T. Grilli, M. Krafczyk, Efficient GPGPU implementation of a lattice Boltzmann model for multiphase flows with high density ratios, Comput. Fluids 93 (2014) 1–17, https://doi.org/10.1016/j.compfluid.2014.01.004.
[431] X. Nie, G. Doolen, S. Chen, Lattice-Boltzmann simulations of fluid flows in MEMS, J. Stat. Phys. 107 (1–2) (2002) 279–289.
[432] S. Succi, Mesoscopic modeling of slip motion at fluid-solid interfaces with heterogeneous catalysis, Phys. Rev. Lett. 89 (6) (2002), https://doi.org/10.1103/PhysRevLett.89.064502.
[433] B. Li, D. Kwok, Discrete Boltzmann equation for microfluidics, Phys. Rev. Lett. 90 (12) (2003), https://doi.org/10.1103/PhysRevLett.90.124502.
[434] F. Toschi, S. Succi, Lattice Boltzmann method at finite Knudsen numbers, Europhys. Lett. 69 (4) (2005) 549–555, https://doi.org/10.1209/epl/i2004-10393-0.
[435] S. Ansumali, I. Karlin, C. Frouzakis, K. Boulouchos, Entropic lattice Boltzmann method for microflows, Physica A 359 (2006) 289–305.
[436] R. Zhang, X. Shan, H. Chen, Efficient kinetic method for fluid simulation beyond the Navier-Stokes equation, Phys. Rev. E 74 (4, 2) (2006) 046703, https://doi.org/10.1103/PhysRevE.74.046703.
[437] Y. Zhou, R. Zhang, I. Staroselsky, H. Chen, W. Kim, M. Jhon, Simulation of micro- and nano-scale flows via the lattice Boltzmann method, Physica A 362 (1) (2006) 68–77.
[438] S.H. Kim, H. Pitsch, I.D. Boyd, Accuracy of higher-order lattice Boltzmann methods for microscale flows with finite Knudsen numbers, J. Comput. Phys. 227 (19) (2008) 8655–8671, https://doi.org/10.1016/j.jcp.2008.06.012.
[439] Y. Shi, P.L. Brookes, Y.W. Yap, J.E. Sader, Accuracy of the lattice Boltzmann method for low-speed noncontinuum flows, Phys. Rev. E 83 (4) (2011) 045701(R).
[440] T.-M. Liou, C.-T. Lin, Study on microchannel flows with a sudden contraction-expansion at a wide range of Knudsen number using lattice Boltzmann method, Microfluid. Nanofluid. 16 (1–2) (2014) 315–327, https://doi.org/10.1007/s10404-013-1200-2.
[441] L.M. Yang, C. Shu, J. Wu, Y. Wang, Comparative study of discrete velocity method and high-order lattice Boltzmann method for simulation of rarefied flows, Comput. Fluids 146 (2017) 125–142, https://doi.org/10.1016/j.compfluid.2017.01.014.
[442] C. Shen, D.B. Tian, C. Xie, J. Fan, Examination of the LBM in simulation of microchannel flow in transitional regime, Microscale Thermophys. Eng. 8 (4) (2004) 423–432.
[443] L.-S. Luo, Comment on "Discrete Boltzmann equation for microfluidics", Phys. Rev. Lett. 92 (13) (2004) 139401.
[444] L.-S. Luo, Some recent results on discrete velocity models and ramifications for lattice Boltzmann equation, in: 8th International Symposium on the Discrete Simulation of Fluid Dynamics (LGA99), Univ Tokyo, Tokyo, Japan, Jul 28-30, 1999, Comput. Phys. Commun. 129 (1–3) (2000) 63–74.
[445] J.E. Broadwell, Shock structure in a simple discrete velocity gas, Phys. Fluids 7 (8) (1964) 1243–1247, https://doi.org/10.1063/1.1711368.
[446] H. Babovsky, M. Padula, A new contribution to nonlinear stability of a discrete velocity model, Commun. Math. Phys. 144 (1) (1992) 87–106, https://doi.org/10.1007/BF02099192.
[447] L. Mieussens, Discrete-velocity models and numerical schemes for the Boltzmann-BGK equation in plane and axisymmetric geometries, J. Comput. Phys. 162 (2) (2000) 429–466, https://doi.org/10.1006/jcph.2000.6548.
[448] H. Cabannes, R. Gatignol, L.-S. Luo, The Discrete Boltzmann Equation: Theory and Applications, Lecture Notes given by Cabannes at University of California, Berkeley, 1980, 2003.

[449] L.S. Andallah, H. Babovsky, A discrete Boltzmann equation based on hexagons, Math. Models Methods Appl. Sci. 13 (11) (2003) 1537–1563, https://doi.org/10.1142/S0218202503003021.
[450] H. Babovsky, T. Płatkowski, Kinetic boundary layers for the Boltzmann equation on discrete velocity lattices, Arch. Mech. 60 (1) (2008) 87–116.
[451] H. Babovsky, A numerical model for the Boltzmann equation with applications to micro flows, Comput. Math. Appl. 58 (4) (2009) 791–804, https://doi.org/10.1016/j.camwa.2009.05.003.
[452] S. Brechtken, T. Sasse, Normal, high order discrete velocity models of the Boltzmann equation, Comput. Math. Appl. 75 (2) (2018) 503–519, https://doi.org/10.1016/j.camwa.2017.09.024.
[453] A.V. Bobylev, A. Palczewski, J. Schneider, On approximation of the Boltzmann-equation by discrete velocity models, C. R. Acad. Sci., Sér. 1 Math. 320 (5) (1995) 639–644.
[454] A. Palczewski, J. Schneider, A.V. Bobylev, A consistency result for a discrete-velocity model of the Boltzmann equation, SIAM J. Numer. Anal. 34 (5) (1997) 1865–1883, https://doi.org/10.1137/S0036142995289007.
[455] W. Wagner, Approximation of the Boltzmann-equation by discrete velocity models, J. Stat. Phys. 78 (5–6) (1995) 1555–1570, https://doi.org/10.1007/BF02180142.
[456] L. Mieussens, Convergence of a discrete-velocity model for the Boltzmann-BGK equation, C. R. Acad. Sci., Sér. I Math. 328 (12) (1999) 1231–1236, https://doi.org/10.1016/S0764-4442(99)80445-5.
[457] Z. Guo, T. Zhao, Y. Shi, Physical symmetry, spatial accuracy, and relaxation time of the lattice Boltzmann equation for microgas flows, J. Appl. Phys. 99 (7) (2006), https://doi.org/10.1063/1.2185839.
[458] V.E. Ambruş, V. Sofonea, Application of mixed quadrature lattice Boltzmann models for the simulation of Poiseuille flow at non-negligible values of the Knudsen number, J. Comput. Sci. 17 (2, SI) (2016) 403–417, https://doi.org/10.1016/j.jocs.2016.03.016.
[459] W.L. Briggs, V.E. Henson, S.F. McCormick, A Multigrid Tutorial, SIAM, Philadelphia, PA, 2000.
[460] U. Trottenberg, C.W. Oosterlee, A. Schuller, Multigrid, Academic Press, London, 2001.
[461] J. Tölke, M. Krafczyk, E. Rank, A multigrid solver for the discrete Boltzmann equation, J. Stat. Phys. 107 (2002) 573–591.
[462] D.J. Mavriplis, Multigrid solution of the steady-state lattice Boltzmann equation, Comput. Fluids 35 (8/9) (2005) 793–804.
[463] D.V. Patil, K.N. Premnath, S. Banerjee, Multigrid lattice Boltzmann method for accelerated solution of elliptic equations, J. Comput. Phys. 265 (2014) 172–194, https://doi.org/10.1016/j.jcp.2014.01.049.
[464] J. Tölke, M. Krafczyk, M. Schulz, E. Rank, R. Berrios, Implicit discretization and nonuniform mesh refinement approaches for FD discretizations of LBGK models, Int. J. Mod. Phys. C 9 (1998) 1143–1157.
[465] D.R. Rector, M.L. Stewart, A semi-implicit lattice method for simulating flow, J. Comput. Phys. 229 (19) (2010) 6732–6743, https://doi.org/10.1016/j.jcp.2010.05.020.
[466] J. Huang, C. Yang, X.-C. Cai, A fully implicit method for lattice Boltzmann equations, SIAM J. Sci. Comput. 37 (5) (2015) S291–S313, https://doi.org/10.1137/140975346.
[467] W. Li, L.-S. Luo, Finite-volume lattice Boltzmann method for nearly incompressible flows on arbitrary unstructured meshes, Commun. Comput. Phys. 20 (2) (2016) 301–324, https://doi.org/10.4208/cicp.211015.040316a.
[468] W. Li, W. Li, P. Song, H. Ji, A conservation-moment-based implicit finite volume lattice Boltzmann method for steady nearly incompressible flows, J. Comput. Phys. 398 (2019) UNSP 108882, https://doi.org/10.1016/j.jcp.2019.108882.
[469] E.J. Ding, Accelerated algorithm for computing the motion of solid particles suspended in fluid, Phys. Rev. E 80 (2) (2009) 025701, https://doi.org/10.1103/PhysRevE.80.025701.
[470] E.J. Ding, Calculation of drag and torque coefficients by time-independent lattice-Boltzmann method, Phys. Rev. E 90 (3) (2014) 033313, https://doi.org/10.1103/PhysRevE.90.033313.
[471] E.J. Ding, Lattice Boltzmann Stokesian dynamics, Phys. Rev. E 92 (5) (2015) 053303, https://doi.org/10.1103/PhysRevE.92.053303.
[472] E.J. Ding, Time-independent lattice Boltzmann method calculation of hydrodynamic interactions between two particles, Phys. Rev. E 91 (6) (2015) 063308, https://doi.org/10.1103/PhysRevE.91.063308.
[473] M. McCracken, J. Abraham, Multiple-relaxation-time lattice-Boltzmann model for multiphase flow, Phys. Rev. E 71 (3) (2005) 036701.
[474] K. Premnath, J. Abraham, Three-dimensional multi-relaxation time (MRT) lattice-Boltzmann models for multiphase flow, J. Comput. Phys. 224 (2) (2007) 539–559.
[475] C. Peng, O.M. Ayala, L.-P. Wang, A comparative study of immersed boundary method and interpolated bounce-back scheme for no-slip boundary treatment in the lattice Boltzmann method: part I, laminar flows, Comput. Fluids 192 (2019) UNSP 104233, https://doi.org/10.1016/j.compfluid.2019.06.032.
[476] C. Peng, O.M. Ayala, J.C.B. de Motta, L.-P. Wang, A comparative study of immersed boundary method and interpolated bounce-back scheme for no-slip boundary treatment in the lattice Boltzmann method: part II, turbulent flows, Comput. Fluids 192 (2019) UNSP 104251, https://doi.org/10.1016/j.compfluid.2019.104251.
[477] H. Liu, Y. Zhang, Phase-field modeling droplet dynamics with soluble surfactants, J. Comput. Phys. 229 (24) (2010) 9166–9187, https://doi.org/10.1016/j.jcp.2010.08.031.
[478] H. Liu, A.J. Valocchi, Y. Zhang, Q. Kang, Lattice Boltzmann phase-field modeling of thermocapillary flows in a confined microchannel, J. Comput. Phys. 256 (2014) 334–356, https://doi.org/10.1016/j.jcp.2013.08.054.
[479] R. Rojas, T. Takaki, M. Ohno, A phase-field-lattice Boltzmann method for modeling motion and growth of a dendrite for binary alloy solidification in the presence of melt convection, J. Comput. Phys. 298 (2015) 29–40, https://doi.org/10.1016/j.jcp.2015.05.045.
[480] K. Yaji, T. Yamada, M. Yoshino, T. Matsumoto, K. Izui, S. Nishiwaki, Topology optimization using the lattice Boltzmann method incorporating level set boundary expressions, J. Comput. Phys. 274 (2014) 158–181, https://doi.org/10.1016/j.jcp.2014.06.004.
[481] L. Zhou, Z.G. Qu, L. Chen, W.Q. Tao, Lattice Boltzmann simulation of gas-solid adsorption processes at pore scale level, J. Comput. Phys. 300 (2015) 800–813, https://doi.org/10.1016/j.jcp.2015.08.014.
[482] Z. Guo, C. Zheng, B. Shi, Force imbalance in lattice Boltzmann equation for two-phase flows, Phys. Rev. E 83 (3) (2011) 036707.
[483] B. van Leer, Computational fluid dynamics: Science or toolbox, AIAA Paper 2001-2520, 2001.
[484] A. Klar, Relaxation scheme for a lattice–Boltzmann-type discrete velocity model and numerical Navier–Stokes limit, J. Comput. Phys. 148 (2) (1999) 416–432, https://doi.org/10.1006/jcph.1998.6123.
[485] S. Jin, Z. Xin, The relaxation schemes for systems of conservation-laws in arbitrary space dimensions, Commun. Pure Appl. Math. 48 (3) (1995) 235–276, https://doi.org/10.1002/cpa.3160480303.
[486] H. Nishikawa, A first-order system approach for diffusion equation. I: second-order residual-distribution schemes, J. Comput. Phys. 227 (1) (2007) 315–352, https://doi.org/10.1016/j.jcp.2007.07.029.
[487] T. Ohwada, On the construction of kinetic schemes, J. Comput. Phys. 177 (1) (2002) 156–175, https://doi.org/10.1006/jcph.2002.7008.
[488] T. Ohwada, S. Fukata, Simple derivation of high-resolution schemes for compressible flows by kinetic approach, J. Comput. Phys. 211 (2) (2006) 424–447, https://doi.org/10.1016/j.jcp.2005.04.026.